



O'Neill, Andrew (2010) *Investigations in molecular structure: from scattering to molecular complexes of brominated compounds*. PhD thesis.

<http://theses.gla.ac.uk/1709/>

Copyright and moral rights for this thesis are retained by the author

A copy can be downloaded for personal non-commercial research or study, without prior permission or charge

This thesis cannot be reproduced or quoted extensively from without first obtaining permission in writing from the Author

The content must not be changed in any way or sold commercially in any format or medium without the formal permission of the Author

When referring to this work, full bibliographic details including the author, title, awarding institution and date of the thesis must be given.

**Investigations in Molecular Structure: From
Scattering to Molecular Complexes of Brominated
Compounds**



**University
of Glasgow**

Andrew O'Neill

Doctor of Philosophy Degree in Chemistry

Department of Chemistry

University of Glasgow

WestCHEM 

Declaration

This thesis has been written in accordance with the University of Glasgow regulations and all work presented here is original and performed by the author unless otherwise stated and referenced in the text.

Andrew O'Neill September 2009

Andrew O'Neill

Abstract

The main focuses of this research were to examine the capabilities of solution techniques to attempt to monitor the nucleation process in crystallisation, and to investigate structural outcomes of crystallisation processes, with reference to polymorphism and intermolecular interactions.

To achieve this, work on the investigation of nucleation and early-stage crystallisation was carried out at the Department of Pharmaceutical Sciences at the University of Strathclyde and also at the central synchrotron facility of Station 2.1 at the SRS Daresbury. Small angle X-ray scattering (SAXS) was carried out on solutions of methyl-4-hydroxybenzoate (pMHB) and 2-bromobenzoic acid. These studies were carried out after developing solution methods to enable us to determine the point at which crystals emerged from solution. This was achieved using Focussed Beam Reflectance Measurements. Structural studies were also carried out on pMHB to examine its polymorphic behaviour and crystal structures were solved at various temperatures from 100K to 300K. The crystal structure of methyl-2,5-dibromobenzoate was also solved at 100K after discovering it sublimes at room temperature. This structure could only be solved from a twinned crystal and indicated the appearance of interesting halogen interactions occurring.

Structural studies have also been carried out using the bromanilic acid molecule as a focus to generate a number of co-crystal complexes to examine their halogen bonding capability and to determine any structural significances in their formation.

Co-crystal complexes of bromanilic acid and a variety of molecules were made in 1:1 and 1:2 ratios to see if any additional halogen interactions could be observed or induced, in addition to the expected hydrogen-binding interactions. The co-crystals included a range of picolines and lutidines as well as bromo-substituted pyridines to attempt to induce halogen interactions. This generated a number of new compounds whose structures were determined using single crystal X-ray diffraction and the interactions were monitored to observed whether any defined patterns with regards to the tendency of bromanilic acid co-crystallisations to produce predictable patterns of intermolecular interactions could be determined.

Acknowledgements

I would like to begin by thanking my supervisors Chick and Alastair for their help, guidance and encouragement throughout the project. Their enthusiasm made the project highly enjoyable and who could forget their karaoke appearances.

I would also like to give special thanks to Lynne for her encouragement / patience with regards to reading and re-reading and also for bullying at the right times to get the work done. Further thanks should go to Andrea for letting me break things in the lab and for generally letting me get in her way but still for showing me the ropes at Strathclyde. Also further thanks should go to Donna for her help with the SAXS experiments and further data analysis.

To all the chicklets who enjoyed a good bit of banter both in the office listening to Damianos tales of Italy and his healthy eating guides and also on those Friday afternoons when wine invariably led to a trip to the Ruby, till they shut it ☹, its been emotional....

Also thanks should go to my fiancée Caroline for putting up with all my notes and papers etc lying all over the flat in some sort of organised mess. Also to my mum and dad who always encouraged me to do what I enjoy. Finally Nicola, Stephanie, Martin, Kelly and Matthew for their own individual ways in which they have helped.

Saturday afternoons at the football again ☺

1 Introduction.....	1
1.1 Polymorphism.....	1
1.2 Nucleation.....	6
1.3 Small Angle X-ray Scattering.....	8
1.4 Studies in the Solid State.....	11
1.5 Solution Studies and Crystallisation Within the Metastable Zone.....	12
1.6 Experimental Structure and Hydrogen Bonding in Molecular Crystals.....	14
1.7 Crystal Engineering and the Importance of Halogen Bonding.....	17
1.8 Co-crystallisations.....	19
2. Theory.....	21
2.1 Crystallography.....	21
2.2 Diffraction Theory.....	22
2.2.1 The Unit Cell and Crystal Lattice.....	23
2.2.2 Miller Indices.....	25
2.2.3 Braggs Law.....	26
2.2.4 The Ewald Sphere.....	27
2.3 Structure Determination.....	28
2.3.1 Diffraction Patterns and Structural Information.....	28
2.3.2 The Phase Problem.....	30
2.3.3 Direct Methods.....	31
2.3.4 The Patterson Method.....	31
2.3.5 Heavy Atom Method.....	32
2.4 Structure Refinement.....	32
3. Techniques and Instrumentation.....	35
3.1 Focussed Beam Reflectance Measurements and Attenuated Total Reflectance Ultra-Violet.....	35
3.2 Synchrotron Radiation.....	39
3.3 X-ray Diffraction Studies of Liquids – Synchrotron and Lab Based Sources...	40
3.4 General Approach to Crystallisations.....	42
3.5 Lab Based X-ray Single Crystal Diffraction.....	44
4. Liquid Studies on Substituted Aromatic Molecules – Methyl-4-hydroxybenzoate.	47
4.1 Introduction.....	47
4.2 Dissolution and Metastable Zone Width Studies.....	48
4.2.1 X-ray Powder Diffraction.....	48

4.2.2 Infrared Spectroscopy.....	49
4.2.3 Calibrations.....	50
4.2.4 Dissolutions.....	53
4.2.5 Metastable Zone Width Studies.....	55
4.3 Small Angle X-ray Scattering Studies of Nucleation.....	61
4.4 Conclusions.....	68
5. X-ray Diffraction Studies of Methyl-4-Hydroxybenzoate – an Investigation of Possible Conformational Polymorphism.....	69
5.1 Variable Temperature X-ray Powder Diffraction.....	70
5.2 Variable Temperature Single Crystal Diffraction Studies.....	71
5.3 Conclusions.....	75
6. Scattering Studies of Bromo-Substituted Compounds: Towards Signal Enhancement and Halogen Interactions.....	77
6.1 Dissolution and Metastable Zone Width Studies of Methyl 2,5-dibromobenzoate	77
6.1.1 Conclusions on Metastable Zone Width Experiments.....	81
6.2 Structural Studies of Methyl 2,5-dibromobenzoate.....	82
6.3 Preliminary SAXS Studies of 2-bromobenzoic acid.....	85
6.3.1 Conclusions.....	89
7. Co-crystals of Brominated Compounds. I. Bromanilic Acid with Picolines.....	90
7.1 Methyl-4-bromobenzoate.....	90
7.2 Co-crystallisations of Bromanilic Acid – Potential Intermolecular Halogen Interactions.....	94
7.2.1 Introduction to Bromanilic Acid.....	94
7.2.2 Initial Studies of Bromanilic Acid.....	97
7.3 Co-crystallisations of Bromanilic Acid with Picolines.....	101
7.3.1 Bromanilic Acid – 3-picoline Co-crystal Structures.....	102
7.3.2 Bromanilic Acid – 2-picoline Co-crystal Structures.....	106
7.3.3 Bromanilic Acid – 4-picoline Co-crystal Structures.....	108
7.3.4 Summary.....	114
8. Co-crystals of Brominated Compounds II Bromanilic Acid with Lutidines.....	115
8.1 Co-crystallisations of Bromanilic Acid and the Family of Lutidine Molecules.	115
8.1.1 Bromanilic Acid, 2,3-lutidine.....	116
8.1.2 Bromanilic Acid, 2,4-lutidine.....	118
8.1.3 Bromanilic Acid, 2,5-lutidine.....	120

8.1.4 Bromanilic Acid, 3,5-lutidine.....	122
8.2 Summary.....	127
8.3 Co-crystals of Bromanilic Acid and Other Bromo-Substituted Molecules.....	128
8.3.1 2-bromo-3-methylpyridine : Bromanilic Acid.....	128
8.3.2 3-bromo-4-methylpyridine : Bromanilic Acid.....	130
8.4 Conclusions / Summary.....	132
9. Conclusions and Forward Look.....	133
9.1 Liquid Scattering Studies.....	133
9.2 Structural studies of methylbenzoate derivatives and the assessment of conformational polymorphism.....	134
9.3 Co-crystal Studies and Attempts to Engineer Halogen Bonding Interactions..	134
References.....	136
Appendices.....	142
Figure 1.1.1: The packing motifs of the two polymorphs of paracetamol.....	2
Figure 1.1.2: Structure of carbamazepine.....	3
Figure 1.1.3: Molecular structure of ROY.....	4
Figure 1.2.1: Illustration of the metastable zone incorporating solubility curve and supersolubility curve.....	8
Figure 1.6.1 a and b: An example of a bifurcated hydrogen bond donor and acceptor	16
Figure 1.7.1 a and b: The crystal structures of the iodo and bromo substituted co-crystal compounds studied by Aakeröy ⁷³	19
Figure 2.2.1.1: A three dimensional unit cell.....	24
Figure 2.2.2.1: Miller indices showing the (222) plane.....	26
Figure 2.2.3.1: Bragg's law.....	27
Figure 2.2.4.1: The construction of an Ewald sphere.....	28
Figure 2.3.1.1: Atomic form factor drop off with increasing angle for X-ray form factors (and absence of fall-off for neutron scattering lengths).....	30
Figure 3.1.1: The ATR-UV probe showing the clear crystal window through which all light passes.....	36
Figure 3.1.2: The Multi-Max system at SIPBS. This shows the reactor vessels in their independent compartments, the possibility for dilution and also the FBRM probe.....	37

Figure 3.2.1: A schematic showing the process of how synchrotron radiation is generated.....	40
Figure 3.3.1 a and b: Station 2.1 at Daresbury showing the beamline (left) and the sample holder (right).....	41
Figure 3.5.1: Chart of requirements prior to publishing crystal structures ⁸¹	44
Figure 4.1.1: Methyl 4-hydroxybenzoate.....	47
Figure 4.2.1: XRPD data from pure and recrystallised pMHB. The pure material is shown in black and the recrystallised in red.....	49
Figure 4.2.2: IR data collected on pure and recrystallised pMHB. The pure material is shown in red and the recrystallised material in blue.....	50
Figure 4.2.3: Absorbance changes with wavelength using varying concentrations of solutions at a fixed temperature.....	51
Figure 4.2.4: Calculated calibration results using varying concentrations of solutions at a fixed temperature.....	52
Figure 4.2.5: Absorbance changes against wavelength at varying temperatures for a fixed concentration of solution.....	54
Figure 4.2.6: The solubility curves calculated from dissolution experiments.....	55
Figure 4.2.7: Chord length distribution profile of the crystallisation process from dissolution to recrystallisation. The temperature profile for the experiment is shown in red.....	57
Figure 4.2.8: Change in CLD as solution is cooled and crystallisation occurs.....	58
Figure 4.2.9: UV absorbance changes as the metastable zone width experiment progresses and temperature is decreased.....	59
Figure 4.2.10: The metastable zone width results plotting the dissolution curve and the best fit curve for the nucleation points as observed during the MZW experiments. 60	60
Figure 4.3.1: Sample cell used with small window for the solution.....	62
Figure 4.3.2: The detector image of pMHB in methanol at 20°C.....	63
Figure 4.3.3: Scattering profile of pMHB (blue) and methanol (red) at 20°C.....	64
Figure 4.3.4: Scattering profile showing an overlay of the data collected at the four studied temperatures (5°C is shown in green, 10°C in pink, 15°C in red and 20°C in blue) showing a marginal increase in intensity as a function of temperature.....	66
Figure 4.3.5: All the data collected on station 2.1, indicating increased scattering from the solute. The methanol solutions all show significantly lower scattering at higher angles and show very little variation as a function of temperature.....	67

Figure 5.1: pMHB indicating the two torsion angles discussed in relation to possible conformational polymorphism.....	69
Figure 5.2: XRPD patterns collected during VT XRPD study (from bottom to top, 100K, 150K, 200K, 250K, 300K).....	71
Figure 5.2.1: The crystal packing of pMHB as viewed along the <i>b</i> -axis at (top) 100K, (middle) 200K and (bottom) 300K.....	72
Figure 5.2.2: The trend in unit cell parameters and cell volume of pMHB with respect to temperature, from the single crystal experiments.....	74
Figure 6.1.1: Methyl 2,5-dibromobenzoate.....	77
Figure 6.1.2: The absorbance changes for each calibration solution as a function of temperature.....	78
Figure 6.1.3: Solubility curves of MDBB from dissolution experiments.....	79
Figure 6.1.4: Solubility and supersolubility curves for MDBB indicating the metastable zone.....	80
Figure 6.2.1: Crystal structure of MDBB viewed along the <i>a</i> axis, with halogen - oxygen bonds and halogen – halogen interactions highlighted.....	83
Figure 6.2.2: Predicted powder pattern of MDBB calculated from the crystal structure solved from the twinned crystal at 100K.....	84
Figure 6.2.3: Powder pattern of MDBB collected at 300K.....	85
Figure 6.3.1: Typical dimer of 2-bromobenzoic acid, with hydrogen bonds and halogen bonds labelled in blue ⁸⁸	86
Figure 6.3.2: Scattering profile of MDBB.....	86
Figure 6.3.3: Scattering profile measured on Station 2.1 showing variations between the scattering from solutions of the two molecules investigated (2-bromobenzoic acid in blue, pMHB in red, both in methanol solvent) and the control (methanol solvent-only) experiment (in pink).....	87
Figure 6.3.4: Scattering profile showing the variations in scattering of 2-bromobenzoic acid with temperature, with the increase between 10°C (red) and 20°C (blue) evident.....	89
Fig 7.1.1: Methyl-4-bromobenzoate.....	90
Fig 7.1.2: Crystal structure of methyl-4-iodobenzoate viewed along the <i>b</i> axis, with an O··I halogen bond highlighted.....	91
Fig 7.1.3: Overlay of representative XRPD patterns of methyl-4-bromobenzoate collected from samples recrystallised from different solvents.....	91

Fig 7.1.4 a-c: Crystal structures of methyl 4-bromobenzoate viewed along the <i>b</i> axis produced at 100, 200 and 300K respectively, with the halogen bond highlighted.....	92
Figure 7.1.5 a and b: The variation of the thermal ellipsoids at 100K and 300K for methyl-4-bromobenzoate indicating that although the precision of the structure remains similar, the thermal motion, specifically around the methyl hydrogens increases considerably as would be expected for a librating methyl group.....	93
Fig 7.2.1: A schematic diagram of bromanilic acid, systematic name 2,5-dibromo-3,6-dihydroxyl-1,4-benzoquinone.....	94
Figure 7.2.2: Crystal structure of bromanilic acid viewed along the <i>c</i> axis showing the four hydrogen bonds that are present from each bromanilic acid molecule ⁹⁶	95
Fig 7.2.3 a and b: An example of a picoline and a lutidine molecule, in this example a. 4-picoline and b. 2,3-lutidine.....	98
Fig 7.2.4: Crystal structure of bromanilic acid collected at 100K. Close contacts are shown with dashed lines.....	100
Figure 7.2.5: XRPD data from recrystallised sample of bromanilic acid.....	101
Figure 7.3.1: Crystal structure of bromanilic acid and 3-picoline in a 1:1 ratio viewed down the <i>a</i> axis collected at 100K.....	102
Figure 7.3.2: Crystal structure of bromanilic acid and 3-picoline in the ratio 1:2 viewed down the <i>a</i> axis, collected at 100K.....	104
Figure 7.3.3: Close contacts involving bromine and the carbon atoms of the bromanilic acid molecule involved in the bifurcated hydrogen bonding with 3-picoline.....	105
Figure 7.3.4: XRPD data showing the 1:1 and 1:2 co-crystal products of co-crystallisations of bromanilic acid and 3-picoline.....	105
Figure 7.3.5: Crystal structure of Bromanilic acid and 2-picoline in the ratio 1:2 viewed along the <i>b</i> axis, collected at 100K.....	106
Figure 7.3.6: XRPD data showing the 1:1 and 1:2 bromanilic acid 2-picoline co-crystal products.....	107
Figure 7.3.7: Crystal structure of bromanilic acid and 4-picoline in a 1:1 ratio determined at 100K.....	109
Figure 7.3.8: Crystal structure of bromanilic acid and 4-picoline in the ratio 1:2 viewed along the <i>b</i> axis, collected at 100K.....	110
Figure 7.3.9: XRPD data showing the 1:1 and 1:2 co-crystal products of bromanilic acid with 4-picoline.....	110

Figure 8.1.1: Crystal structure of bromanilic acid and 2,3-lutidine in a 1:1 ratio viewed down the a axis, collected at 100K.....	116
Figure 8.1.2: All the interactions from one molecule of bromanilic acid in the co-crystal structure with 2,3-lutidine.....	118
Figure 8.1.3 a and b: a shows the existence of the four molecule interaction in bromanilic acid 2,4-lutidine and b shows that each of these four molecule interactions has staggered four molecule interactions layered below it providing π - π stacking interactions.....	119
Figure 8.1.4: Crystal structure of bromanilic acid and 2,4-lutidine in a 1:1 ratio collected at 100K showing the halogen bonding and how it links the four-molecule units.....	119
Figure 8.1.5: Crystal structure of bromanilic acid and 2,5-lutidine in a 1:1 ratio viewed along the a axis, collected at 100K.....	121
Figure 8.1.6: The layers in the bromanilic acid 2,5-lutidine co-crystal that are present as a result of π - π stacking interactions between the four molecule units.....	122
Figure 8.1.7: Four molecule interaction of bromanilic acid with 3,5-lutidine.....	123
Figure 8.1.4.2: Crystal structure of bromanilic acid and 3,5-lutidine in a 1:1 ratio viewed along the b axis, collected at 100K.....	124
Figure 8.3.1: Crystal structure of bromanilic acid and 2-bromo-3-methylpyridine showing the interactions present around each bromanilic acid molecule collected at 100K.....	129
Figure 8.3.2: The crystal packing of bromanilic acid (ba) and 2-bromo-3-methylpyridine (mp) showing apparent a-b-a-b type layers, when viewed along the a axis.....	130
Figure 8.3.3: Crystal structure of bromanilic acid and 3-bromo-4-methylpyridine in a 1:1 ratio viewed along the b axis, collected at 100K.....	131
Figure 8.3.4: Four molecule unit in crystal structure of 3-bromo-4-methylpyridine and bromanilic acid.....	132
Table 2.2.1.2: Unit cell types with associated unit cell requirements and possible Bravais lattices.....	24
Table 5.1: Torsion angle data from low temperature form (LT), room temperature form (RT), our 100K data and our 300K data.....	75

Table 7.1: Distances and angles for the bifurcated hydrogen bond in the bromanilic acid (Ba) picoline (pic) complexes and other important close contacts. The angles shown represent the plane of the bifurcated hydrogen bond.....112

Table 7.2: The crystallography data produced from single crystal diffraction.....113

Table 8.1: Distances and angles for the bifurcated hydrogen bond in the bromanilic acid (ba) lutidine (lut) complexes and brominated methylpyridines (mepyr) complexes and other important close contacts. The angles shown represent the plane of the bifurcated hydrogen bond.....125

Table 8.2: The crystallography data produced from single crystal x-ray analysis...126

Chapter 1. Introduction

1.1: Polymorphism

Polymorphism in molecular crystals is defined as the ability of a substance to exist in different molecular arrangements or different molecular conformations within the lattice under similar external conditions. The wide range of molecules that exhibit polymorphism can be explained by Ostwald's law of stages, which states that "when leaving an unstable state, a system does not seek out the most stable state, rather the nearest metastable state which can be reached with loss of free energy"¹. This describes the idea that when crystallisation occurs the molecules, as they assemble, will simply fall to the nearest minimum energy state with a loss in free energy and can then continue to seek out the most stable form. This can ultimately result in changes in the polymorphic form adopted even after an apparently stable structure appears to be found. The co-crystal structure of carbamazepine and isonicotinamide shows that through a solvent mediated transformation the initial needles produced (form II) will be replaced with plate like crystals of form I over time².

Polymorphism can generally be traced back to the work of Mitscherlich in the early 1800s and he is widely credited with the first recognition of the phenomenon from his studies on crystals of certain phosphates and arsenates³. Since this discovery polymorphism has become an area of huge study and of critical importance in many areas, including the food and speciality chemicals industries, however arguably the most significant of these would be the pharmaceutical industry. This can be highlighted in many major studies including that of Ritonavir¹, a drug developed for the treatment of HIV. The discovery of a second more thermodynamically stable form of Ritonavir, changing the physical properties and characteristics and making the original formulated form disappear from the production process, led to a complete stop on production and ultimately cost the manufacturer (Abbot Laboratories) millions of dollars in lost sales and in R&D for reformulation. It should be mentioned that even after a polymorphic form 'disappears' it can be possible to generate this initial form again but a different route will have to be found. There are many other examples of disappearing polymorphs^{4,5,6}, causing a great deal of concern among

researchers in the field as this finding shows that an apparently ‘simple’ process such as crystallisation in fact could not be controlled.

Another common example of polymorphism in pharmaceuticals is the case of paracetamol, a widely used analgesic that has for a long time been known to have two distinct crystal forms in which single crystals can be produced. Form I, the common form, is monoclinic⁷, while form II is known to be orthorhombic⁸. Subsequent studies using variable temperature x-ray diffraction, on Form II,⁹ and neutron diffraction, on Form I,¹⁰ have been carried out to characterise the structures fully. Form I is the thermodynamically stable modification⁹ at room temperature, whereas form II is the metastable form under ambient conditions. This is a rather simple example of polymorphism where the two forms that can be solved by single crystal diffraction have unique crystal systems (Figure 1.1.1).

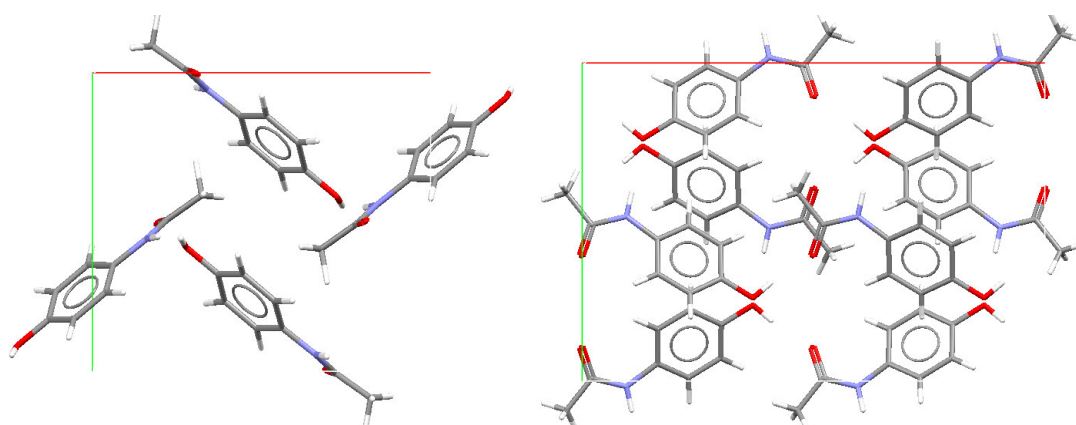


Figure 1.1.1: The packing motifs of the two polymorphs of paracetamol

There are also several more complicated instances of polymorphism, many of which have been widely studied over the course of many years. One of these is the heavily studied anticonvulsant drug carbamazepine (Figure 1.1.2). There are four known polymorphs of carbamazepine^{11,12,13,14}, however solvates and hydrates are also known to exist and in one particular automated parallel crystallisation study Forms I-III were found along with one hydrate form and no fewer than 8 organic solvates¹⁵.

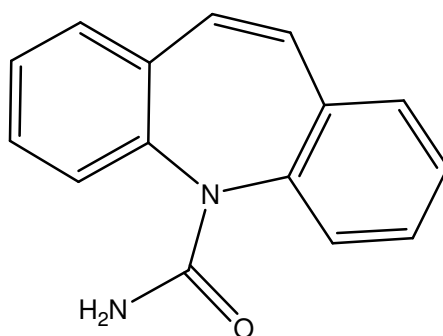


Figure 1.1.2: Structure of carbamazepine

Due to the significant polymorphism present in this material computational studies have also been carried out as there are clear advantages in being able to predict any occurrence of polymorphism. The computational studies carried out were concerning the predictability of forms II-IV, as current computational prediction models do not permit the study of structures where Z' is greater than 1. The two monoclinic polymorphs forms III and IV were found to be the most stable structures alongside a third, currently unobserved structure. Forms I and II were 6 and 8 kJ/mol above the global minimum, where the energy for Form I was generated from the known crystal structure, and along with many other potential structures in the energy landscape would have been unlikely to be suggested as possible polymorphs¹⁶. This study emphasises how important it is to develop computational techniques further, with the aim of benefiting crystal structure prediction.

The material with the most known polymorphs is 5-methyl-2-[(2-nitrophenyl)amino]-3-thiophenecarbonitrile (ROY; Figure 1.1.3)). This is known as ROY due to the characteristic colours of the distinguishable polymorphs that are known to exist. These forms are orange needles, yellow prisms, red prisms, orange plates, yellow needles and orange-red plates¹⁷.

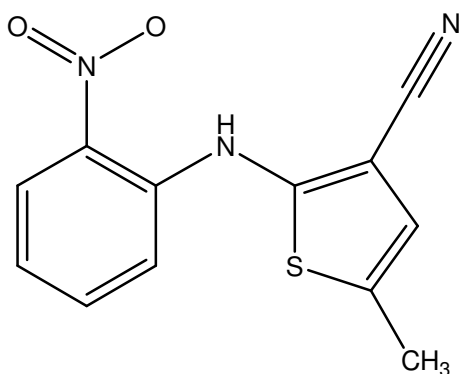


Figure 1.1.3: Molecular structure of ROY

The six polymorphs mentioned above are all available in single crystal forms from recrystallisation from solvents, with no solvates known. This is a unique case and makes ROY the organic compound with the most available polymorphs from simple recrystallisation. There are also now three further polymorphs that have been discovered from less studied routes^{18,19}. This goes to show the importance of alternative approaches to polymorph screening to include not only solvent crystallisations, but also allowing for the discovery of further polymorphs via unusual routes.

The terminology surrounding polymorphism is a major area of ambiguity with many terms relating to small subtle changes in the crystal structure, which may or may not be evidence of a new polymorph being produced. These include pseudopolymorphism and conformational polymorphism¹. The first of these relates to the formation of solvates and hydrates of which there are many in a wide range of studied compounds as highlighted by Jacco van de Streek²⁰. The second is a much more complicated term as any small changes in crystal structures, with reference to changing temperature or pressure, *etc*, of a specific study could be described by the author as an incidence of conformational polymorphism. The potentially narrow scope of this field in trying to attribute the occurrence of polymorphism can be identified in the study of methyl 4-hydroxybenzoate where a stable crystal structure was known to exist²¹. Further work was carried out on the crystal structure and a reported conformational polymorph was discovered²². The small changes with reference to the original crystal structure, solved at room temperature, were largely due to a torsion angle change of less than 6°. This prompted further discussion and

disagreement²³, illustrating how an apparent polymorphic transition can sometimes be defined at the authors' discretion.

The relationship between polymorphs and their most stable forms can be described as monotropic or enantiotropic²⁴. If the polymorphs are related monotropically, transformation from the metastable form to the stable form is irreversible independent of the physical processes that are applied to the structure – a return to the metastable crystal structure will not occur. If the polymorphs are related enantiotropically however, the transformation is reversible. In this case a transition point exists, where the free energies are identical, and at temperatures above this, one form is more thermodynamically stable than the other, whereas this is the opposite at lower temperatures. There are two proposed mechanisms for such transitions, solid state transitions (SST) and solution mediated transformations (SMT)²⁵. SST are influenced by the environment of the crystal, such as pressure and temperature, and also by the presence of crystal defects and impurities. SMT typically occur in solvent and can be driven by the change in solubility between the two forms, however at higher temperatures it is also possible for a second, less stable, state to be accessed due to the increase in energy as a result of heating.

The massive increase in the study of polymorphism has given rise to a significant improvement in techniques for monitoring the modifications in crystal structure. The instrumentation available for the detection, characterisation and identification of new polymorphs has increased at a significant rate in terms of both *in-situ* techniques and also off-line techniques.

With regards to off-line techniques that are used most regularly these can typically be subdivided into four areas; crystallographic, spectroscopic, microscopic and thermal. Crystallographic techniques include both single crystal diffraction and powder diffraction, from both X-ray and neutron sources. The significant increase has come increasingly in the powder diffraction side with it now becoming routine to solve crystal structures to a publishable standard using the quality of powder data and structure solution programs now widely available. Spectroscopic techniques include infrared spectroscopy and Raman spectroscopy, and while not able to solve structures in terms of the 3-dimensional connectivity, these can give quick analysis of samples

to indicate similarities and changes from the starting materials. Microscopic analysis is used to examine the optical properties of crystals for example using electron microscopy. Thermal techniques include differential scanning calorimetry (DSC) and thermal gravimetric analysis (TGA) and these are routinely carried out together to examine changes in the physical properties of the compounds.

X-ray powder diffraction (XRPD) is still the most routinely used and arguably the most important technique for quick determination of products. It is now possible in high throughput labs to produce hundreds of samples each day and using XRPD to carry out analysis quicker than ever. However these techniques require preparation of appropriate samples and especially in the example of XRPD, grinding of the samples into a fine powder is sometimes able to in itself produce enough energy to produce a new polymorph^{26,27}.

1.2: Nucleation

Crystal nucleation is generally viewed as essentially a two-step process, which involves the initial formation of clusters followed by the organisation of these clusters into ordered crystalline arrangements²⁸. These clusters are determined to be at nucleation when the critical nuclei size is reached. This point is unique for every system investigated and even for polymorphic forms of the same molecule this can be different.

Homogeneous nucleation, in which nucleation will occur spontaneously with only molecules of the crystallising materials present, will very rarely occur in large volumes of solution as these are highly difficult to prepare without the presence of impurities. It is believed that homogeneous nucleation can be controlled experimentally by many variables including solubility and temperature². Precipitation in small volumes has been used to study homogeneous nucleation processes. An example of this is the generation of the metastable polymorph of nabumetone via capillary based crystallisation²⁹. Due to the increased evaporation time this can also promote the growth of larger crystals in an environment much more likely to induce homogeneous nucleation than that of the common sample vial. Further studies include the use of emulsion systems to study homogeneous

nucleation, this involves the separation of heteronuclei in the dispersion of a melt and from the remainder of the drop homogeneous nucleation can occur^{30,31}. This technique was carried out on meta-chloronitrobenzene (m-cnb) from 2 solutions containing a mixture including para-chloronitrobenzene (p-cnb). This also involved seeding with m-cnb and the resulting crystallisation resulted in a highest purity of 99.7% for both of the solutions prepared.

Heterogeneous nucleation processes are significantly more important in pharmaceutical systems since extra surfaces can act as nucleation points to promote the crystallisation of different crystal structures. This process can occur *via* many pathways from scratching of the walls of the vessel to accidental nucleation by dust or a strand of hair. This sensitivity to environment is what makes the nucleation process so hard to define. In laboratory and large-scale crystallisations it is often found that the nucleation process appears to originate in one section of the reaction vessel. This can be at different areas such as at a cooling spot or the surface of a liquid. It can also be found that a particular spot on the vessel wall or the stirrer can also be the centre around which nucleation occurs, this is generally due to faults in the glassware, which are impossible to avoid. In the case where the same glassware is being used for another experiment, there may be a seed left behind that will lead to erroneous results³².

Whilst thermodynamic models are available to predict polymorphism computationally, they do not currently accommodate kinetic factors such as nucleation and crystal growth resulting in an inclination to overestimate the tendency to form polymorphs¹⁵. There are three well defined regions associated with crystallisation (Figure 1.2.1). The first is a stable, unsaturated, zone where crystallisation is impossible. The second is the metastable zone between the solubility and supersolubility curves, where crystallisation is improbable, however if seeds were to be implanted in a metastable solution then growth would occur on it³³. This is the preferred region to carry out controlled crystallisations as this helps to prevent any unwanted nucleation from occurring³⁴. Crystallisation within the metastable zone is not common due to the stability of the solution and beyond this metastable zone the system is said to be labile, and this is where spontaneous nucleation can occur. Tuning the cooling rate of a supersaturated solution until the

first indications of crystallisation can be seen, can control the onset of nucleation. This is referred to as the nucleation point.

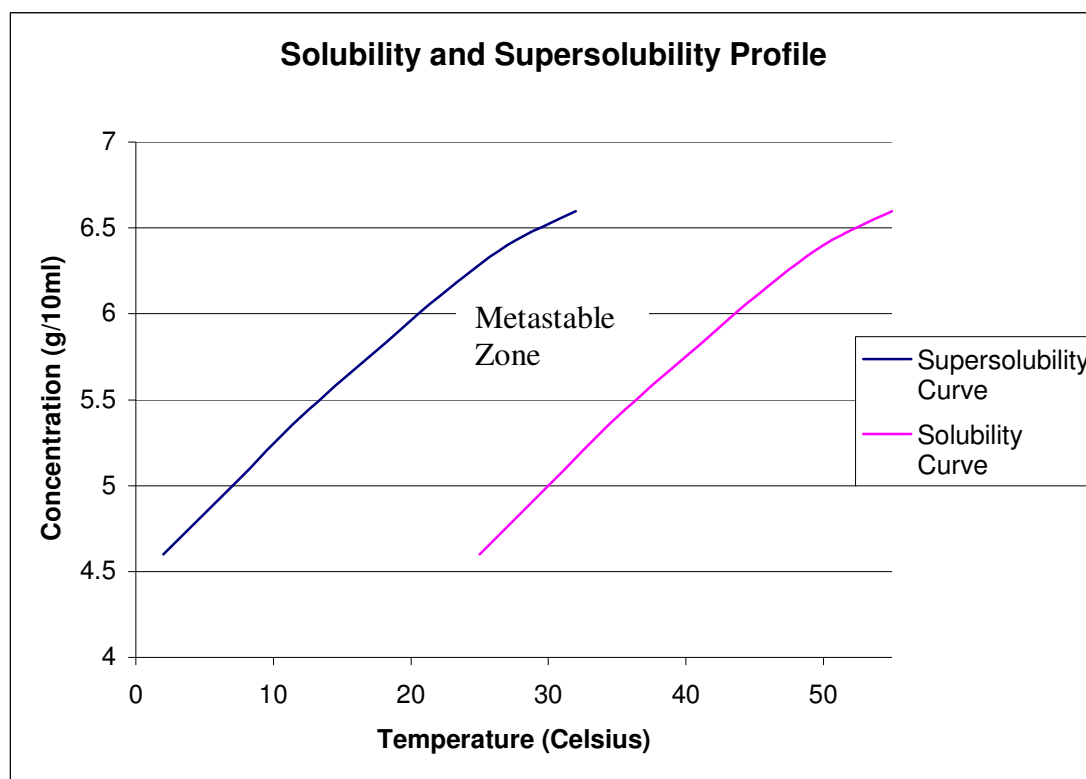


Figure 1.2.1: Illustration of the metastable zone incorporating solubility curve and supersolubility curve.

In many cases the best way to control the crystallisation product is to add seeds from previously grown crystals^{35,36} thus being able to control the final product of the crystallisation. Seeding can be carried out either intentionally or unintentionally, which leads to the idea of homogeneous and heterogeneous nucleation. The effectiveness of crystal seeding in controlling crystallisation outcomes relies on the potential of solid surfaces to promote heterogeneous or secondary nucleation, while avoiding heterogeneous nucleation mediated by unknown contaminants. Roger Davey, through the simple example of brown sugar, highlights this theory where just one granule is used to produce numerous others of a uniform size and shape³⁷.

1.3: Small angle x-ray scattering (SAXS)

X-ray and also neutron small angle scattering are both powerful probing techniques that can be used *in-situ* to study the growth of particles and monitor solution changes^{38,39}. SAXS is widely used to analyse low resolution structure and conformational changes of native biological macromolecules in solution⁴⁰ and has come a long way since A. Guinier developed the main principles behind the technique during his studies of metallic alloys³⁹. Progress in these fields have led to the manufacturing of significant high – flux dedicated x-ray synchrotron radiation beams, such as station 2.1 at the SRS, Daresbury Laboratories, which was used to collect some of the data presented in Chapter 4 and 5. Such a beamline can generate huge amounts of data during *in-situ* experiments, though the analysis of these can be difficult and time-consuming.

Low angle scattering can be important for studying the onset of crystallisation in solution as at the onset of crystallisation there is no crystallinity, merely the start of ordering of molecules in solution. This allows larger d-spacings to be investigated. Such studies are hugely important and could in principle be used to aid in the prediction of polymorphism if ever a reliable kinetic profile of crystallisation can be produced. SAXS can also be used as a complementary technique with wide angle x-ray diffraction (WAXS) which can also be used to study structural changes in solution. When used together they provide complementary methods for determining size, size distribution, structural profile and ‘order’ in the solution state. SAXS focuses on the low scattering angles, $<10^\circ$, and WAXS from $3/4-60^\circ$.

SAXS measurements typically are concerned with scattering angles $<10^\circ$. As dictated by Bragg's Law ($n\lambda=2d\sin\theta$), the diffraction information about structures with large d-spacings lies in this region. In Bragg's law, n is an integer, λ is the wavelength of the incident and diffracted beam, d is the spacing between the planes in the crystal and θ is the scattering angle. Therefore the SAXS technique is commonly used for probing large length scale structures such as high molecular weight polymers, biological macromolecules and self-assembled superstructures. When used in the study of proteins and other macromolecules it routinely provides information on the size, shape and the radius of gyration of the sample under study. SAXS measurements are technically challenging because of the small angular separation of the direct beam (which is very intense) and the scattered beam. Large specimen-to-detector distances

and high quality collimating optics are used to achieve good signal-to-noise ratio in the SAXS measurement. This relies on the availability of SAXS programs which can reveal significant signal from the scattering region at low scattering angles.

SAXS has been used in conjunction with Raman spectroscopy in the study of fibrillin rich microfibrils⁴¹. This enabled the packing of the microfibrils contained in the tissue and the organization to be monitored. A combination of these techniques enabled changes within the microfibrils to be noted on a macromolecular and submolecular level to be noted when the tissue was extended and strained. With the development of SAXS it is possible to carry out experiments such as this and determine the overall change in structure on such small scales.

Amorphous carbon films have also been studied using SAXS to develop the technique away from purely biological science, and be applied to determine their porosity. The films studied were produced by plasma enhanced chemical vapour deposition (PECVD)⁴², which deposits films at varying argon pressure. As SAXS probes the whole structure, the changes in pore size were able to be determined using GNOM⁴³. This enabled 8nm pores to be detected in carbon films produced at high argon pressure. With such determination at small sizes the possibilities for the technique are very wide ranging.

SAXS has also been used to monitor solution structures. This can lead to significant prospects with regards to molecular binding in the body. Glyceraldehyde-3-phosphate dehydrogenase (GAPDH) was studied in relation to the method by which it transported into the cell surface where glycolytic enzymes are not routinely found³⁸. Crystallographic studies found that GAPDH formed dimers whereas all other GAPDH type structures formed tetrameric structures. Through SAXS studies, however, it was noted that the protein was in fact tetrameric in solution but it is the arrangement of the dimers that alters from previous studies. Using SAXS it was also possible to monitor the impact of the structure upon binding to NAD⁺, which contracted significantly.

A further study involving solution structures was carried out on the human natural killer inhibitory receptor Irp60⁴⁰. SAXS data was able to determine that Irp60 is monomeric in solution with distinct molecular shape. This is even though there is no

crystallographic data available for this specific protein, showing that in the absence of such data SAXS is still able to determine shape in solution.

1.4: Studies in the Solid State

Crystal engineering is the design and production of molecular solid state structures based upon their functional group capabilities. This can be done with the aim of controlling subsequent physical properties that the molecules will possess. Crystal engineering has become an area of wide scale study and has been developed widely in terms of predictability of interactions that are likely to occur. Being able to predict structures is still proving a great challenge, including computationally, so there is still a lot of knowledge to be gained before crystal engineering will result in confident predictions. This area is open to a great deal of ongoing work and relies on a lot of experimental trial and error before reliable predictions will ever be made.

The basic technology project; CPOSS (Control and Prediction of the Organic Solid State) project was set up to try and combine the theoretical prediction of polymorphism with the practical side of growing polymorphs to push the boundaries of polymorph prediction, which would ultimately lead to the ability to confidently predict the lowest energy conformation of a specific compound, and the number of polymorphs present. The project, led from University College London, reaches out to experimentalists carrying out high throughput XRPD and monitoring early stage polymorph formation using solid state NMR and links in with computational studies. These computational studies produce energy landscapes to show what is predicted to be the lowest energy polymorph. There have been occasions that this has been able to generate the most stable polymorph even taking into account hydrates⁴⁴, however the kinetics behind crystal growth are not well enough understood to be incorporated into the calculations and for this reason relative energies of known polymorphs are not always predicted correctly, and many possible polymorphs are missed.

The progress incorporated in such a research activity can be measured when both experimental data and computationally predicted structures are combined such as in the case of the 5-substituted uracils⁴⁵. This approach compared the experimentally

produced crystal structures of twelve uracils substituted at the 5-position and the energy predictions associated with the most likely forms. The computational studies in this work calculated the experimentally produced crystal structures to be within 3kJ mol⁻¹ of the global minimum. This implies that these structures produced were indeed within reasonable range of the computationally produced global minimum and are determined to be thermodynamically feasible.

The computational methods currently in place still rely purely on energy calculations but through computational program development, crystal structure prediction is now able to study compounds with $Z' > 1$, more flexible compounds and now co-crystals. There are obvious limitations in the reliability of polymorph prediction using the current techniques, however there has been progress in terms of crystal structure prediction and a way to evaluate this is via the four blind tests carried out so far^{46,47,48,49}. These blind tests, organised by the Cambridge Crystallographic Data Centre, are on compounds without widely available structural data and in fact an independent figure holds the structural data for the compounds in the tests. Each of the groups that takes part is allowed three predictions, ranked, for each molecule. For the first time in blind test 4 it has been possible for a group (Neumann, Leusen and Kendrick) to predict all four molecules correctly and as their top ranked guess, however the technique used requires a great degree of computational time. This however proves that significant progress has been made since the first blind test where from many attempts only seven guesses were 'classified as correct' though with numerous structures available around the global minimum even this was inconclusive. For this reason it is essential that efforts to improve crystal structure energy prediction continue and that inclusion of kinetic factors is developed to aid with the difficulties that lie within polymorph prediction.

1.5: Pre-Nucleation Studies and Crystallisation Within the Metastable Zone

Pre-nucleation studies are fundamental with respect to increasing knowledge about how crystallisation occurs. Using focussed beam reflectance measurements (FBRM) and particle vision and measurement (PVM) it has been possible to monitor a polymorphic transition of mannitol^{50,51}. These techniques enable in-situ monitoring of

particle changes without sampling and whilst FBRM records the changes in the chord length distribution, PVM enables visual monitoring. This can have benefits with regards to monitoring dissolution and recrystallisation to examine the forms as they are being produced. This also eliminates the need for supplementary techniques to examine whether a change has occurred such as XRPD, which as mentioned above in itself can sometimes promote a polymorphic transition due to the grinding necessary.

FBRM has also been used to monitor the particle size changes in solution^{52,53}. The FBRM probe has a measurement range of 1-1000 μm and can collect data measurements every five seconds and transfer them to chord length distribution plots (CLD). Making use of this with an imaging technique such as process video imaging (PVI) provided evidence that below 1 μm the FBRM was not highly sensitive signifying that although the FBRM probe generates an idea of what is in solution it is not sufficiently sensitive to provide any evidence on crystallisation kinetics.

Other techniques involved in solution studies include the use of attenuated total reflectance ultra-violet (ATR-UV). This is another in-situ technique that has been successfully developed to monitor concentration changes of an organic compound⁵⁴. The UV absorption data acquired can be simply transformed to concentration using the Beer Lambert law for the absorbance

$$A = e c l.$$

where A is the absorption coefficient, e is the molar absorptivity of the absorber, c is the concentration and l is the path length.

The metastable zone refers to the region of supersaturation where spontaneous nucleation cannot occur and a seed of the crystal is required to initiate growth. The width of the metastable zone indicates the stability of the solution, the larger the zone width the more stable the solution³³.

A solute is maintained in solution until a sufficiently high level of supersaturation has been developed; this in turn encourages spontaneous nucleation to occur. It is

important to characterize the metastable zone width (MZW) under a specific set of operating conditions, which relate closely to the conditions of the final scale crystallisation. The polythermal technique⁵⁵ involves cooling a saturated solution at a fixed rate until nucleation occurs. This is repeated several times at a variety of cooling rates until a reliable MZW can be determined. The MZW can be considered to be characteristic for each crystallisation system as each is unique. The induction period of nucleation is defined as the time that elapses between the instant when the supersaturated state is generated and the point of time at which solid phase particles become detectable. This includes the time required for the generation of a critical nucleus in supersaturation and the growth to a detectable range, which can be as low as 1 μ m in the FBRM⁵⁶.

Understanding the MZW is of fundamental importance in being able to control crystal growth and is widely studied in this field¹. In depth solubility studies and supersolubility studies of a single compound are needed and temperature control is crucial. Reliable dissolution profiles can be determined and these are fundamental in the pharmaceutical industry in particular. This is due to the increase in discovery of new polymorphic forms of molecules and the corresponding changes in their key physical properties such as solubility. For this reason it is vitally important to be able to carry out these experiments in a clean and controlled environment as even the smallest contaminant such as a speck of dust can be known to initiate nucleation.

1.6: Experimental Structure and Hydrogen Bonding in Molecular Crystals

Hydrogen bonding is known to be the strongest non-bonding interaction with the strongest being similar in strength to that of some conventional covalent bonds. It is proven to be vitally important in both structural chemistry and biology where hydrogen bonds provide, for example, vital interactions in the structure of DNA. Hydrogen bonds are known to affect the smallest of molecules, such as ice and essentially provide the glue that holds a structure together. Techniques such as infrared spectroscopy and NMR can be used to monitor the dynamics and strengths of hydrogen bonding systems, however crystallography can tell us precise information

about the atomic positions in specific crystal systems and hence about the detailed geometry of hydrogen bonds.

From a crystallographic perspective, hydrogen bonding interactions are known to be the strongest non covalent interactions with energies ranging from 0.5 – 40 kcal mol⁻¹. Pauling first freely used the term hydrogen bond in 1935 to account for the interactions in ice⁵⁷, though the prospect of hydrogen bonding had been advanced previously by Latimer and Rodebush (1920)⁵⁸ and Huggins (1922)⁵⁹ and has been progressively used since. Pauling stated that in a hydrogen bonding system, X-H...A, only if X and A were highly electronegative would there be an electrostatic interaction between H and A that would in turn be sufficiently high to be termed a hydrogen bond⁶⁰. This theory however restricts the phenomenon of hydrogen bonding to interactions where X and A are any of; F, O, Cl, N, Br or I. This has led to further quantification and led Steiner and Saenger in 1993 to put forth their own definition that ‘any cohesive interaction X-H...A where H carries a positive and A a negative charge and the charge on X is more negative than on H’ can be deemed to be a hydrogen bond⁶⁰. This definition still holds value today.

Hydrogen bonding is routinely split into three types according to their energy: weak < 4 kcal mol⁻¹, moderate 4-15 kcal mol⁻¹ and strong 15-40 kcal mol⁻¹⁶¹. Unusually activated donors and acceptors, often in an intramolecular situation, form very strong hydrogen bonds⁶⁰. Most often they are formed between an acid and its conjugate base, X-H...X⁻, or between a base and its conjugate acid, X⁺-H...X. The distinctive characteristic of such interactions is that their bonding is covalent in character, for example the X-H and H-A distances are comparable. An energy range of 15-40 kcalmol⁻¹ is to be found for this category. The main examples include [F...H...F]⁻ and [N...H...N]⁺.

The moderate region with regards to hydrogen bond strength is the most common and is frequently observed in organic compounds. Many functional groups that have hydrogen bonding capabilities are to be found in this region. This area of hydrogen bonding represents a change from the almost covalent nature of the bonding involved in the very strong hydrogen bonds, towards the electrostatic character that is typical of hydrogen bonding systems. These systems are also known to be most common for

undergoing hydrogen transfer between donor and acceptor compounds and have been widely studied^{62,63}. For example Schmidtman *et al.* studied hydrogen transfer in pentachlorophenol – dimethylpyridine (lutidine) complexes⁶⁴. By matching the pK_a of these compounds they could examine how a change in which lutidine isomer was used would affect the hydrogen atom position, since even though the lutidine isomers are from the same family, their pK_as are not identical.

Weak hydrogen bonds are numerous throughout most crystal structures but are not widely studied due to the presence of stronger interactions, which are common in many crystal structures. The strongest of these bonds such as O-H... π , are electrostatic in nature and have energies that are comparable to a bond such as O-H...O-H. The energy of these interactions typically lies in the 2-4 kcal mol⁻¹ range. This is in contrast to the weakest of the interactions containing C-H donors, which are barely stronger than dipole-dipole interactions or dispersion forces⁶⁰.

Hydrogen bonds are long range and directional interactions and because of this a group X – H can be bonded to more than one acceptor at the same time. In a situation where there are two acceptors, A₁ and A₂, this is called a bifurcated hydrogen bond (Figure 1.6.1).



Figure 1.6.1 a and b: An example of a bifurcated hydrogen bond donor and acceptor

The term bifurcated can also be used to describe the action of an acceptor molecule. This has mainly been observed for systems containing weak hydrogen bonds or in organometallic compounds. This is because organometallic systems can be donor rich when weak donors are taken into account and in these circumstances bifurcated acceptors can occur frequently depending on the ligands surrounding the metal centre. This is not a new discovery and in fact can be found to exist in important compounds such as glycine⁶⁵, while a study of tetrachlorohydroquinone also discovered bifurcated

hydrogen bonding⁶⁶. The three angles associated with a bifurcated hydrogen bond can also be used to give an example of the environment of the hydrogen. That is to say that if the three angles add up to 360° , the hydrogen will lie in the plane of the hydrogen bonds, however the smaller the angle becomes the more raised above the plane the hydrogen atom becomes. In the literature it is often noted that a bifurcated hydrogen bond is written as $X-H \cdots A_1(A_2)$ ⁶⁰. This is due to the presence of a dominant hydrogen bond and in many cases the weaker bond will be ignored. It is very rarely, if at all, seen that the hydrogen atom will lie equidistant from both acceptor atoms. The dominant interaction will always have the shorter bond distance and the angle associated will lie closer to 180° . This will become apparent in the co-crystallisation work carried out in Chapter 7 with bromanilic acid.

1.7: Crystal engineering and the importance of halogen bonding

Hydrogen bonding has always been recognised as the strongest intermolecular interaction due to its directionality resulting in strong crystal networks. In this regard conventional strong hydrogen bonds such as $O-H \cdots O$ and $N-H \cdots O$ can form a predictable network of interactions and are routinely used in terms of crystal engineering building blocks. These interactions are not the only ones currently being studied in terms of crystal engineering and there are currently a lot of investigations into trying to use weaker interactions such as $X \cdots O$, $X \cdots N$ and even $X \cdots X$ where X represents a halogen atom. These interactions are considered to be similar in strengths to moderate hydrogen bonds, with energies in the region of $4-15 \text{ kcal mol}^{-1}$.

It is known that the halogens Cl, Br and I form short non-bonded interactions in crystal structures⁶⁰. These close contacts between halogens are deemed to be potentially significant in stabilising a structure based on the distance between them being less than the sum of their respective van der Waals radii. These contacts are also of high importance in crystal engineering as they form the basis of the “ 4\AA chloro rule” described by Schmidt for planar dichloroaromatic compounds⁶⁷. This rule in itself is however questionable and the nature of the interactions is the cause for some debate. Price *et al*⁶⁸ believe that these short contacts are the result of anisotropy, whereas Desiraju⁶⁹ believes that there are special attractive forces present

between halogen atoms in the crystal lattice. Atomic polarisation is an important factor as this induces directional interactions formed by the halogens with O and N atoms and has been studied in terms of crystal engineering⁷⁰. Halogens can give rise to a variety of interactions depending on their size and environment where it is most likely that fluorine and chlorine atoms will interact mainly in terms of C – H- - - X and less in terms of X- - - X, while bromine and iodine atoms tends towards X- - - O interactions⁶⁰. This is likely to be due to the increased polarisability of the heavier halogen atoms giving more directionality.

Whilst halogen bonds, X- - - O, N, have been found to exhibit orientation preferences this is not true for halogen – halogen interactions. It is recognised that halogen bonding may be strong enough to be of prime importance in the arrangement of molecules in a crystal lattice, however this is certainly not true of halogen – halogen interactions. Nyburg and Faerman⁷¹ found the sum of van der Waals radii of the halogens varies as a function of the direction of the interaction, i.e. head-on or side-on. The values are noticeably higher in the side-on position indicating the importance of anisotropy of the electron density of the atom. Halogen bonding has been studied with regards to four *p*-phenyl-substituted *cis*-9,10-diphenyl-9,10-dihydroanthracene-9,10-diols, with the para substituent being either chloro, bromo, iodo or methyl substituted⁷². This study showed that the O-H- - - O hydrogen bond was present throughout, however the methyl substituted compound was found to crystallise in the monoclinic P2₁/c space group whereas the other three halogen containing compounds were discovered to crystallise in the P-1 space group each containing competing halogen – halogen interactions. This also provides further evidence against the existence of a chloro-methyl exchange rule.

Christer Aakeröy *et al.* have studied the effect of combining hydrogen bonding and halogen bonding interactions in terms of developing supramolecular strategies to generate target molecules. This was done *via* a series of co-crystallisation experiments between a molecule containing two sites with possibilities of hydrogen or halogen bonding and a secondary molecule containing a weak and a strong hydrogen bond donor and a potential halogen bond donor, where bromo, chloro and iodo substitutions were all attempted in this secondary molecule⁷³. These co-crystal studies proved that the strong hydrogen bond interactions, in this case oxime dimers,

are always formed. Only in the iodine-containing secondary molecule was a halogen bond formed, for the chloro and bromo substituted molecules the weak hydrogen bond was formed (figure 1.7.1).

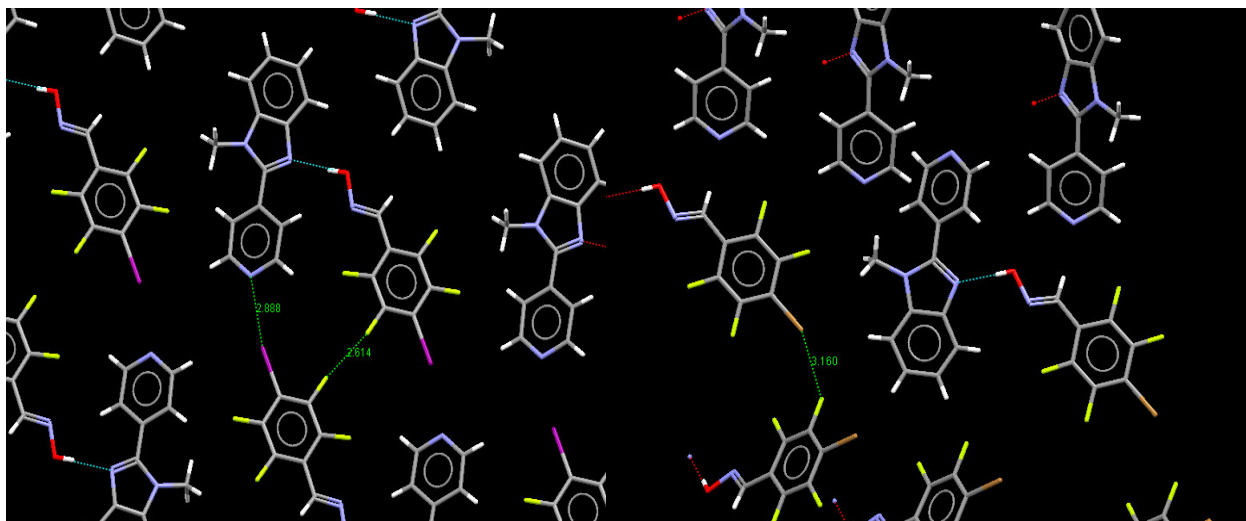


Figure 1.7.1 a and b: The crystal structures of the iodo and bromo substituted co-crystal compounds studied by Aakeröy⁷³.

Figure 1.7.1 a shows the I - - N halogen bond formed alongside the F - - F halogen – halogen interactions. In the bromo substituted analogue only Br - - F halogen – halogen interactions are found to exist, these link the molecules in three dimensions.

Further work has, however, led to the successful generation of halogen bonds to supplement the presence of strong hydrogen bonds in co-crystal compounds⁷⁴.

1.8: Co-crystallisations

Co-crystallisations are becoming more widely used with regards to trying to develop complexes with specific physical properties, and there is a large market for this in the pharmaceutical industry in particular. An example of this is where a co-crystal can be formed to encourage the formulation of an active pharmaceutical ingredient in a form that will be taken up in the body, for example with favourable solubility properties. In crystallography terms the terminology surrounding co-crystals can still be slightly

contentious, especially with regards to co-crystals involving hydrogen transfer where these may be more accurately referred to as salts. Co-crystals are commonly described as ‘structurally homogeneous crystalline materials that contain two or more neutral building blocks’⁷⁵. This definition however can lead to ambiguity as any co-crystal that shows hydrogen transfer should be described as a salt. Problems can then arise if studying the hydrogen transfer as a function of temperature as the hydrogen atom has sometimes been shown to migrate towards an acceptor atom as a function of temperature, meaning originally the two were neutral, however as temperature has changed this is no longer the case. During the work presented here, these will be referred to as co-crystals to remove any ambiguity with regards to situations where hydrogen transfer occurs and others where hydrogen transfer does not occur.

Co-crystals are often produced in an attempt to generate a specific interaction and to determine how reliable such an interaction is in a family of related molecules. The production of such an interaction may not ultimately be successful, however it is still important to try and determine which interactions occur and are therefore more dominant. A lot of this chemistry is however trial and error with regards to crystal engineering, however there is more progress being noted in this field also. A crystal engineering approach was recently undertaken with caffeine to attempt to produce a co-crystal that is stable at high relative humidities⁷⁶. Caffeine was co-crystallised with a series of dicarboxylic acids and a predicted intermolecular hydrogen bond motif was produced.

Chapter 2: Theory

2.1 Crystallography

Crystallography is the best way of obtaining detailed atomic structural information from a well ordered solid material. This allows analysis of crystalline solids most commonly by use of X-ray or neutron diffraction. These techniques allow the examination of a wide range of materials and provide precise information about the location of atoms in the structure. X-ray diffraction is the most commonly used and is the most widely available especially in terms of in-house equipment. Neutron diffraction is less widely used due to the specialised sources and equipment required and this tends to involve significant cost and time at specialised central facilities such as ISIS, RAL, Oxfordshire, UK or the ILL (Institut Laue Langevin) facility in Grenoble, France. It should also be noted that high intensity X-rays are also available at central facilities, at synchrotron radiation sources such as the Diamond Light Source in Oxfordshire, and previous to that at SRS, Daresbury Laboratory. The high intensity of these synchrotron sources allow the study of very small or weakly scattering samples, for example, that are not amenable to study in the home laboratory.

X-ray and neutron diffraction are very different to each other because of the different mechanism by which they interact with the crystal. X-rays are electromagnetic radiation and interact with the electron clouds of atoms *via* an electrostatic interaction, whereas neutrons interact with the nuclei of atoms via the strong nuclear force. The X-ray scattering factors increase strongly with atomic number ($\sim Z$, with intensities varying as Z^2), whereas the neutron scattering length shows a fairly random trend of value with increasing atomic number; there is a very slight tendency to increase with Z , but there is a large amount of fluctuation in the absolute values. For this reason neutron diffraction is highly important with regards to finding precise hydrogen atom positions as these can often be poorly resolved, or hidden by the presence of heavier atoms when studying by X-ray diffraction especially in the presence of many heavy atoms.

The hydrogen atom position found *via* X-rays is also generally not accurate, with shortened bond distances due to the electron (from which the X-rays scatter) being pulled into the covalent bond. For this reason it is recognised when considering hydrogen bonds then it is best to use donor – acceptor distances from X-ray determinations rather than distances from the calculated hydrogen atom position. This is not the case in neutron experiments where the nuclear position is found and due to the scattering length of hydrogen being negative for neutrons, hydrogen atoms appear as a very distinctive trough in a difference Fourier map rather than the usual peaks. Neutrons also travel much further through crystals than X-rays probing far more of the material, due to only weak interactions with matter. However, this, combined with the fact that the sources have a low flux, means that larger crystals are required to be generated before neutron diffraction can be carried out. Both single crystal techniques make use of the same fundamentals of diffraction theory, however there are advantages and disadvantages for the use of either.

Single crystal crystallographic techniques are employed to determine details of the molecular and crystal structure of the solid – bond lengths, bond angles, intermolecular interactions – and are the source of some of the most precise data on these structural features.

X-ray diffraction is a technique routinely carried out in-house making it a reasonably accessible source for crystal structure determination. It should also be stated that both neutron and X-rays have powder diffraction capabilities and whilst X-ray powder diffraction is still routinely used for sample identification purposes there are now emerging examples of crystal structure determination from powder diffraction alone⁷⁷. This has been made possible due to high resolution powder data being available and also the substantial progress in the programs available for solving structures from powder data.

2.2: Diffraction Theory

Much of the theory that is fundamental to crystallography and solving crystal structures was known well before it was trialled experimentally on a crystalline

material. The fundamentals rely on the theory of diffracted light and also the use of mathematical models describing the geometry of crystal lattices. This, coupled with the discovery of X-rays⁷⁸ enabled von Laue to demonstrate that crystals could diffract X-rays⁷⁹. The first structure solved was the structure of salt in 1913⁸⁰. From this the field of crystallography has grown and become a significant process in terms of chemistry, materials science and biology. Diffraction methods are often used not only with regards to crystal structure determination but also to distinguish between different polymorphs of the same material, examine the purity of a product and also to closely examine the bonding and interactions within a crystal structure.

2.2.1: The Unit Cell and Crystal Lattice

A crystal is built up of a basic pattern of points repeated in three dimensions; this is called the crystal lattice. A repeating motif can be placed onto each lattice point to build up the three dimensional structure by translation, which occurs whether there are any other forms of symmetry or not. If each repeating molecule is represented by a single point, the result of this translation will show a regular array of points, which indicate the repeating motif. This array of points is the lattice.

Defining the repeating geometry of the structure, the unit enclosed by lattice points that is repeated by translation to produce the crystal is called the unit cell, where the unit cell usually contains the equivalent of one lattice point (though this can be more). The unit cell can contain either one molecule, or a combination of many molecules. In three-dimensions, each unit cell has a shape size defined by six parameters; lengths a , b and c and angles α , β and γ (Figure 2.2.1.1).

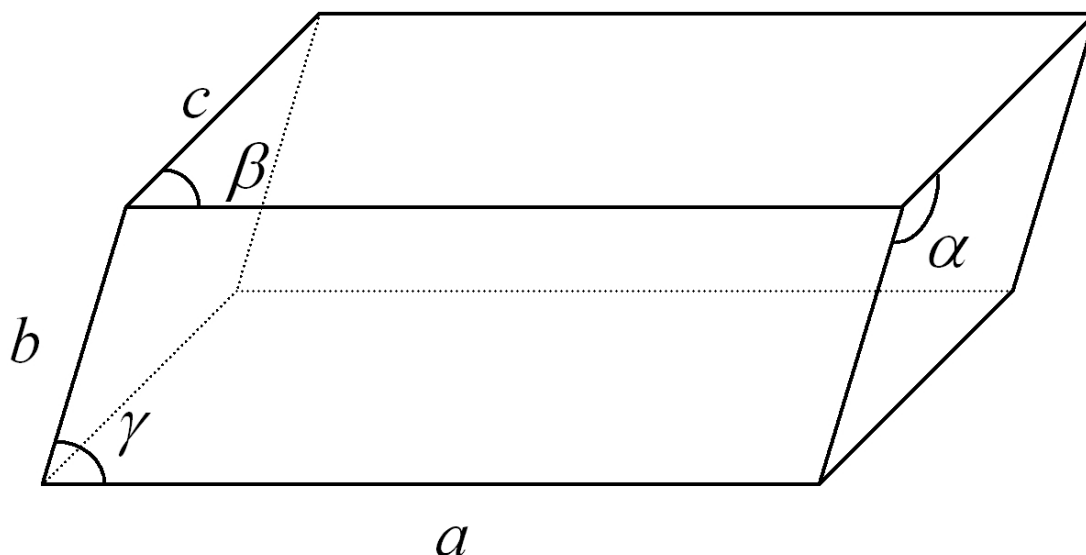


Figure 2.2.1.1: A three dimensional unit cell.

Rotation and reflection symmetry impose restrictions on the unit cell parameters and while every three-dimensional lattice has inversion symmetry, the restrictions applied result in crystal systems being divided into seven types (Table 2.2.1.2). In addition to these seven crystal systems, the presence of different numbers of lattice points inside the unit cell (called cell centrings) generates the Bravais lattices, and internal symmetry elements present within the unit cell lead to the definition of the space group defining the overall symmetry of the crystal contents, which is dependent on the crystal system. The crystal system adopted by a crystal does limit the number of space groups available.

Crystal System	Unit Cell Restrictions	Unit Cell Types
Triclinic	No restrictions	P
Monoclinic	$\alpha = \gamma = 90^\circ, \beta \neq 90^\circ$	P, C
Orthorhombic	$\alpha = \beta = \gamma = 90^\circ$	P, C, I, F
Tetragonal	$a = b, \alpha = \beta = \gamma = 90^\circ$	P, I
Trigonal	$a = b, \alpha = \beta = 90^\circ, \gamma = 120^\circ$	R
Hexagonal	$a = b, \alpha = \beta = 90^\circ, \gamma = 120^\circ$	P
Cubic	$a = b = c, \alpha = \beta = \gamma = 90^\circ$	P, I, F

P = primitive, C = centred, I = body – centred, F = face-centred, R = rhombohedral

Table 2.2.1.2: Unit cell types with associated unit cell requirements and possible Bravais lattices.

A primitive unit cell contains lattice points only at all 8 corners and all of these are equivalent, however centred cells are sometimes used, generating a larger cell which contains more than one lattice point. When lattices are described in this manner the six primitive lattices must be combined with eight centred lattices and this generates the 14 Bravais lattices. The asymmetric unit is the most basic repeating unit, which relates molecules in one unit cell to each other. This is only usually a small part of the unit cell and when the symmetry operations are carried out on the asymmetric unit the unit cell contents can be defined and thus the entire crystal can be generated. Adding the symmetry elements to the possible lattices leads to a total of 230 unique space groups into which every regular structure must belong. The space group is the collection of all symmetry elements for an infinitely repeating pattern.

Molecules can undergo rotation symmetry in crystals, however only certain rotations are permitted in the crystal system, these are C_2 , C_3 , C_4 and C_6 . Other symmetry elements can be observed in crystals by combining translation symmetry with rotation or reflection to generate screw axes and glide planes. In a simple two-dimensional example of glide plane symmetry, this would include a reflection and a displacement of half the repeating unit pattern. A screw axis involves a rotation followed by translation along the direction of the axis.

Systematic absences arise when glide planes and screw axes cause particular subsets of reflections to have zero intensity, due to patterns of destructive interference of X-rays that are completely out of phase because of the unit cell symmetry, leading to no scattering being observed. These are distinct for the various space groups. For example the space group $P2_1/n$ produces a unique set of systematic absences in its diffraction pattern. The screw axis, parallel to the b axis causes reflections $0k0$ to be absent when k is odd. The glide plane, perpendicular to the b axis, and with its glide plane direction along the ac face diagonal, causes reflections $h0l$ to be absent when $h+l$ is odd.

2.2.2: Miller Indices

When the atoms present in a crystal diffract X-rays, a series of spots with defined positions and intensities are produced and these relate to the symmetry and specific

atoms present in the crystal. This is to say that a bromine atom would scatter X-rays with a greater intensity than that of carbon for example due to the extra electrons possessed by the bromine atom. The planes which give rise to these observed reflections are called lattice planes and their orientation may be defined by Miller indices h , k and l . The unit cell is bound by the (100), (010) and (001) planes and the Miller indices are defined by their intercept with the a , b and c axes respectively. A simple example of this would be to examine the intercepts halfway along each axis. The Miller indices would thus be described as $a/2$, $b/2$, $c/2 = a/h$, b/k , c/l and thus describing the (2 2 2) plane (Figure 2.2.2.1).

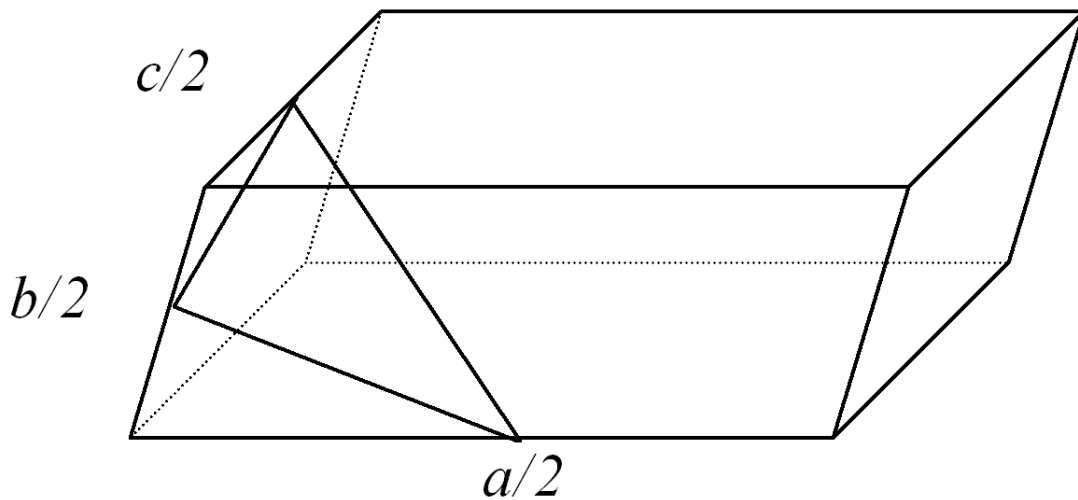


Figure 2.2.2.1: Miller indices showing the (222) plane.

These Miller indices then correspond to a reciprocal lattice point in the diffraction pattern.

2.2.3: Bragg's Law

A diffraction spot of measurable intensity is only generated when the diffracted beams from a series of parallel planes are in phase and give constructive interference (Figure 2.2.3.1). For this to happen, the path difference between these two diffracted beams must be equal to an integral number of wavelengths.

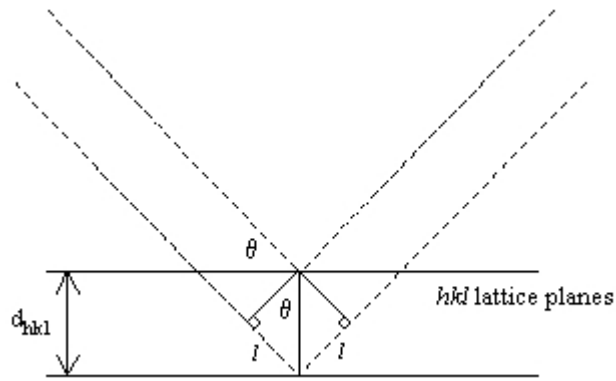


Figure 2.2.3.1: Bragg's law.

This leads to Bragg's Law:

$$\text{Equation 2.1: } n\lambda = 2d \sin\theta$$

In Bragg's law, n is an integer, λ is the wavelength of the incident and diffracted beam, d is the spacing between the planes in the crystal and θ is the scattering angle.

2.2.4: The Ewald Sphere

The analysis of X-ray diffraction patterns can be aided by the use of the Ewald sphere. This is centred on the crystal (C) and a circle with radius $1/\lambda$ is drawn around it such that its edge sits on the origin of the reciprocal lattice. From Bragg's law a reflection is superimposed and the reflected beam cuts the sphere at point P. Figure 2.2.4.1 indicates that a diffraction spot will be observed if the scattering vector is equal in length and in the same direction as the reciprocal lattice vector QP. Thus to satisfy Bragg's law the reciprocal lattice point must touch the surface of the Ewald sphere.

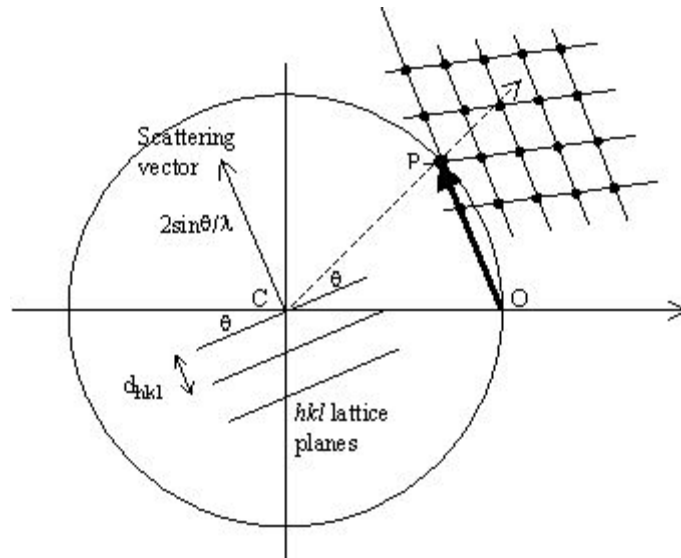


Figure 2.2.4.1: The construction of an Ewald sphere.

Figure 2.2.4.1 shows a simplistic two-dimensional view of an Ewald sphere with parallel planes representing Bragg's law and layers of diffraction. From this it can be seen that Bragg's law is only adhered to if scattering from the next layer produces a diffracted beam in phase with the one shown and a reciprocal lattice point located on the surface of the sphere.

2.3: Structure Determination

2.3.1: Diffraction patterns and Structural Information

The experimental diffraction pattern collected for a crystal structure allows determination of the unit cell parameters, the space group and the intensity data related to each individual diffraction spot, which each have their unique Miller indices corresponding to their positions. Each individual diffraction spot of intensity $I(hkl)$ has a related structure factor, F_{hkl}^o , where $I \propto |F_{hkl}^o|^2$, which results in the phase problem. These are converted via a Fourier transformation into the observed scattering density, the problem in carrying out this transformation being that initially there is no phase information available in the observed structure factors. Each Fourier component, the structure factors F_{hkl}^o , can have a different value, which depends on

the internal atomic structure of the unit cell. The structure factor can thus be written in terms of scattering from individual atoms making up the crystal structure:

$$\text{Equation 2.2: } F_{hkl}^0 = \sum f_j \exp [2\pi i(hx_j + ky_j + lz_j)]$$

where the summation is over j atoms in the unit cell at coordinates (x_j, y_j, z_j) . The scattering of each atom in the cell is given by the atomic scattering factor f_j .

There are several factors that can affect the structure factor including the temperature factor as indicated by the Debye-Waller effect. This describes the fact that as each atom is not in a fixed position and vibrates around their equilibrium position that the structure factor will be reduced as a factor of temperature and this affects each atom individually. This amount will depend on the local environment in which the atom sits within the structure. This will be reflected in the scattering factor f_j indicated in equation 2.2.

The Fourier transformation relating the scattering density to the observed structure factors can be expressed as:

$$\text{Equation 2.3: } \rho(x,y,z) = (1/V) \sum F_{hkl} \exp[-2\pi i(hx + ky + lz)]$$

where (x,y,z) represent the fractional coordinates in the unit cell. It is the interpretation of this scattering density, which enables atoms to be identified in the crystal structure. This summation is carried out over all values of h, k and l and therefore all reflections in the diffraction pattern contribute towards it.

The Debye-Waller effect reduces the scattering factor as it leads to a reduction in intensity due to smearing of the electron density as a function of thermal motion. This leads to a reduction of the structure factor by:

$$\text{Equation 2.4: } (F_{hkl}^0)_T \sim \exp[-BT_j(\sin^2\theta/\lambda^2)] F_{hkl}$$

where each atom has a separate temperature factor B_j . $B=8\pi^2U$, where U represents the thermal parameters. This is accounted for in modern refinement programs where

the refinement is carried out allowing the average amplitudes of vibration for each atom in the structure to vary independently, and in fact these are usually allowed to adopt non-spherical vibrations, undertaking anisotropic thermal vibrations. From equation 2.4 it can also be seen that those reflections at smaller Bragg angles will be less affected than those at larger Bragg angles.

The atomic form factor reflects the strength of scattering of an individual atom (for X-rays this is proportional to the number of electrons), and also how rapidly the intensity of reflections decrease with increasing diffraction angle. Figure 2.3.1.1 indicates how rapidly this occurs for hydrogen and carbon atoms. Also shown in this figure is the fact that this form factor fall-off does not occur for neutron scattering.

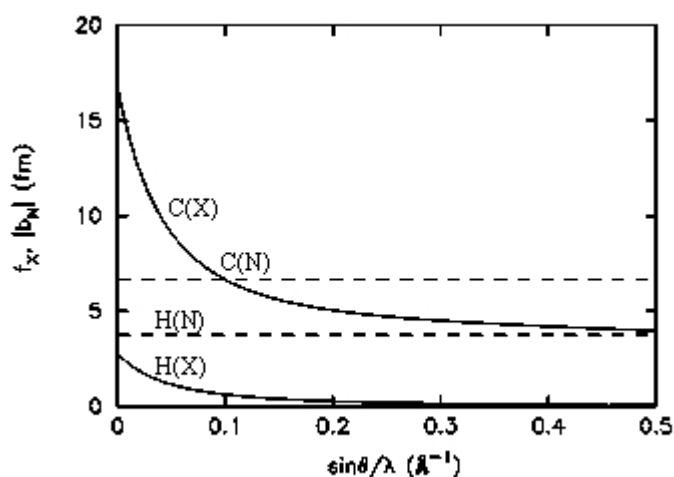


Figure 2.3.1.1: Atomic form factor drop off with increasing angle for X-ray form factors (and absence of fall-off for neutron scattering lengths).

2.3.2: The Phase Problem

To be able to solve a crystal structure it is necessary to know the intensity, $I \propto |F_{hkl}^o|^2$, and the phase of the individual reflections, however the structure factor can only be determined from the observed scattering intensity, thus the phase information is lost. The structure factor 2 can be expressed as:

$$\text{Equation 2.5: } F_{hkl}^o = |F_{hkl}^o| \exp(i\alpha_{hkl})$$

where $|F_{hkl}|$ represents square-root of the measured intensity and α_{hkl} is the phase. The phase information is not collected experimentally however so only the magnitude is known. This means that a simple Fourier transform will not generate the electron density and this is referred to as the phase problem. There are now several methods for solving this phase problem and the most commonly used include: direct methods, the Patterson method and heavy atom methods.

2.3.3: Direct Methods

Direct methods is the most commonly used method for solving the phase problem and is incorporated in most structure solution programs. These can examine the relationships between the intensities of the reflections and lead directly to solving the phase problem. The mathematical constraints used for direct methods are based on fundamental features of electron density, that the integrated electron density must be positive and finite, as defined by Sayre. The methods currently employed can be directly related to the work of Karle and Hauptman who received the Nobel Prize for Chemistry in 1985. This is based on the triplet relationship which relates the values of the three phases of reflections involved in the triplet for example if the intensities of three reflections such as (3 2 1), (-2 -1 0) and (-1 -1 -1), where the sum of the indices within the triplet are (0 0 0), are all strong, then it is probable that the sum of their phases will be close to zero. Many of these probabilistic relationships can be set up in a diffraction data set and the method performs many trials to generate the best set of estimated phases producing a model with the best figure of merit, which subsequently can be used to determine atomic positions from the calculated electron density map. This technique is known to have a high success rate for small – medium sized organic compounds.

2.3.4: The Patterson Method

The Patterson method avoids the phase problem by making use of the known intensities. The Patterson method generates a map of interatomic vectors (u, v, w) via $|F_{hkl}^o|^2$ values.

Equation 2.6: $P_{uvw} = 1/V \sum |F_{hkl}^o|^2 \cdot \cos[2\pi(hu + kv + lw)]$

The origin of the cell (000) will always have the highest peak as every atom will be mapped onto itself. The Patterson function is a map of vectors between pairs of atoms in the structure. Therefore for every peak seen in the Patterson map (u, v, w), there must be two atoms in the structure whose x coordinates differ by u, y coordinates differ by v and z coordinates differ by w. These Patterson peaks show where the atoms lie with respect to each other but not with regards to the unit cell origin, which is essentially what we are most interested in.

When an organic molecule containing many of the same atoms is mapped *via* Patterson methods the resulting map will be hard to interpret due to the presence of many overlapping vectors, however when dealing with structures containing heavy atoms these vectors will be strong and the separations of two lighter atoms will give much smaller peaks. Using the phases calculated from the heavy atoms positions now determined, a subsequent Fourier synthesis should determine the positions of the lighter atoms.

2.3.5: Heavy Atom Method

The heavy atom method as suggested relies on the presence of one or more heavy atoms being present in the unit cell. These heavy atoms can be found *via* a map of the interatomic vectors and from this position a set of phases can be produced. This can then be built up to generate phase information for the whole structure. The heavy atoms present need to scatter with a significant difference in scattering power from the rest of the atoms for this method to succeed. If such an atom is present the phases can be deduced from this atom and a build up of phases for the structure can be generated until such stage that a Fourier map will be able to determine the positions of the remaining atoms.

2.4: Structure Refinement

The aim of a structure refinement is to generate calculated structure factors that best fit the observed structure factors. It is possible to map the measured reflection intensities by value of an electron density map, also known as a Fourier map.

$$\text{Equation 2.7: } \rho(x,y,z) = \sum |F_{hkl}^o| \exp(-2\pi i(hx + ky + lz) + \alpha_{hkl}^c)$$

With each Fourier map produced a better model of the structure is produced and this improves the phase information to be used in the next cycle of Fourier calculations. This creates a cycle that ultimately closes in on the most accurate crystal structure available from the measured diffraction intensities.

The positions of the atoms are known to be the peaks on the Fourier map, however to model the structure correctly a description of the atoms has to be refined to give a model that best fits the observed data. Varying the positional and thermal parameters for each atom using the least squares method gives the best structure refinement. Even for small molecule crystallography the number of parameters that can be varied is high so during the least squares refinement an R factor is used to rate how good the structure model is.

$$\text{Equation 2.8: } R = \frac{\sum |F_o| - |F_c|}{\sum |F_o|}$$

$$\text{Equation 2.9: } wR2 = \sqrt{\frac{\sum w(F_o^2 - F_c^2)^2}{\sum w(F_o^2)^2}}$$

The R-factor is used to assess the agreement between the measured amplitudes and those calculated from atomic positions during refinement. If the model and the structure are identical the R-factor would be zero, however this is unlikely to occur as there are always errors present throughout data collection and analysis. The lower the R-factor the better and ideally the R-factor would be between 0.02 and 0.08 for publication of small molecule structures. The weighted R-factor (wR) works in the same way but is based on the squared structure factor values where each structure factor has its own weighting factor. A better model results in a better R-factor, with

the improving phase information generating better Fourier maps and thus generating a better model for refinement.

Another important value for evaluating the structure quality is the goodness of fit, S .

$$\text{Equation 2.10: } S = \sqrt{\frac{\sum (w(F^o_{hkl}{}^2 - F^c_{hkl}{}^2))}{n - p}}$$

In terms of refinement, the more successfully collected reflections the better the data set providing better information to refine the structure. The more parameters that are refined the more data is required – typically data/parameter ratios of greater than 10 should be sought. The value for the goodness of fit for a good data set should be roughly 1 though can be marginally below or above.

Chapter 3: Techniques and Instrumentation

3.1: Focussed Beam Reflectance Measurements and Attenuated Total Reflectance Ultra Violet

There has been significant development in *in-situ* techniques that do not require sampling and give real time data analysis such as Attenuated Total Reflectance – Ultra Violet (ATR-UV), Focussed Beam Reflectance Measurements (FBRM) and Attenuated Total Reflectance – Fourier Transform Infrared (ATR-FTIR). The theory of attenuated total reflectance is based on light passing from a material of high refractive index, for example a crystal, to a material of lower refractive index, for example a solution. Light travels to the reflection surface and can be partially absorbed by the solute before being reflected back to the probe. The reflected light is therefore attenuated, causing a measurable reduction in the output signal dependent on the absorbance of the solution⁵⁴. Each probe has two fibre optic cables, one for transmission of the light from the light source to the measuring head of the immersion probe, while the second conducts the signal, which is the light that has passed through the sample and back to the spectrophotometer. ATR-UV probes are suitable for the direct measurement of strongly absorbing solutions in which the UV absorption of the solvent does not mask the solute absorption.

The main advantage of using an ATR-UV probe (Figure 3.1.1) for measuring solubility and crystallisation in solution is that no sampling is required and that this is a real time process. Other advantages are that the probe is relatively insensitive to the presence of particles in solution as the probe is based on surface measurements and the probe is suitable for an easy set up. However in deciding to use the ATR-UV probe it must also be considered whether the solute has a significant UV absorption compared to the solvent in which the process is carried out so that it can be measured in the presence of the solvent. The UV absorption of the solute is directly proportional to the concentration of the solution according to the Beer-Lambert law and so provides a convenient method for accurate *in-situ* real time measurement of solute concentration when compared to other techniques. This process comes into its

own during cooling crystallisation processes, enabling a significant solubility profile to be compiled from solubility to crystallisation.



Figure 3.1.1: The ATR-UV probe showing the clear crystal window through which all light passes.

ATR-UV can also be used in connection with Focussed Beam Reflectance Measurements (FBRM). FBRM uses a highly focussed laser beam projected through the sapphire window of the FBRM probe to rapidly scan over a small region. The beam is rotated at a fixed high velocity allowing rapid scans across particles flowing across the path of the beam. This high speed scanning movement of the beam is significant as this means that the motion of the particles is insignificant. A particle entering the beam path produces back scattered light, which is picked up by a stereoscopic system. The crystal continues to back-scatter light until the beam reaches the other edge of the crystal. The time period of back-scattering is recorded and multiplied by the scan speed of the beam to give the distance between one edge of the crystal and the other⁵³; this is known as the chord length. These chord lengths that are measured are profiled in a chord length distribution (CLD) plot.

The Mettler Toledo Multi Max system (Figure 3.1.2) installed in the solid state research laboratory in the Strathclyde Institute of Pharmacy and Biomedical Sciences (SIPBS) was used to carry out all experimental work using Attenuated Total

Reflectance – Ultra Violet (ATR-UV) and incorporating Focussed Beam Reflectance Measurements.

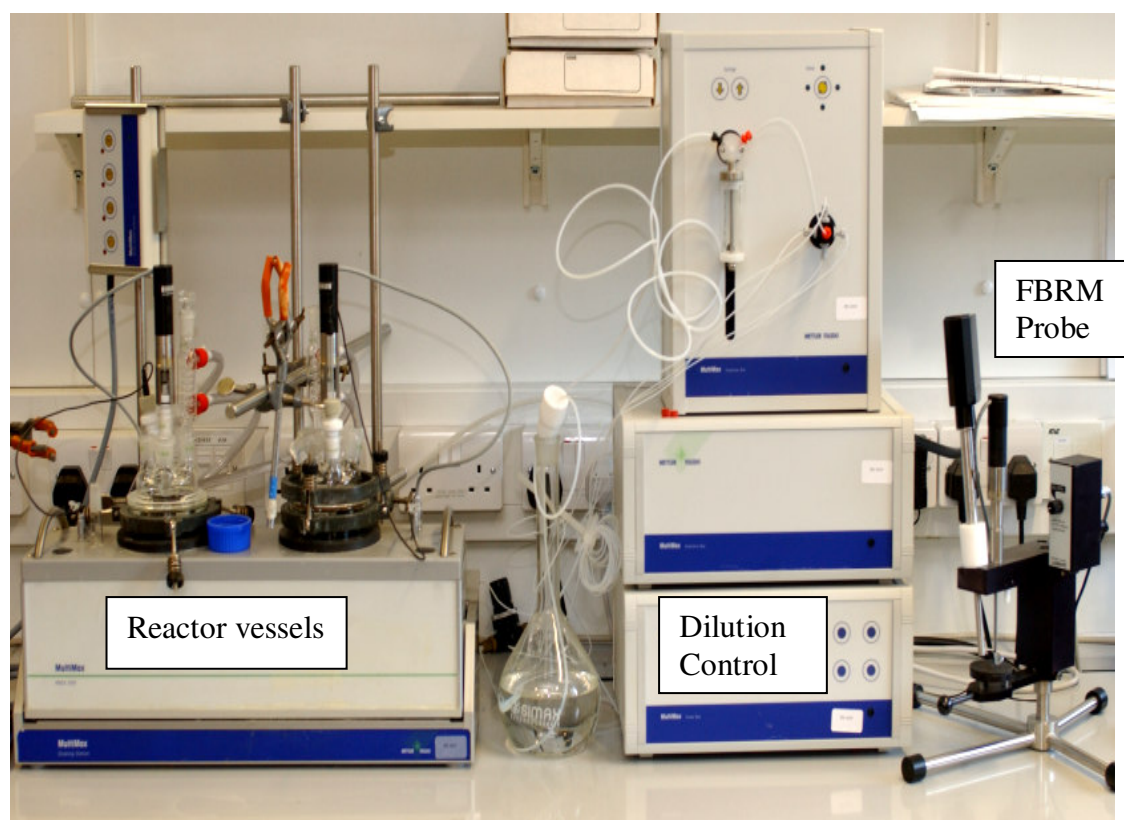


Figure 3.1.2: The Multi-Max system at SIPBS. This shows the reactor vessels in their independent compartments, the possibility for dilution and also the FBRM probe.

The Mettler Toledo Multi-Max system gives a great degree of control over the desired reaction conditions mainly involving the temperature of the reactor vessel and the rate at which the solution is stirred. The reactor vessels, by means of the control box, allow simultaneous reactions to be measured without adversely affecting either reaction, for example one reactor vessel could be heated whilst the other is being cooled and the reactor temperatures are maintained independently. By running the ATR-UV probe in parallel with the Multi-Max system, it is possible to see changes in UV absorbance as the reaction proceeds, with an accurate knowledge of the temperature at which any changes occur. This is required during calibration and subsequent dissolution methods.

This is achieved *via* an automated set up which enables the Multi-Max, ATR-UV and FBRM to be linked. The FBRM and ATR-UV measurements are all computer controlled and independent of each other, however the data can be extracted and comparisons can be made as a function of time, which leads to knowledge being generated about the crystallisation process under precise conditions. This enables experiments to be carried out *in-situ* and data collected while experiments are ongoing with no need for sampling. This is of course a huge advantage as with real time measurements and no sampling required, analysis can be carried out while experiments are in progress.

For each different part of the liquid studies that had to be carried out as part of the present work a distinct method had to be followed. The three distinct areas that have to be studied to develop a reliable metastable zone width include calibration, dissolution to produce the solubility curve, and finally the metastable zone width experiments themselves. The calibration procedure, carried out before any sample measurements are made, are the same for every compound and it is imperative that these are reliable. These calibrations are compound dependent as each compound has differing solubilities, and thus the range of the study has to incorporate this. Furthermore, different compounds have different melting points and this does play a part in determining the range of temperatures through which the experiments can be carried out. Calibration profiles rely upon a range of solutions being prepared and controllably ramped from the low T range to the high T range. At defined intervals, the temperature is kept steady and left to equilibrate for a period. This ensures that the absorbance is constant and therefore a specific concentration at each point is calculated. This is subsequently carried out for the full range of temperatures required.

Dissolution experiments are usually carried out on pharmaceutically important compounds to determine the rate of uptake into solution, however this is not required for the studies being carried out by us as chemists. The fundamental differences between the interests of pharmacologists and chemists is that pharmacologists are interested in how much can be dissolved into an aqueous medium and how quickly, thus adding of the solute is not carried out until the experiment is running. Whereas

from a chemistry viewpoint the important feature is the concentration, which is a measure of the amount of material dissolved at a certain point. For this reason, and because of the high solubility of the compounds selected, the solute was already present in the reactor vessel prior to the experiment commencing. Dissolution experiments rely on controlled heating to set temperatures and then leaving for long periods to ensure that full dissolution has occurred at each temperature. This is carried out at a series of temperatures and a full solubility curve can then be calculated.

Metastable zone width experiments are the only set of experiments that require all three components of the Multi-Max, ATR-UV and FBRM to be linked together. These experiments rely upon a solubility curve that is reliable and solutions are prepared according to this. The solutions prepared correspond to a specific point on the solubility curve and then controlled cooling is carried out while the FBRM monitors any changes that are occurring in solution. Recrystallisation is easily observed by the sudden increase in particles detected by the FBRM and the sharp decrease in UV absorbance. These experiments have to be repeated many times to ensure a reliable point for crystallisation under these conditions has been determined and for many different solutions lying on the solubility curve until a supersolubility curve can be generated and a metastable zone width defined.

3.2: Synchrotron Radiation

A synchrotron is a huge scientific machine designed to produce very intense beams of X-rays, infrared and ultraviolet light, called synchrotron light. Electrons generated in the electron gun are accelerated to very high speeds by the linear accelerator, the booster synchrotron and finally maintained at high speed in the storage ring. The storage ring (Figure 3.2.1) is made up of bending magnets, which are used to steer the electrons around the ring, and in 3rd generation synchrotrons, insertion devices that are more complicated arrays of magnets. As the electron beam encounters each magnet it is accelerated by changing direction and this results in the emission of radiation that can be channelled into each beamline in the form of light. Light generated by electrons in the storage ring passes into beamlines, where the experiments are carried out. Each beamline is optimised for a different kind of experiment, but each

beamline contains an optics hutch, where the light is filtered and focussed, and an experimental hutch, where the experiments are carried out. There is also a control hutch where the experiment is programmed.

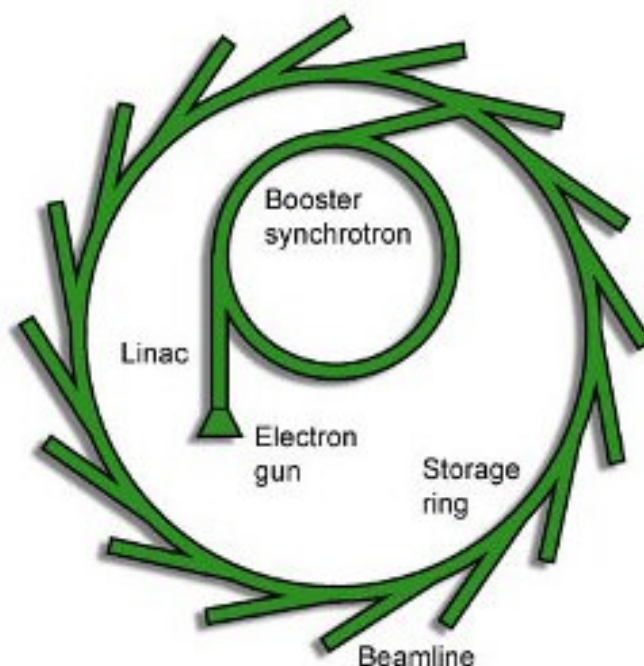


Figure 3.2.1: A schematic showing the process of how synchrotron radiation is generated.

The synchrotron radiation generated has many uses from chemistry and materials science to life science and earth science, showing the wide range of studies that can be carried out at synchrotron sources. The original synchrotron radiation source in the UK was the Synchrotron Radiation Source (SRS) at the Daresbury Laboratory. The SRS, at which the SAXS studies described here were carried out, operated from 1981 until 2008, when it was superseded by the development of the new 3rd generation Diamond Light Source synchrotron in Oxfordshire.

3.3: X-ray Diffraction Studies of Liquids – Synchrotron and Lab Based Sources

Station 2.1 at the SRS Daresbury Laboratory (Figure 3.3.1) was a fixed wavelength small angle X-ray scattering station. The station was widely used in the field of structural biology to obtain structural information relating to the shape and size of their compounds. The wavelength at station 2.1 was fixed at 1.54Å, with a variable

camera length between 1 and 8.25m. This enabled the user to examine a wide range of d-spacings.

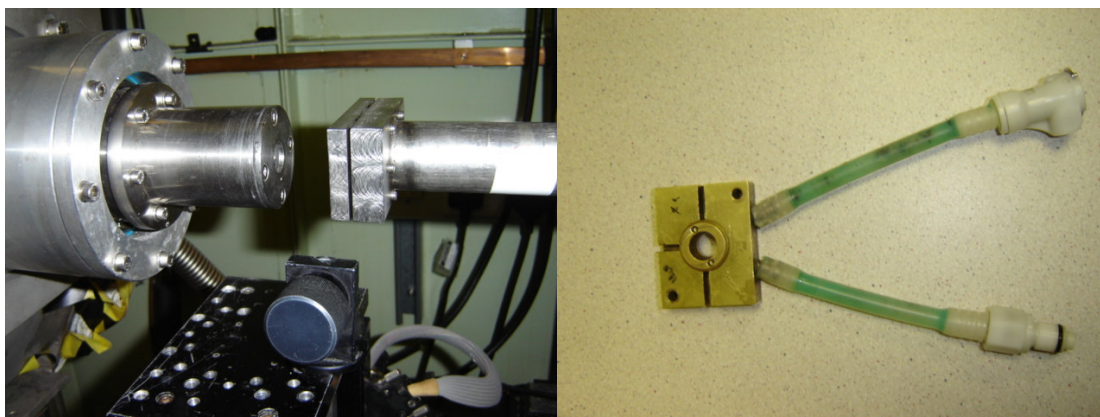


Figure 3.3.1 a and b: Station 2.1 at Daresbury showing the beamline (left) and the sample holder (right).

Before each experiment, the instrument has to be calibrated and the beam collimated and centred without a sample in place. The sample window is designed to be very narrow, and the camera length determines how much scattering is observed and the range of scattering angles accessible. In the experiments carried out during this work, liquid samples were used, in which it was hoped to induce nucleation/crystallisation assemblies that could be observed. Scattering from liquids is weak and therefore most scattering is observed on the detector in regions around the beam stop. The temperature control in the sample holder system used (Figure 3.3.1) was simple and experiments had to be paused in between temperature changes to enable heating or cooling to be carried out. As the mica window is in the vertical position, there is a potential problem as it cannot be reliably predicted where any crystallisation event will occur. It is thus difficult to ensure that this lies in the path of the beam and not around the sides of the sample holder where it will not be detected.

SAXS can also be carried out in the laboratory rather than at the synchrotron. Prof Tim Wess and his group in the Optometry school at Cardiff University have helped install and develop the Bruker AXS Nanostar small angle scattering system. This has enabled the highest flux beam that is currently possible for SAXS studies outwith synchrotron sources. The Bruker AXS Nanostar, with its intense, collimated primary

beam and 2-dimensional detector, has a similar design to a synchrotron SAXS beamline. The Nanostar features a strong X-ray source, which combined with multi-layer optics, provides an intense and narrow incident beam upon the sample. As mentioned in Chapter 1, SAXS yields information such as particle sizes and size distributions from dimensions of 1 to 100 nm, as well as shape and orientation distributions in liquid, powders and bulk samples. The Wess group routinely use such techniques for the study of collagen samples to examine the structure and probe the mechanical properties.

A further development in the instrumentation for studying liquids that was attempted in work related to this project is the Rigaku R-axis/Rapid Curved Image plate diffractometer, used as a WAXS instrument in this context. This contains a large curved image plate, which enables scattering to large angles to be measured in a single image.

Solutions for SAXS studies of crystallisation must be prepared in a clean place and filtered into sample vessels to avoid any possible contamination or undissolved particulate being found in solution. It is ideal to prepare as concentrated a solution as possible that will not recrystallise spontaneously in a sealed solution, or in contact with the droppers required to load the sample vessel.

3.4: General Approach to Crystallisations

There are almost endless ways in which crystallisation can occur as it is ultimately a random process and still nearly impossible to control fully due to the lack of knowledge about the early stages of crystallisation. In this sense, the approach to crystallisation that is taken is fairly simple. The main variables that are often changed include temperature, whether that be constant temperature or a temperature profile involving controlled heating and cooling regimes, or varying fractions of solute, this is true for both co-crystals and single component samples and solvents, where there is a huge library potentially available.

Recrystallisation can have two meanings in the study of chemistry. Firstly in the organic chemistry field recrystallisation is often incorporated in the purification and

synthesis of compounds. This involves rapid precipitation to improve yields and would not be routinely used by crystallographers. In a crystallographic sense where the object is to generate large single crystals the recrystallisation has to be carried out slowly *via* a variety of methods. The main methods used for crystal growth are solution methods. Recrystallisation from solvents is by far the most widely used *via* slow evaporation, however if the solution dries out crystals can become deformed and not single. Anti-solvents (solvents in which the molecule is not soluble) can also be used to help crystal growth as this reduces the solubility and can enable larger crystals to grow. A variety of methods exist for crystal growth from solution including: cooling from a hot, near saturated solution; convection which relies on the presence of a temperature gradient across the solution, and various diffusion techniques.

Following recrystallisation to produce a solid, often polycrystalline, sample, it is generally commonplace to obtain X-ray powder diffraction (XRPD). For a single component system this is generally to see if there has been any polymorphic transitions during the recrystallisation or solvent/hydrate formation depending on the conditions. Powder generation can occur naturally in the recrystallisations vial or can be produced from grinding of a single crystal. Grinding is known however to produce enough energy to initiate reactions that may not be desired, so must be employed with caution. Other techniques that are routinely used to ascertain whether any changes have occurred during a reaction include techniques such as infrared spectroscopy (IR), differential scanning calorimetry (DSC) and thermal gravimetric analysis (TGA). DSC and TGA can be used simultaneously to monitor energy and weight changes as the molecule is heated up towards the melting point, often this can show polymorphic changes occurring or whether a single phase is present throughout.

Often the use of single crystal diffraction is beneficial to allow structure determination and refinement. There are many novel ways to attempt to grow single crystals, from the traditional slow evaporation through to more modern machines such as the React Array Microvate used routinely throughout this work. This instrument allows twelve separate rows of independently temperature controlled conditions for crystallisation to be trialled simultaneously and with four individual vessels in each row this allows for up to 48 different experiments in twelve separate temperature conditions to be carried out simultaneously. These are small scale vessels, typically containing mg of

material, and can give results in a far shorter time period than slow evaporation techniques. The Microvate allows ramping and cooling profiles to be set up in each row and can lead to positive identification of the conditions that may lead to the best crystal growth. If a single crystal is grown successfully, it is necessary to examine its quality under the microscope to check whether it is single, more than one crystal or even whether there are deformations on the surface, prior to running the sample on the single crystal diffractometer for structure determination.

3.5: Laboratory Based X-Ray Single Crystal Diffraction

With X-ray diffraction having developed much in recent years it is now routine to solve crystal structures from crystals as small as 0.1mm x 0.1mm x 0.1mm, using laboratory based single crystal methods (Figure 3.5.1). Crystal selection is carried out using an optical microscope with cross polarisers used to determine the extinction of the crystal. A crystal with clean edges and faces is selected to ensure no cracks or defects are present on the crystal. When a suitable crystal has been selected it is necessary to mount it on a glass fibre and onto the pip of the goniometer before mounting on the diffractometer. The goniometer head is then attached onto the diffractometer, which has screws to adjust the alignment and ensure the crystal is central in the X-ray beam. This can be viewed using the built in microscope.

Diagram of a Typical Crystal Structure Analysis

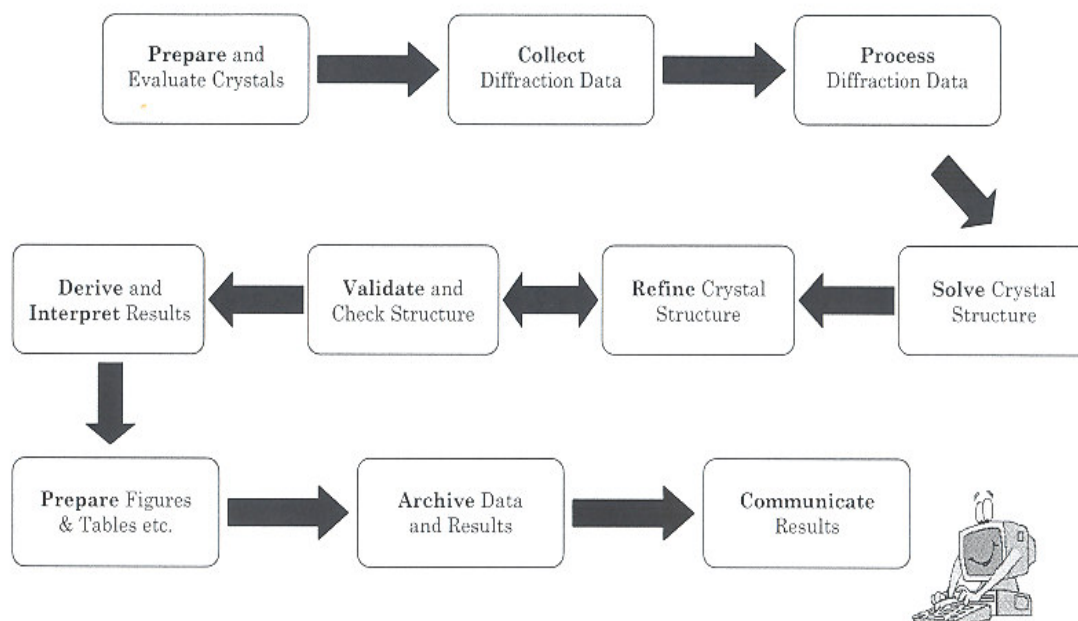


Figure 3.5.1: Chart of requirements prior to publishing crystal structures⁸¹.

The single crystal X-ray diffraction work carried out and reported here was carried out on a Bruker AXS Apex II single crystal CCD detector diffractometer and the structures solved and refined using either SIR⁸² incorporated in CRYSTALS⁸³ or SHELXS⁸⁴ and SHELXL⁸⁴ in the WinGX program⁸⁵.

These programmes, together with the Apex II software for data collection and processing⁸⁶, can be used for all single crystal structure determinations. The diffractometer software provides a quick and easy way to assess crystal quality and to set up the data collection. Incorporated in the instrument software, the primitive unit cell can be determined using a preliminary set of frames. The reflections in these frames are indexed to generate a primitive unit cell and crystal orientation, which can be done manually by selecting the sharpest, best-defined reflections with no sign of smearing or double spots, or automatically and then are refined. The orientation matrix is the solution which best indexes the observed peaks. At this point it is important not to overestimate the symmetry of the molecule or else not enough reflections may be collected to enable a full crystal structure determination.

Within the diffractometer software, a strategy can be determined to maximise the detection of unique reflections corresponding to the crystal system selected and ensure a complete dataset as far as it can be reasonably expected. For example, the more symmetry that is present in a crystal structure, the less crystal orientations have to be measured, less reciprocal space has to be explored, and thus the data collection will be shorter. This can be illustrated as in the absence of any symmetry (triclinic) a crystal would have to undergo an 180° rotation to collect all the reflections needed, and due to Friedel's law, this will result in a multiplicity of two. However if there is a four-fold axis of symmetry present in the crystal, then providing the correct 45° angle can be found, only a 45° rotation is required. A data collection strategy can last for a few hours to a day or longer depending on the size of the crystal, the strength of the diffraction and its symmetry. On completion of the data collection an *hkl* file is produced after integrating the data and introducing correction factors such as; absorption, extinction and Lorentz corrections. The *hkl* file is then input into either CRYSTALS⁸³ or WinGX⁸⁵ where the structure can be solved by direct methods, and refined.

It is also possible to carry out variable temperature single crystal data collection making use of the Oxford Cryosystems low temperature device installed in the diffractometer. This enables reliable temperature control to 100K in the laboratory and undertaking data collections every 50K between 100K and 300K is now commonplace to monitor any temperature-dependent effects, such as disorder, that may occur. For the study of disorder in hydrogen bonding systems, a common theme in the group, this can be used to give supporting evidence in terms of proposals for beamtime at a neutron source where the hydrogen atoms will be able to be located with less error. In the case where multiple temperature data sets are collected, the sample has to be re-centred for each data collection to account for any contraction or expansion of the sample during each run.

Chapter 4. Liquid Studies on Substituted Aromatic Molecules

4. Methyl 4-hydroxybenzoate

4.1: Introduction

Alkyl hydroxybenzoate compounds are used in foods, drugs and cosmetics as preservatives due to their antimicrobial properties. Methyl 4-hydroxybenzoate (pMHB; Figure 4.1.1) has also been well studied for many years due to its potential use as a nonlinear optical material⁸⁷. Lin Xianti *et al* first solved the crystal structure, using X-ray diffraction, and published it in 1983²¹. It was found to be monoclinic with the space group Cc, and unit cell dimensions of $a = 13.568(5) \text{ \AA}$, $b = 16.957(7) \text{ \AA}$, $c = 12.458(6) \text{ \AA}$ and $\beta = 130.10(3)^\circ$. Solubility and metastable zone width studies had also been carried out varying both pH and temperature⁸⁷. Presented here are the new approaches taken to monitor the solubility curve and then subsequently generate the metastable zone, for this reason it was imperative to have models for comparison. This also made use of techniques outlined previously for a different system⁵⁴. The aims were to monitor concentration changes *in situ* before further nucleation studies could be carried out.

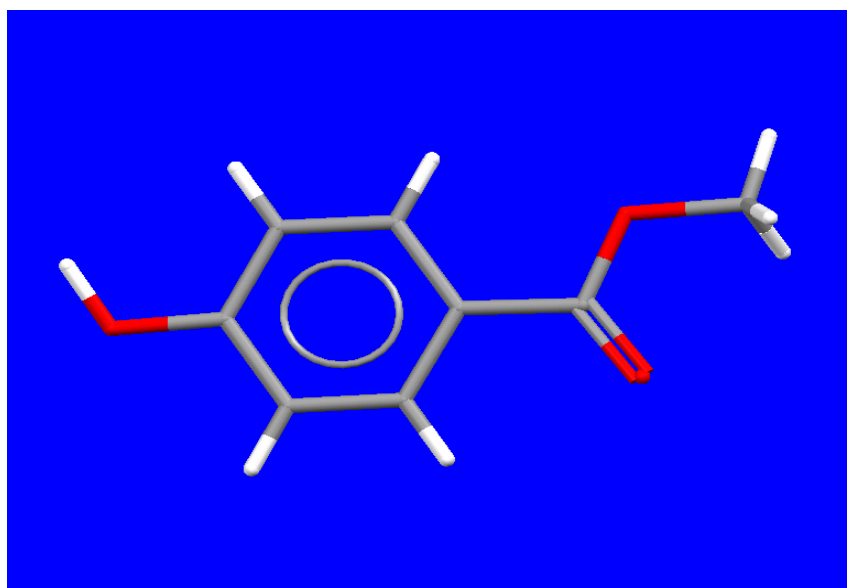


Figure 4.1.1: Methyl 4-hydroxybenzoate

4.2 Dissolution and Metastable Zone Width Studies.

Methyl-parahydroxybenzoate (pMHB) was selected as the initial compound to test and develop dissolution methods and to determine the metastable zone width (MZW). This work took place in the Department of Pharmaceutical Sciences in the Strathclyde Institute of Pharmacy and Biomedical Sciences at the University of Strathclyde where analysis of the pure compound was carried out. X-ray powder diffraction (XRPD) was used to identify the physical form before and after recrystallisation from methanol to ensure that this was a suitable solvent for our studies. The scan was carried out over a 4-40° 2 θ range at room temperature. Differential Scanning Calorimetry (DSC) was also carried out on samples of pMHB before and after recrystallisation to ensure that only one physical form was present. The DSC apparatus was programmed to cool to -40°C then heated past the melting point at 125-129°C before being crash cooled back to -40°C and heated back up to the melting point again. This is used to assess the stability of the compound even in the harshest of conditions and to ensure that rapid cooling would not cause transformations in the subsequent liquid studies. To assess the stability of the compound, a range of recrystallisations were carried out in a wide variety of solvents available in the solvent library at the University of Strathclyde solid-state laboratory. The recrystallised material was analysed by IR spectroscopy and XRPD to assess any changes that may have occurred from the raw material.

4.2.1 X-ray Powder Diffraction

Figure 4.2.1 shows the XRPD pattern collected from the bottle-fresh (pure) pMHB and the recrystallised form. All peaks are found to match and are aligned, thus the only slight changes between the two patterns are in the intensity of the peaks. This would indicate that either form would be able to be used in the solubility studies, which is necessary as pMHB is found to have very high solubility in methanol, which is to be used for the liquid studies.

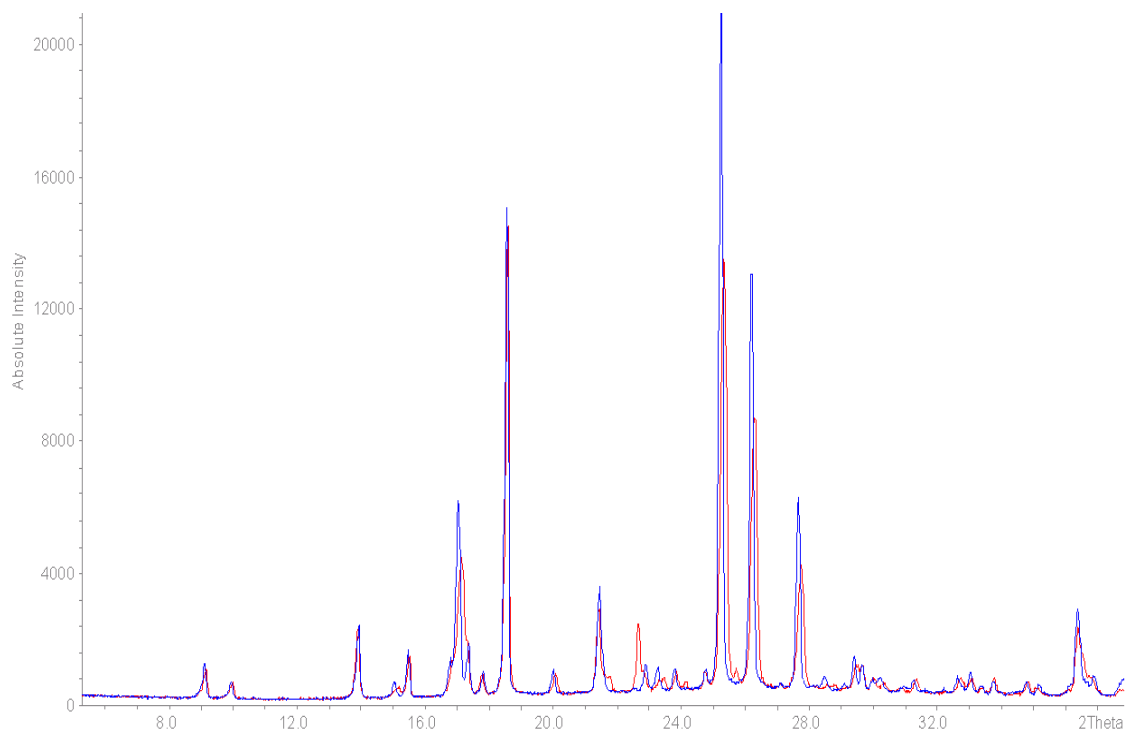


Figure 4.2.1: XRPD data from pure and recrystallised pMHB. The pure material is shown in black and the recrystallised in red.

4.2.2 Infrared Spectroscopy

Recrystallisations were carried out in a wide variety of solvents and analysed by IR spectroscopy to examine if there were any possible differences and potential polymorphs being produced. The IR data (Figure 4.2.2) shows an overlay between pMHB pure material (red) and a sample of pMHB recrystallised in methanol (blue). This shows that all peaks are present in both spectra and only the reflectance of these peaks varies.

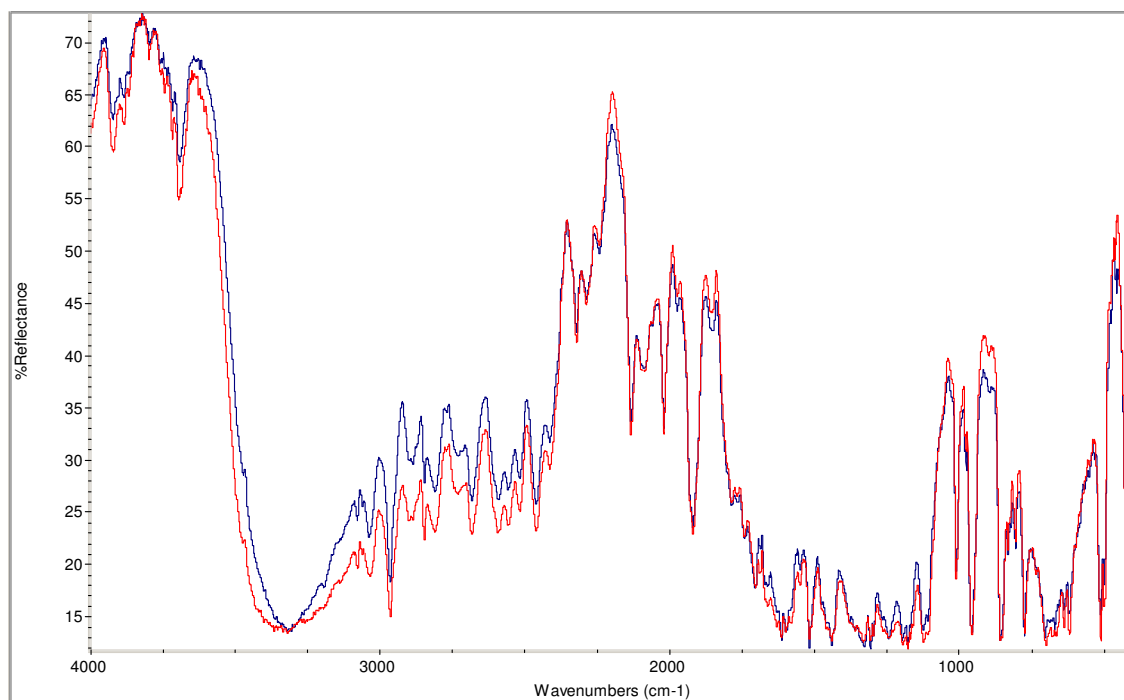


Figure 4.2.2: IR data collected on pure and recrystallised pMHB. The pure material is shown in red and the recrystallised material in blue.

On comparison of the IR data from the raw material and from the solvents tested, it is suggested that the compound did not recrystallise in any other polymorphic forms.

4.2.3 Calibrations

A calibration series is necessary to assess dissolution concentrations and was carried out using the MT Multi-Max system in conjunction with the ATR-UV probe. Calibrations were carried out over a constant temperature ramp starting from 25°C and increasing up to 55°C over a 6 hour time scale, with a stirring rate of 1000rpm. This time scale allows gradual heating between temperatures to ensure minimisation of temperature errors, which occur when the solutions are heated too quickly. The ATR-UV probe was blanked in air above the solution before being placed in the solution where readings would be taken every minute. Taking so many readings allows the ability to monitor the absorbance changes of the solution as a function of temperature. Unlike previous solubility work carried out on the compound⁸⁷ where the temperature range investigated was 20°C to 50°C, it was decided that readings

would be taken at 5°C increments from 25°C to 55°C inclusive thus producing a calibration series that is closer to the boiling point of methanol, the solvent to be used during the experiments.

To provide the most accurate calibration standard possible, five solutions were prepared; 5%, 12.5%, 20%, 27.5% and 35%w/w (solute/solvent) solutions; this is in comparison to only three concentrations that were used in the published method. All weighings were carried out manually and solutions filtered into the reactor vessel to try to protect the system from any impurities affecting the results.

A sample solution was run under these conditions from 200-700nm to determine where the maximum absorbance of the solution occurred. As a result of this, the study was focussed over the 200-300nm range and each solution was run individually over this scale (Figure 4.2.3). In this region the absorbance of methanol is negligible so any change in the UV spectra is solely due to the presence of pMHB in the solution.

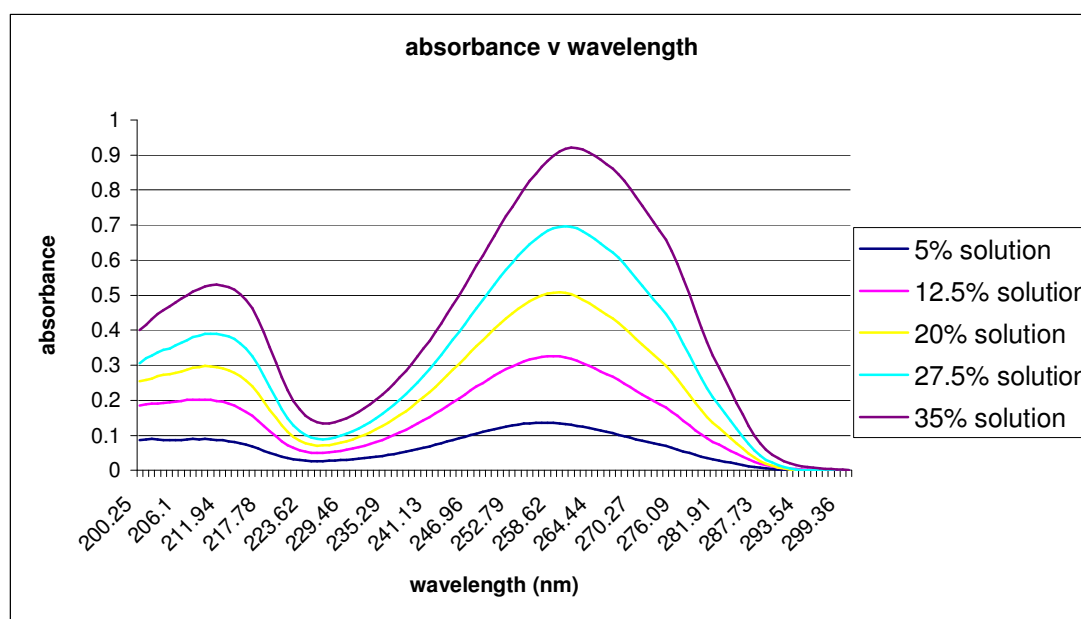


Figure 4.2.3: Absorbance changes with wavelength using varying concentrations of solutions at a fixed temperature.

The major absorbance peak at roughly 260nm was used for the concentration calculations. It should also be noted that the UV absorbance for methanol at this

wavelength is negligible and there is better separation between concentrations of solution.

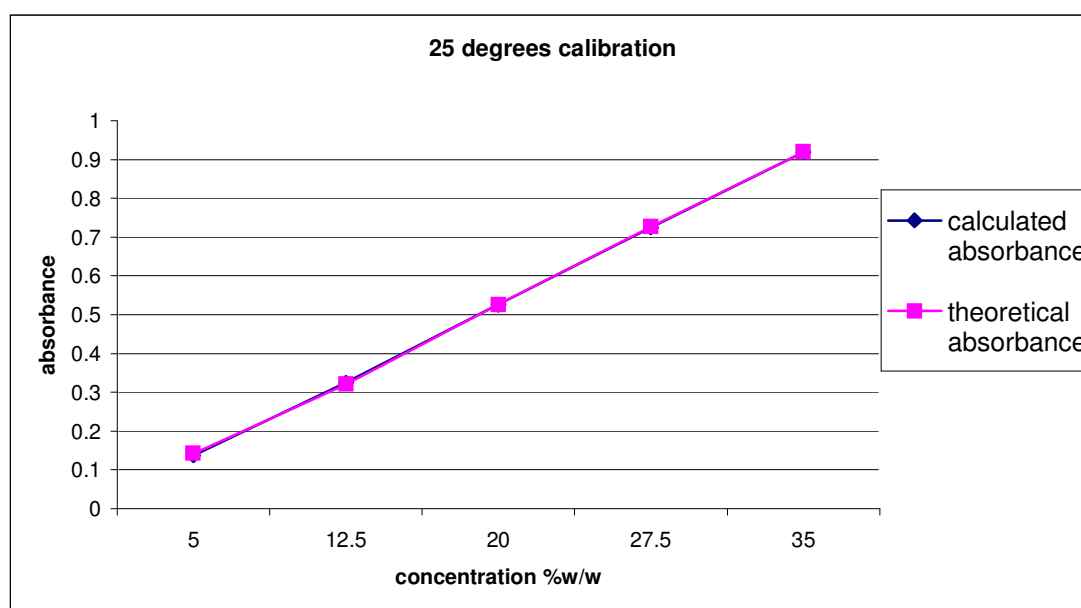


Figure 4.2.4: Calculated calibration results using varying concentrations of solutions at a fixed temperature.

Figure 4.2.4 shows the results of a calibration carried out at 25°C. The darker line is the experimental results and as expected there is an increase in UV absorbance with increased concentration of solution. The equivalent values obtained from the Area Max software for the theoretical absorbance, calculated from a manually input concentration of solution, gives an almost perfect agreement. This is vital before carrying out dissolution experiments as at 25°C this calibration result will be used to calculate the concentration of the saturated solution in the presence of excess pMHB.

Similar calibrations were carried out at all the measured temperatures indicated and all calibration results showed similar profiles, all with a very high degree of similarity to the experimental results. This indicates that the ATR-UV probe, which is used for monitoring concentrations *in situ*, is highly accurate and can be used to reliably calculate solution concentrations.

4.2.4 Solubility Studies

Solubility experiments are fundamental when investigating pharmaceutical compounds as this is the method by which the solubility of the compound is assessed. For the purpose of this work however, the solubilities at set temperatures are fundamental for the knowledge of the concentrations of solutions to be prepared for the metastable zone width studies. This is required as a reliable solubility curve must be determined prior to the generation of a supersolubility curve and thus the metastable zone being determined. The method again makes fundamental use of the MT Multi-Max system and the ATR-UV probe in unison.

Two solubility experiments were carried out to directly compare the results and increase the reliability of solubility curve for pMHB when compared with previously collected data⁸⁷. The experiments were carried out using 150g of methanol as the solvent - this allowed results to be produced that could be directly compared against the calibrations previously carried out where the ratio used was grams of pMHB per 100g of methanol.

An experimental protocol was set up to ramp to each of the desired temperatures and then held until the maximal absorbance remained stable. The stirring rate was again set at 1000rpm, however unlike most dissolution experiments where the compound is added during the experiment, due to the tremendous solubility of the compound in methanol, the compound was added directly to the vessel in prepared solution before it was sealed. The first temperature that was used was 25°C and the solution was held at that temperature until the absorbance was stable before being increased by 1°C every 4 minutes to 30°C where the next absorbance was monitored. The temperature ramp had to be increased very slowly at this stage to minimise any over-shoot in reactor temperature when it reached the desired temperature. Due to the excellent control of the Multi-Max system it should be possible at this rate to minimise this occurring and generate the most accurate dissolution profile possible. This was carried out at the same seven temperatures as in the calibration sequence increasing the temperature in the same manner by 5° each time. During these experiments, especially at higher temperatures, the solution had to be monitored to ensure that there was always an excess of the compound in the solution.

The ATR-UV absorbance readings, during the dissolution experiments, were taken every 30 seconds as this gave a continual monitoring of the UV absorbance and enabled the user to see easily when the absorbance reached a plateau. When analyzing the results from the dissolution, the calibrations were used, in conjunction with the Aspect Plus program, to calculate the concentration of the solution at any given temperature.

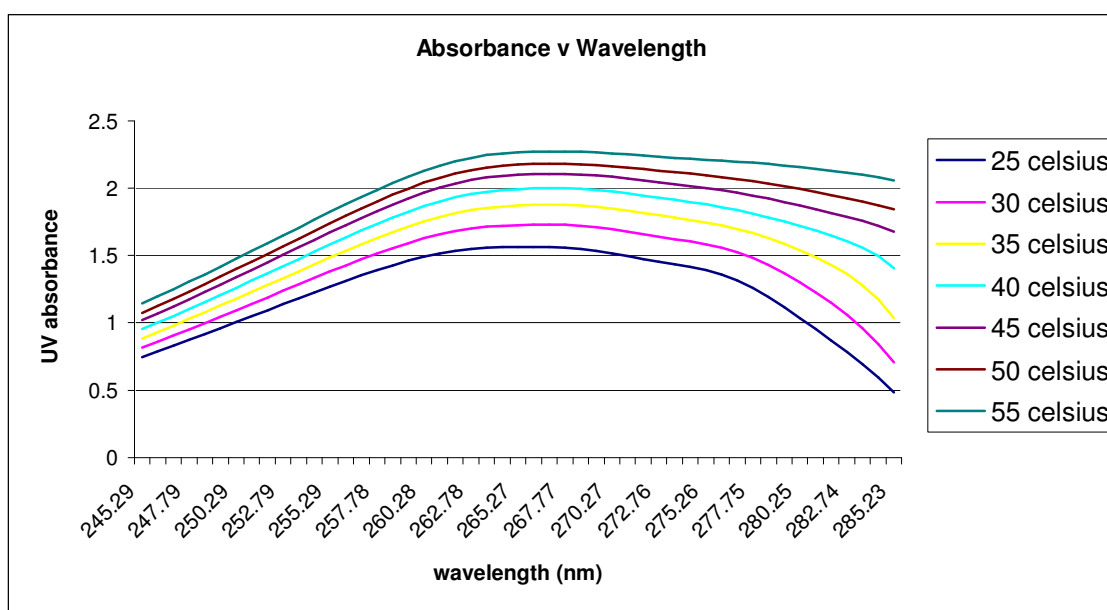


Figure 4.2.5: Absorbance changes against wavelength at varying temperatures for a fixed concentration of solution.

Figure 4.2.5 shows the ATR-UV data from the solubility experiments and from this it is easy to notice the change in absorbance as a function of temperature. As expected, the solubility increases as a function of temperature. These values were the basis for the MZW experiments to aid with the preparation of near supersaturated solutions.

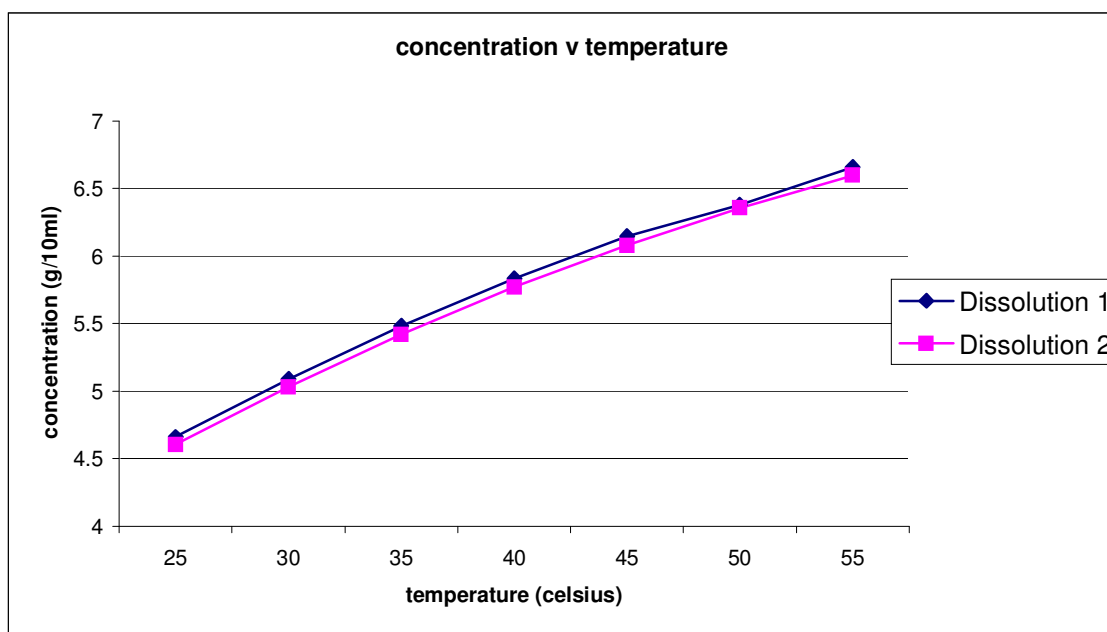


Figure 4.2.6: The solubility curves calculated from solubility experiments.

Figure 4.2.6 shows the two solubility curves calculated from the UV absorbance data collected at each temperature. This was carried out using the Area Max program, which took the experimental UV absorbance data and used the calibration profile at a set temperature to calculate the concentration of the solution at the set temperature. This was subsequently used as the solubility curve. The two curves show a close correspondence to each other and to the previously published results⁸⁷. There is a slight difference in the two solubility experiments, however, this can be explained by the difference between using fresh pMHB and pMHB which had been recrystallised from a previous experiment.

4.2.5 MZW Studies:

Metastable zone width (MZW) studies monitor the changes in chord length of the solution as the temperature is cooled and give a clear idea of the point at which the particles start to emerge from solution. It is important at this stage to note that this point need not necessarily be the nucleation point for the molecule: it is simply the point at which the probe can detect the presence of particles in the solution and not necessarily the formation of a critical nucleus. This links the MT Multi-MaxTM, the

ATR-UV probe and also the FBRM probe, since when the particles start to emerge from solution this will result in a decrease in the UV absorbance of the solution. The set up is defined so as to monitor the fine particles in solution, resulting in a highly sensitive method that is able to analyse any change in the solution. The FBRM probe can be set up to monitor up to eight different characteristics simultaneously. For the interests of the MZW studies only four were of extreme significance, these were:

1. number of chords per second, no weighting factor, 9-27 microns
2. number of chords per second, no weighting factor, 24-90 microns
3. number of chords per second, no weighting factor, 88-102 microns
4. number of chords per second, no weighting factor, 93-102 microns

Using these sets of conditions it was expected that as the particles started to emerge from the solution the number of chords per second picked up by the probe of the smallest length would be increased greatly and this would indicate where the nucleation point occurred. The significant values to monitor during the MZW experiments are shown above as these clearly show the particles emerging from solution and the subsequent growth that occurs after nucleation.

To carry out the MZW studies, saturated solutions, using concentrations obtained from the dissolution experiments, had to be prepared manually at the relevant temperatures. The first solution was prepared at 25°C and cooled at 0.25°C per min until the emergence of particles from solution was detected by the FBRM probe. The stirring rate was kept constant at 1000rpm and this was repeated to assess the reliability of the results. The solutions were prepared by using a hot plate with stirring function and a sealed container and then filtered into the reactor vessel to prevent contaminants entering the system.

The same method was used for all of the seven temperatures before the metastable curve could begin to be populated. This will be plotted against the calculated solubility curve thus giving an indication of the width of the zone width of the molecule.

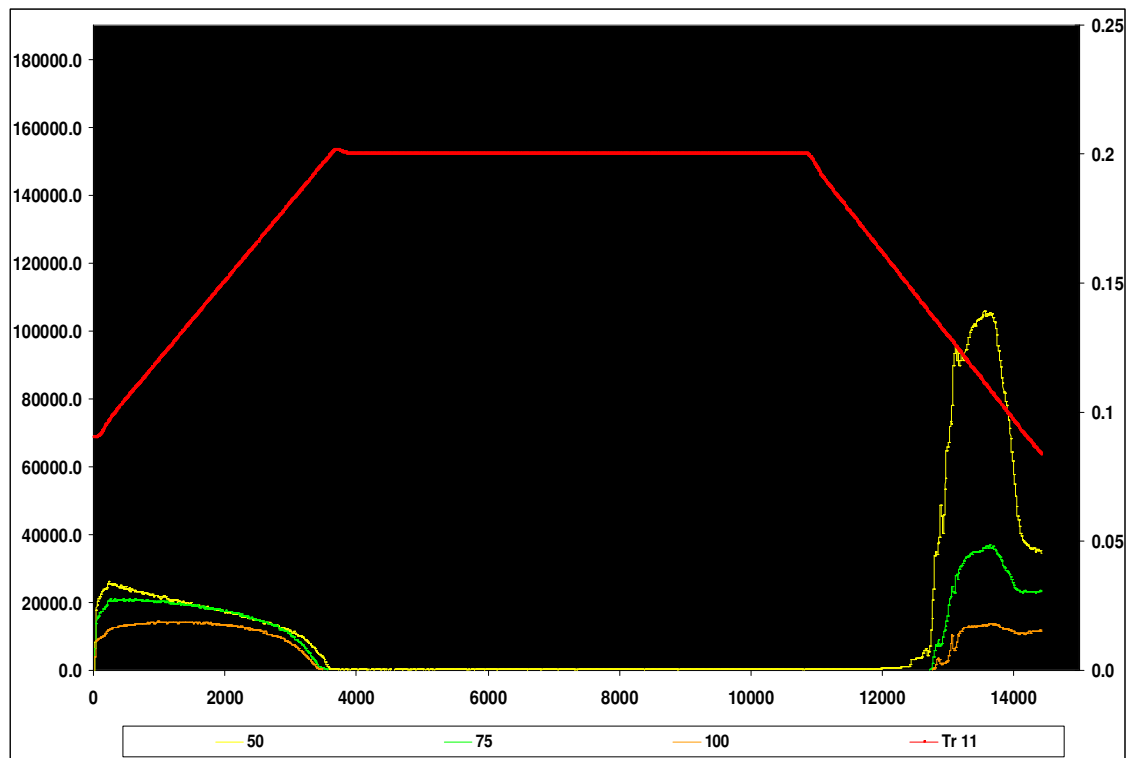


Figure 4.2.7: Chord length distribution profile of the crystallisation process from dissolution to recrystallisation. The temperature profile for the experiment is shown in red.

Figure 4.2.7 shows a chord length distribution (CLD) profile collected during MZW experiments. Initially as the temperature is ramped the particles all start to dissolve into the solution. The solution is then maintained at a constant temperature for a period of time to ensure that all particles are stable in solution and not going to emerge without a cooling ramp being applied. The solution is then cooled at a steady rate until particles start to emerge from the solution. This occurs rapidly for smaller particles (yellow) then gradually for larger particles (green and orange). The nucleation point occurs as soon as the first signs of emergence are detected by the FBRM probe.

This can be easily observed when looking at small particles in the 9-27 μ m range. Values are taken every minute from the initial starting temperature until the nucleation point is reached and the particles all emerge from solution. The other values that the FBRM were set up to monitor were not as significant when monitoring

the emergence of particles from solution and can therefore be ignored when it comes to viewing the results graphically. This is due to nucleation already having occurred and therefore only the significant data is shown.

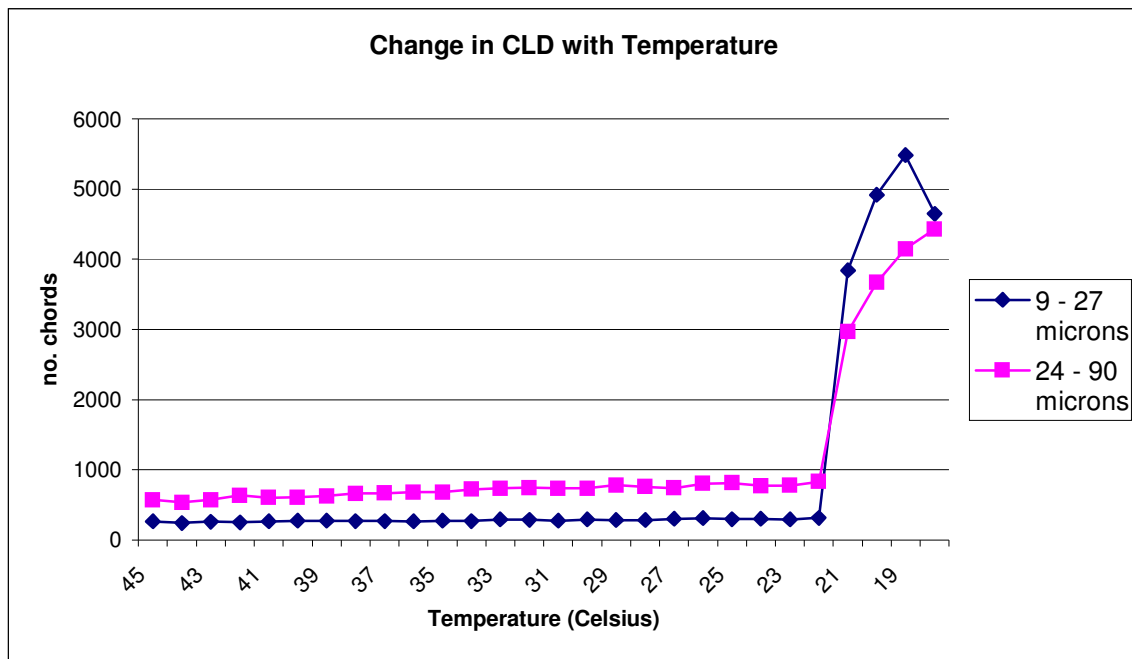


Figure 4.2.8: Change in CLD as solution is cooled and crystallisation occurs.

Figure 4.2.8 shows the number of chords that are detected in the 9-27 μ m and in the 24-90 μ m range and how these both grow at a rapid rate from the nucleation point as the particles start to emerge from solution. The solutions were then reheated and the process was carried out again to try and duplicate results to assess the reliability of the data that is being generated.

From Figure 4.2.8, it is clear that the chord count remains constant until the nucleation point, when the chord count then increases rapidly as the particles emerge from the solution. The chord count is not zero due to the stirring of the solution generating bubbles which are picked up by the FBRM probe and thus result in a chord count even though all the particles are still in solution. This is the same pattern that is noticed when cooling from all temperatures. After recrystallisation has occurred, the profile for the 9-27 μ m region starts to decrease. This is due to crystal growth occurring as a subsequent result of crystallisation. The profile for the larger chord

lengths will subsequently start to grow at this point, though this region is not significant for determining the metastable zone width.

Figure 4.2.9 shows the UV changes as the MZW experiments progress. When the solution is cooled from the starting point, determined from the dissolution experiments, there is an initial small increase in the UV absorbance. This is due to the solvent evaporation that occurs from the solution. This results in an increase in the concentration of the solution and therefore an increase in the UV absorbance as determined by ATR-UV. This is maintained until the particles start to emerge from solution and at this stage the absorbance drops rapidly as crystallisation and subsequent crystal growth occur.

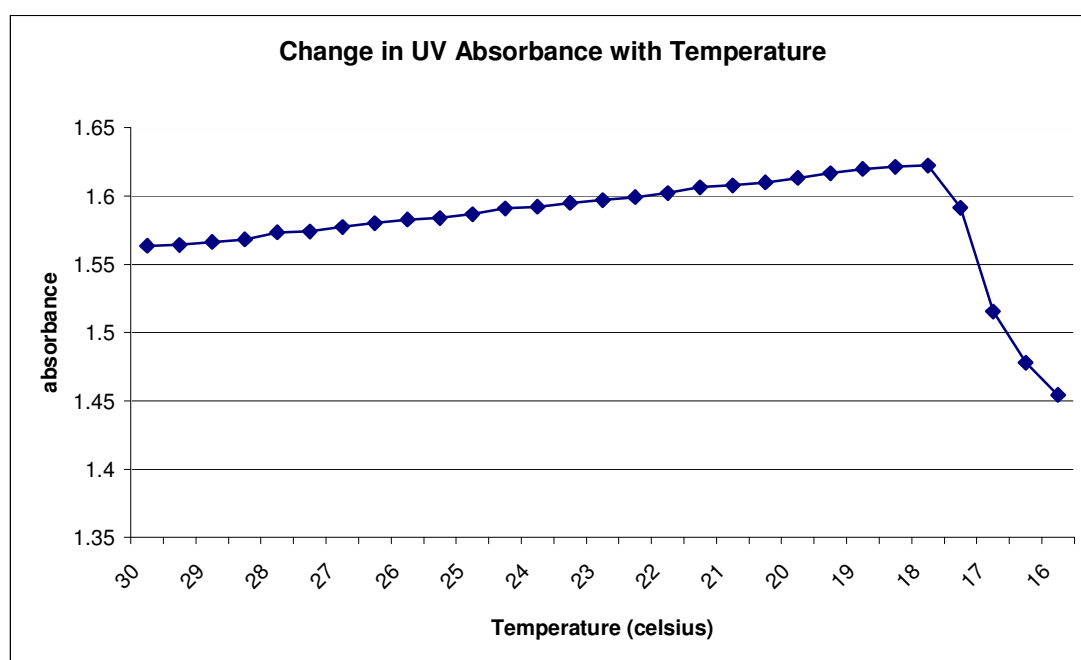


Figure 4.2.9: UV absorbance changes as the metastable zone width experiment progresses and temperature is decreased.

Preparing the solutions by using vacuum filtration ensured that the solution had no small elements of crystalline material present in the reactor vessel. The cooling rate of the solution and the stirring rate of the solution were maintained at 0.25°C/min and 1000rpm respectively. This has led to the successful generation of the MZW graph, Figure 4.2.10.

The results for the MZW experiments were extremely positive considering nucleation is an entirely random process and to attain results of this quality shows that in the right conditions it should be possible to control crystallisation from solution. Having to prepare the solutions at set temperatures prior to filtering into the reaction vessels leads to a slight decrease in the concentration of the solution present for the reaction. This is due to the fact that a small amount crystallises during filtration due to the changes in temperature between the solution and the filtering equipment.

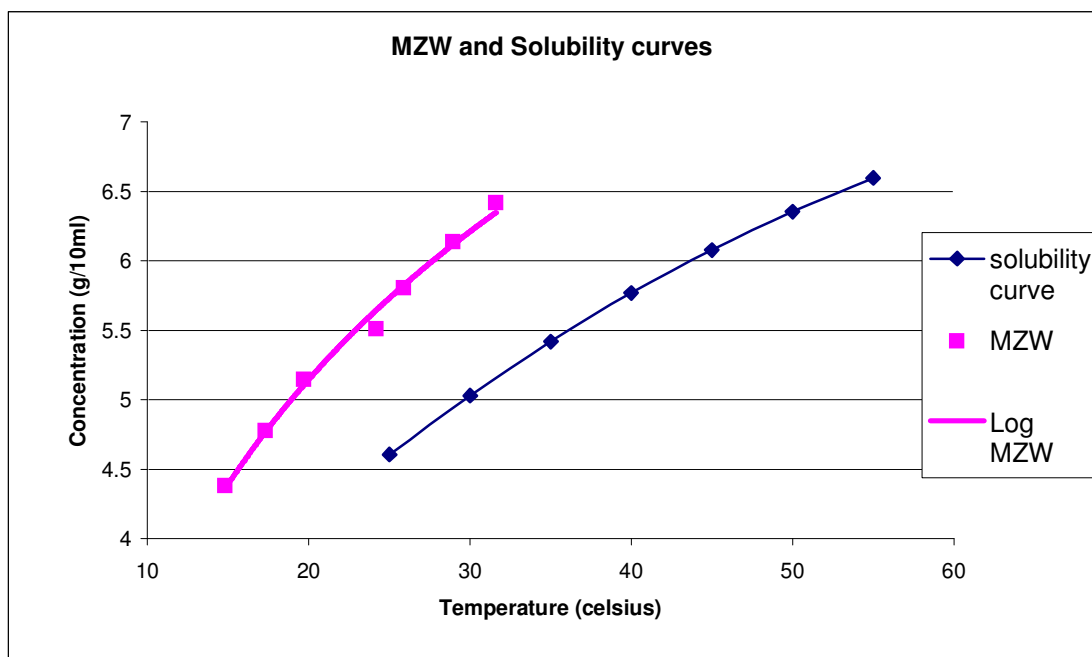


Figure 4.2.10: The metastable zone width results plotting the dissolution curve and the best fit curve for the nucleation points as observed during the MZW experiments.

The significance of the MZW can be understood due to its width. In this sense the wider the metastable zone the easier it would be to control crystallisation within this zone *via* methods such as seeding. The narrower the metastable zone signifies that the solution in itself is not inherently stable and that if left long enough then crystallisation is likely to be automatic.

4.3 Small Angle X-ray Scattering Studies of Nucleation

The main objectives behind the SAXS studies were to find a range of data for the initial nuclei, including their number, size and type, from organic materials that may exhibit polymorphism. This is carried out using SAXS to probe solution studies as crystallisation occurs. The particle size distribution in nucleating solutions is important in distinguishing the factors involved in competitive crystallisation within solutions, while also providing information on particle homogeneity and uniformity. The structural information obtained from macromolecules in solution obtained by SAXS has been used to provide confirmation of computationally modelled protein structure³⁹ and this furthers the belief that vast information can be obtained from SAXS studies.

Two days beam time on Station 2.1 at the SRS Daresbury were allocated for a preliminary SAXS study to investigate the pre-nucleation solution scattering of our test material methyl p-hydroxybenzoate. SAXS is generally used to look at larger molecules in solution, such as proteins, however this project involved trying to monitor pre-nucleation of small organic materials and to determine the initial particle size, which exist in solution prior to crystallisation and whether these are mono- or polydisperse in nature. It was anticipated that these particles would vary in size as a function of temperature as the temperature can significantly affect the formation of the crystals (in terms of both their quality and size and in terms of which polymorph may form) during the crystallisation experiments.

During the experiment, time was spent developing the techniques required, including preparing suitable sample cells. The low viscosity of the solutions dictated that extra care had to be taken to seal the cell and prevent the solution from leaking from the cell during the data collection. This problem was compounded by the ready crystallisation of the samples when in contact with a surface as this acts as a nucleation site and subsequently promoted crystal growth due to the high concentration of the solution. The sample cell used (Figure 4.3.1) had a volume of 200µl and the solution was injected between two mica windows by syringe.



Figure 4.3.1: Sample cell used with small window for the solution.

The problems with maintaining a fixed concentration of solution and the fact that it was hoped to collect data at two camera lengths meant that much of the data were collected with a beam current several orders of magnitude lower in intensity than recorded after the refill and the ring was only operating on one refill per day. The statistics of the data from some of the measurements were therefore not sufficiently high and overnight data collections were not effective. Data were collected at 5°C intervals between 25°C and 5°C and observed signal above the background and solvent level for all cases. The data were collected over a minimum of 30 mins at each temperature and longer when the beam was becoming weaker. The solution used initially was a 0.8g/ml pMHB / methanol solution, however this recrystallised too rapidly around the surfaces of the cell and on the syringe used for injecting the solution. Having learned from this, the rest of the data were collected using a 0.7g/ml concentration.

Despite these complications, on correcting the data for solvent and background levels, it was possible to observe significant scattering arising from the solute. Our results show a significant small angle peak due to the solute and then a return to a flat signal as seen in pure methanol solution. This small angle peak is present throughout the data collection even at low temperatures, though the intensity does not appear to vary radically. Significant features in a small angle diffraction pattern do not appear as

sharp peaks; rather, subtle changes in the slope of the small angle peak and very broad peaks at higher scattering angle are observed. These broad features may not be identifiable when looking at the scattering directly, only becoming apparent when a Fourier transform of the diffraction data has been calculated. Determination of the particle size in the form of the radius of gyration depends on a number of assumptions including the particle shape, which in its simplest case can be modelled as spherical.

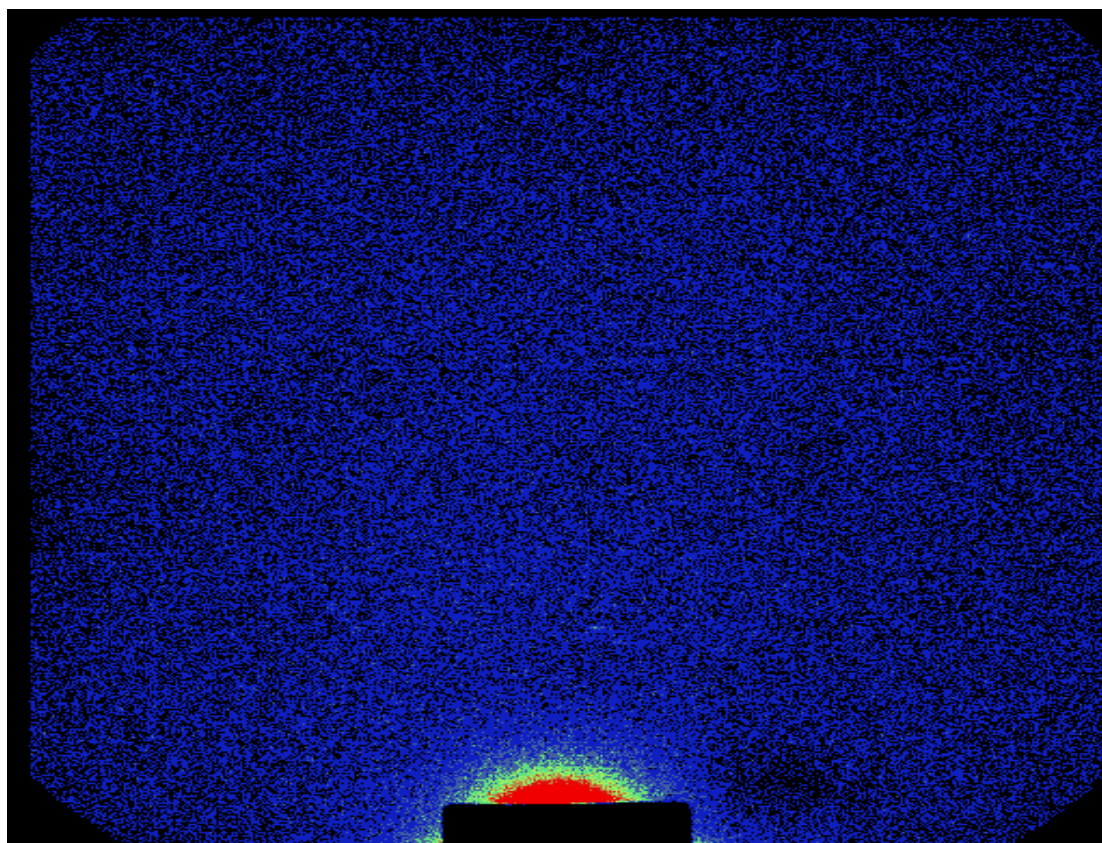


Figure 4.3.2: The detector image of pMHB in methanol at 20°C.

Figure 4.3.2 shows precisely how difficult analysis from SAXS data can be. The majority of the scattering from the X-rays occurs around the beam stop with only minimal scattering seen elsewhere and the intensity of the data away from the beam stop is not sufficiently high to enable any significant data analysis of this region. The significant scattering that occurs around the beam stop shows low angle scattering and represents interactions between the molecules in solution.

Using SAXS specific programs, available through Dmitri Svergun⁴³ and used routinely for assessing protein solution scattering it has been possible to analyse the data to a basic extent.

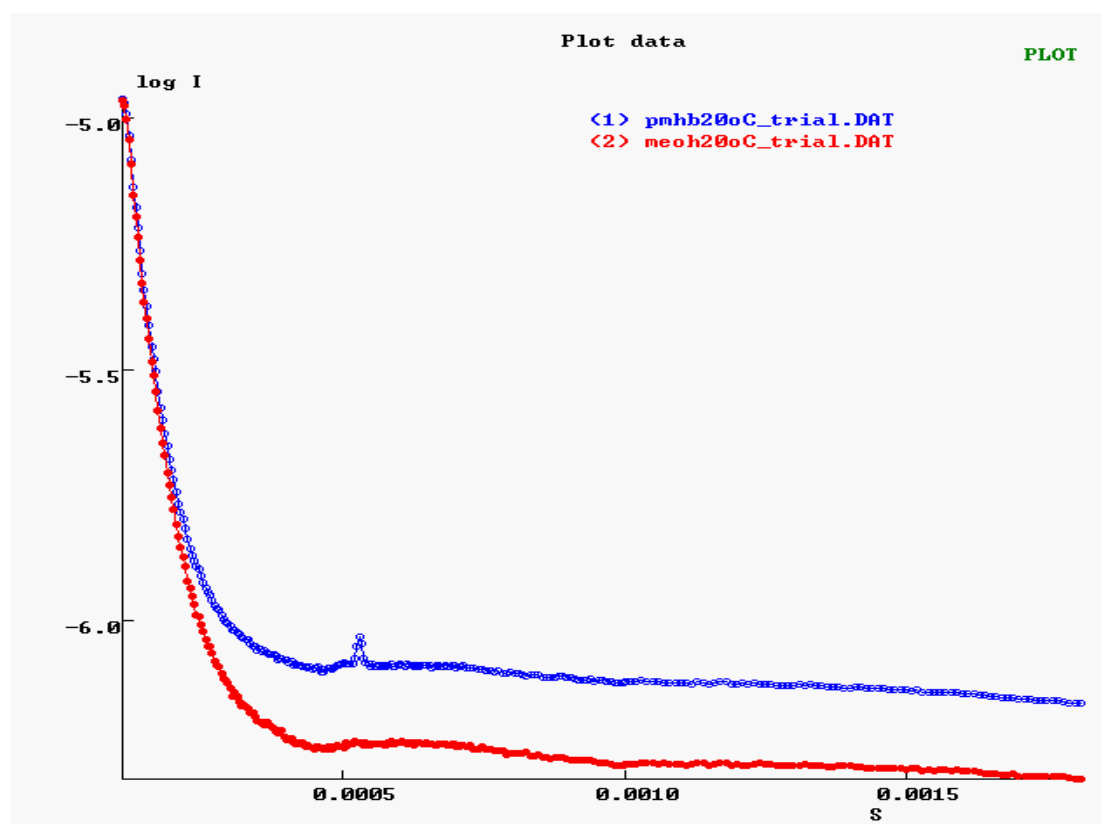


Figure 4.3.3: Scattering profile of pMHB (blue) and methanol (red) at 20°C.

Figure 4.3.3 shows the change in scattering profiles between pMHB and pure methanol solution. The significant areas to examine are at the lowest angles as it is seen to be that this is the region of scattering where the majority of the signal occurs. It should be noted that the scattering from the solute is not highly different from that at methanol at the smallest of angles but does lie higher at larger angle. The slope of the small angle peak is also observed to differ. This does not give the best view to changes during the crystallisation process but gives an initial view that scattering from the solute is being observed. It should also be noted that in the pMHB scattering profile at 20°C, a sharp small peak is observed in addition to the main peak. This is likely to be an artefact in the data, as any changes in particle size in solution will give rise to only broad features in the scattering pattern. This sharp feature was not observed for any of the other temperature measurements.

Figure 4.3.4 shows an overlay of the pMHB data collected at the four separate temperatures. The data were analysed using the program PRIMUS⁴³. The four lines, each corresponding to a separate temperature, show a virtually perfect overlay, which indicates that the molecule was stable in the solution. This could be seen during the experiment as no crystallisation appeared to be occurring during the cooling process or even when the sample was removed at the end of the experiment. Due to the small volume used in the SAXS studies, especially in comparison to the previous solubility studies and less nucleation sites, it proved to be a difficult study. The SAXS study uses 200µl of the concentrated solution prepared, whereas the metastable zone width experiments that were carried out all require a minimum of 150ml to ensure that the FBRM and ATR-UV probes are submerged in the solution. This sort of volume change, as well as the presence of stirring in the MZW experiments will always result in major differences between the two techniques.

Due to the nature of the crystallisation being monitored, organic molecules with no heavy atoms to increase scattering, the scattering is much weaker than for the proteins routinely studied using this technique, however it should be noted as a positive that it has been possible to see scattering from solutions and this will be progressed by adding in heavy atoms into the organic molecules being studied. This theoretically will increase the scattering from the solution, for example the presence of bromine will increase the scattering of an organic molecule greatly as it is a much larger atom than any of the others that are currently involved in the compound. This works for X-ray scattering from crystals due to the number of electrons that bromine has so it is expected that this will also be the case in enhancing signals in the SAXS studies.

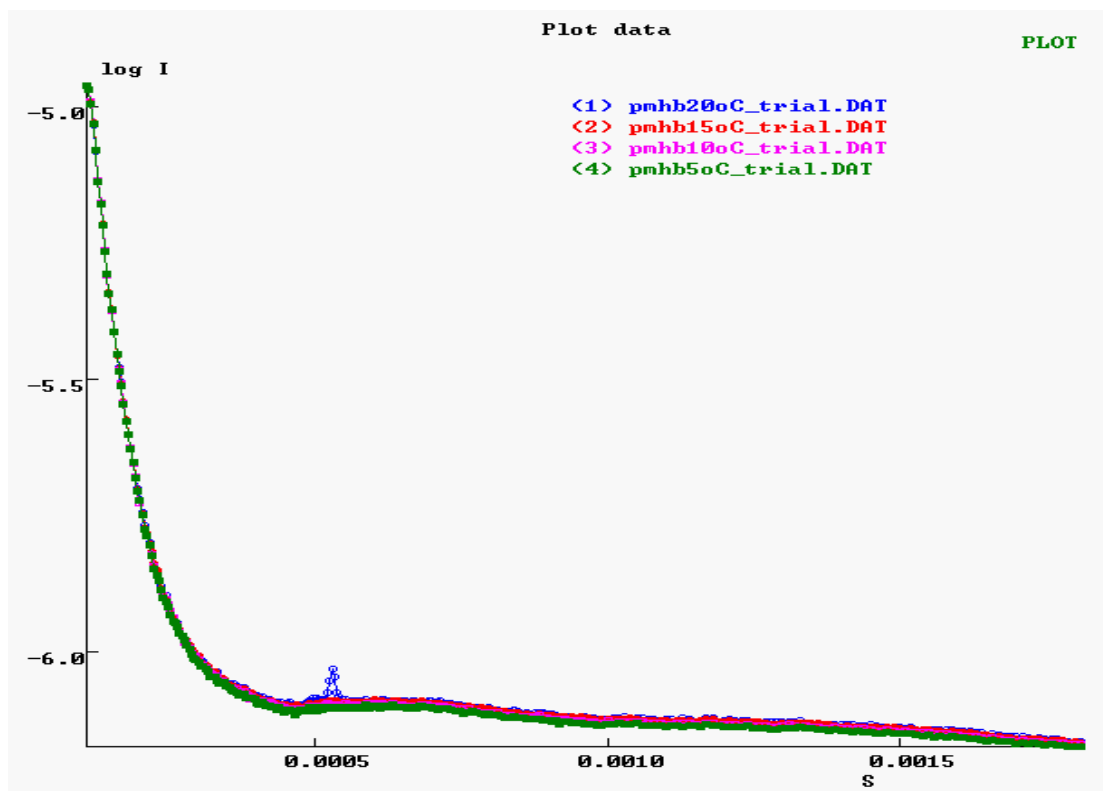


Figure 4.3.4: Scattering profile showing an overlay of the data collected at the four studied temperatures (5°C is shown in green, 10°C in pink, 15°C in red and 20°C in blue) showing a marginal increase in intensity as a function of temperature.

The scattering profiles for both pMHB and methanol solutions showed similar traits, however with an increased scattering coming from the solute. The intensity of signal is maximised at low angle, due to the lack of scattering ability of solutions. The intensity of scattering drops significantly and results in an almost constant level of scattering that is the background for the solute. This range is not as significant as the low angle region as most of the interactions in solution occur around this region leading to increased ordering and intensity. This is clearly visible even in the solution scattering that is occurring from such a small molecule.

Figure 4.3.5 shows an overlay of the data collected at each temperature for pMHB and for the control experiments containing purely methanol. This is the best way to visualise the changes that occurred between the control experiments and the experiments that were carried out containing pMHB. This clearly shows that there is not a significant difference in the scattering in the temperature range studied but does

indicate that there is scattering visible from the solute. This is indicative of broad range ordering in the solution.

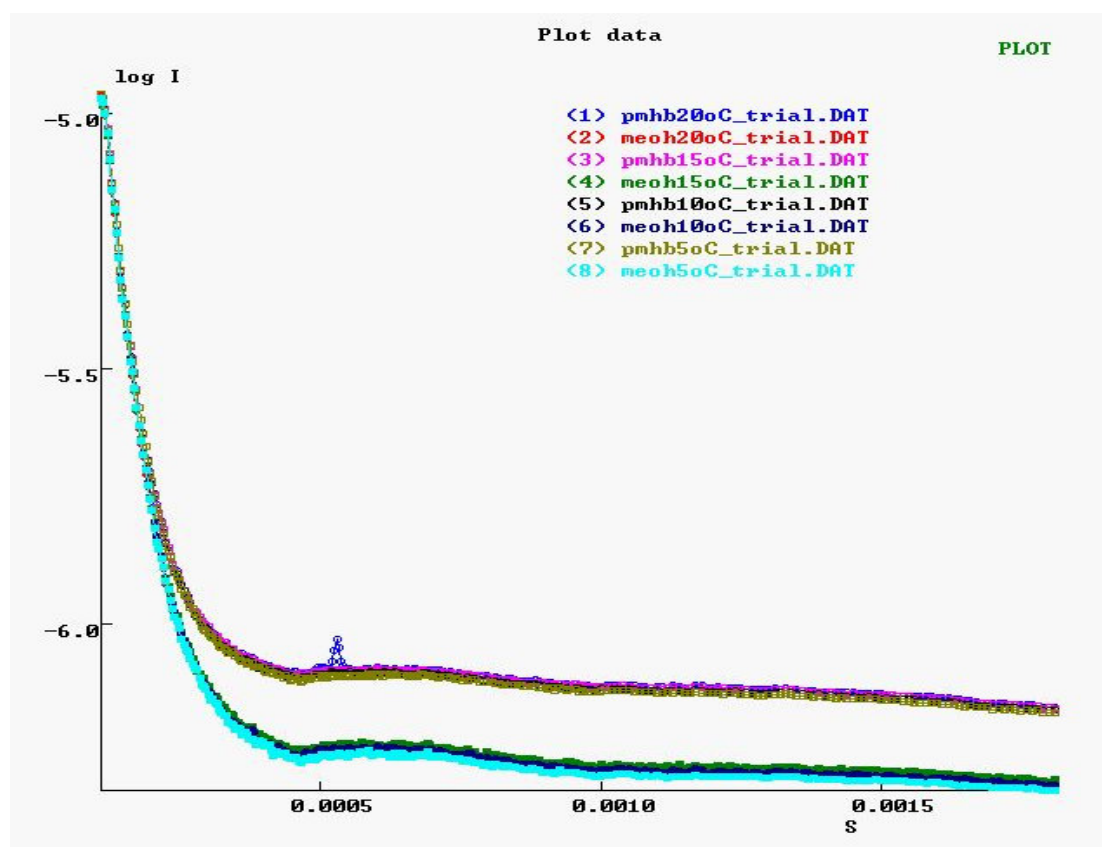


Figure 4.3.5: All the data collected on station 2.1, indicating increased scattering from the solute. The methanol solutions all show significantly lower scattering at higher angles and show very little variation as a function of temperature.

The analysis of this data was not to a sufficient standard due to the weak scattering and it was therefore not possible to determine an accurate radius of gyration (R_g) for the molecules coming together in solution in spite of a range of attempts to carry this out reliably. This will therefore not be reported. The data were analysed using PRIMUS⁴³ and GNOM⁴³ and the scattering pictures available via FibreFix⁴³, however these programs are all specifically designed for much larger molecules where the observed scattering is significantly distant from the beam stop. To increase the scattering from the solution it would be necessary to collect data for a much greater length of time on a more powerful beam and then it may be possible to progress our knowledge of the process of crystallisation by monitoring the interactions before crystallisation occurs.

SAXS studies were also carried out at the University of Cardiff in collaboration with Professor Tim Wess and Dr Donna Lammie using the Bruker AXS NanostarTM. This has a similar design to a synchrotron SAXS system, however the intensity of the beam is obviously reduced. This resulted in further reduced scattering from the solute and no significant data were produced to augment the Station 2.1 data reported above.

4.4 Conclusions:

Although initial liquid studies were successful in the generation of a MZW, the ultimate goal was to attempt to study the nucleation process. In this sense the model compound that was selected was not ideal for the purpose. Scattering was observed due to the pMHB being present, however a more suitable target molecule containing heavy atoms would scatter X-rays more strongly and perhaps be able to produce data that can be analysed using the available analysis programs. This study has therefore been significant in the development of reliable solubility and the use of MZW data that is required for SAXS studies on highly concentrated solutions. However it is our belief that to be able to make significant progress a target molecule with heavier atoms would be more beneficial.

Chapter 5. X-ray diffraction studies of methyl 4-hydroxybenzoate – an investigation of possible conformational polymorphism

Methyl 4-hydroxybenzoate (pMHB; Figure 5.1) is a well studied non-linear optical material⁸⁷. The crystal structure of pMHB was originally solved by Lin *et al.* at room temperature²¹. It shows no signs of other polymorphic forms. Given this, it had been assumed that the most stable form was already known. However, a recent study, by Vujovic *et al.*²² has indicated the possibility of a low temperature phase transition, claiming to have discovered a previously unknown form at low temperature. This study, carried out at 113K, led to the postulation of a new polymorph, although both forms crystallised in the monoclinic non-centrosymmetric Cc space group with three $Z'=3$ and $Z=12$.

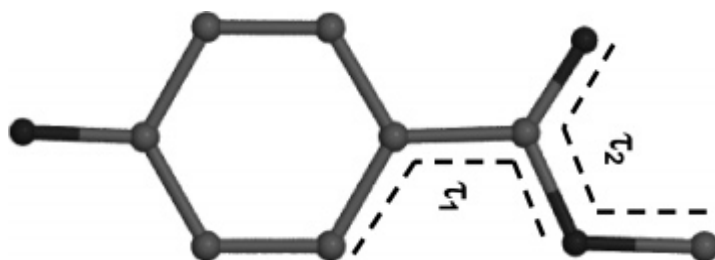


Figure 5.1: pMHB indicating the two torsion angles discussed in relation to possible conformational polymorphism

In the low temperature structure, there is a lengthening of the b axis and an apparent twist in the ester group (shown by changes in the torsion angles indicated in Figure 5.1), when compared with the original structure. These factors result in changes in the calculated powder X-ray patterns that were deemed to be sufficient enough to indicate that a conformational polymorph had been found. In the case of pMHB, any conformational polymorphism occurring would be thought to be due to a ‘displacive’ phase transition where a small change would not have to overcome significant energy barriers²⁴ and that can be readily reversed.

This finding has been disputed by Threlfall *et al*²³, who argue that, although slight differences can accumulate over a large temperature or pressure range to produce a substantial structural difference, this does not of itself produce a new phase or new polymorph. He further states that the slight changes in lattice parameters can be justifiably accounted for in terms of minor conformational changes. This latter interpretation has been backed up by the work presented here using variable temperature X-ray powder diffraction and single crystal studies.

5.1 Variable temperature XRPD

To investigate these reported changes in calculated powder patterns a variable temperature XRPD study was carried out to examine any changes that may show up as temperature was increased from 100K to 300K. These experiments were carried out using a Bruker-AXS D8 powder diffractometer with temperature control provided by an Oxford Cryosystems low temperature Cryostream device. Any significant changes in crystal structure will result in changes to XRPD patterns and will easily be determined as a function of temperature and the temperature range in which these changes occur. For this reason diffraction patterns were collected every 50K over a scattering angle range of 5-55° 2 θ at 1° per minute. Figure 5.1.1 shows that as temperature was increased the peaks at 16.5-18, 25-26 and 27.4-28.4° 2 θ (marked * in the Figure) start to get closer together until there is ultimately one single strong peak at 300K. This is a typical process in all powder data in which the unit cell dimensions are varying as a function of temperature and should be noted, does not represent a significant change in structure. Throughout the variable temperature XRPD experiment, all the peaks are present throughout or can be accounted for by this gradual coalescence of peaks into one single peak at high temperature.

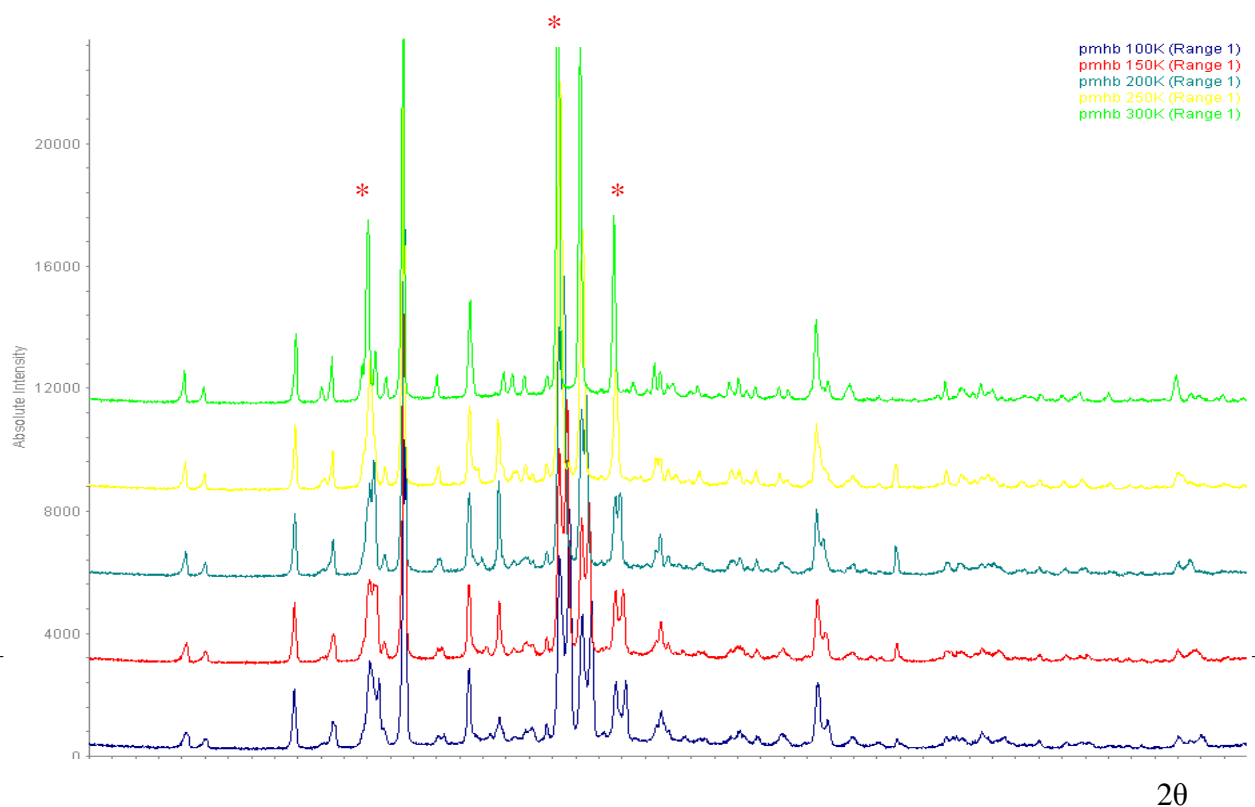


Figure 5.2: XRPD patterns collected during VT XRPD study (from bottom to top, 100K, 150K, 200K, 250K, 300K).

At low temperatures the XRPD thus does not give any supporting evidence for the claim of a phase transition reported to occur at 113K, and can merely be explained by a thermal expansion of the unit cell as the temperature is increased.

5.2 Variable Temperature Single Crystal Studies

Variable temperature single crystal X-ray diffraction studies have been carried out using a Bruker AXS Apex II diffractometer and through this it has been possible to generate good quality structure determinations at various temperatures between 100K and 300K. It was found that throughout the study that pMHB crystallized in the monoclinic non-centrosymmetric Cc space group with three independent molecules in the asymmetric unit and Z=12. This was in agreement with previous studies and also it was found that the *b*-axis did elongate as temperature was decreased. This is unusual as it is common for all three axes to contract with decreasing temperature, however the reason for this elongation is unknown. The crystal structures shown in

Figure 5.2.1 were determined at 100K, 200K and 300K. These are viewed along the *b*-axis and generally show the same characteristics throughout.

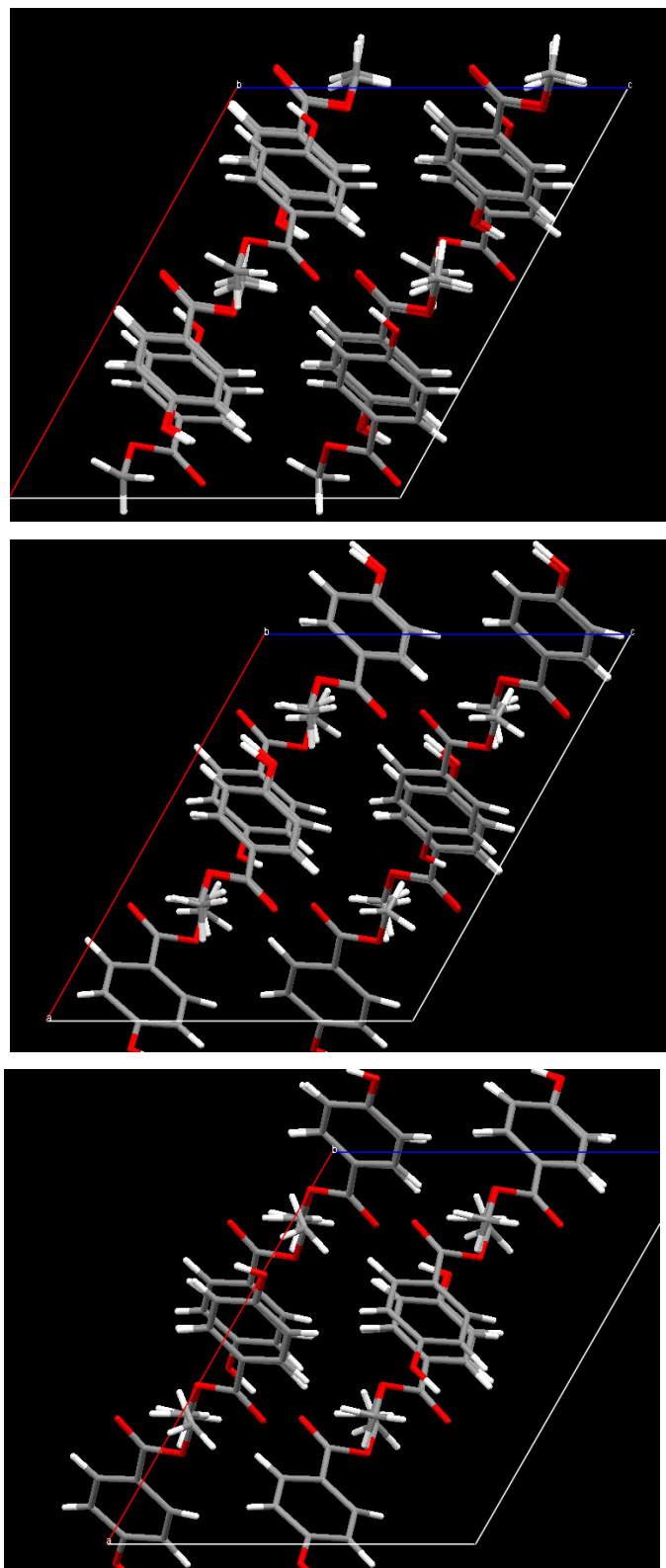
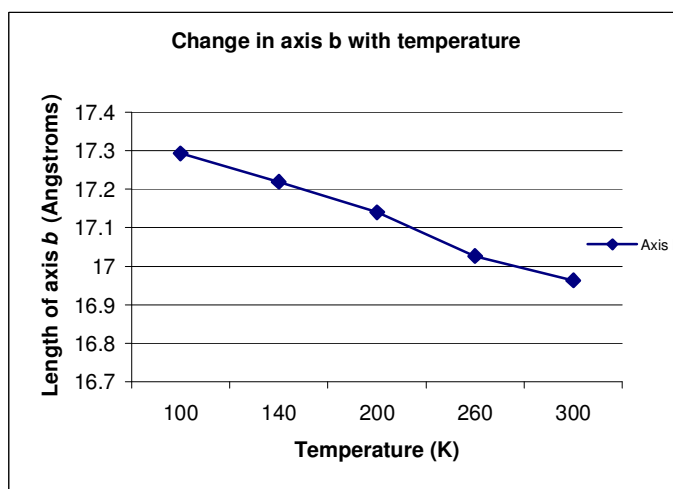
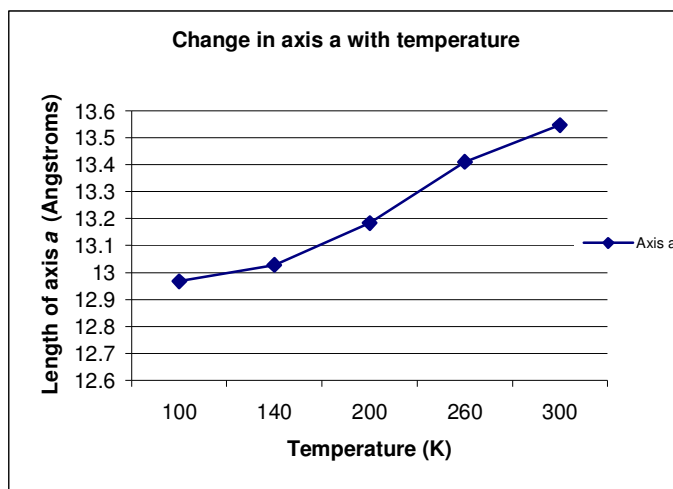


Figure 5.2.1: The crystal packing of pMHB as viewed along the *b*-axis at (top) 100K, (middle) 200K and (bottom) 300K.

Figure 5.2.2 shows the trend in the unit cell parameters determined from the single crystal studies as a function of temperature (unit cell determinations were also carried out at 140 and 260K). This further supports the hypothesis that a simple unit cell contraction is occurring as the temperature is cooled, and there is no abrupt change that would indicate a polymorphic transition.



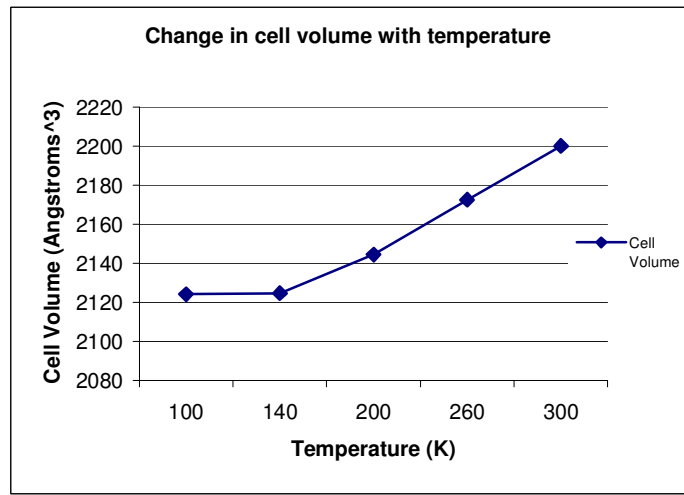
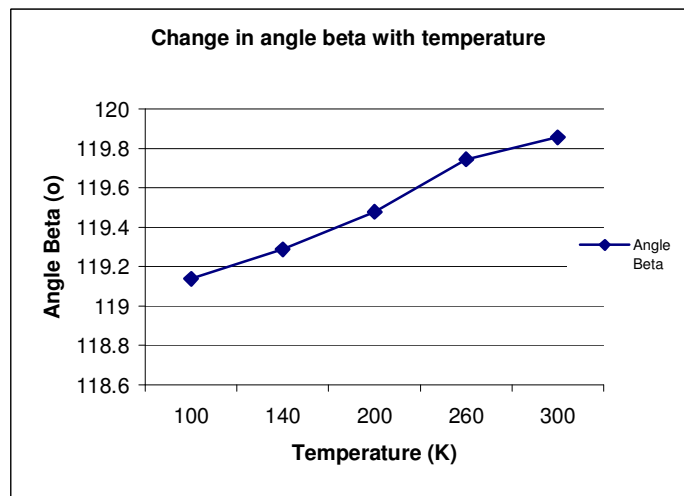
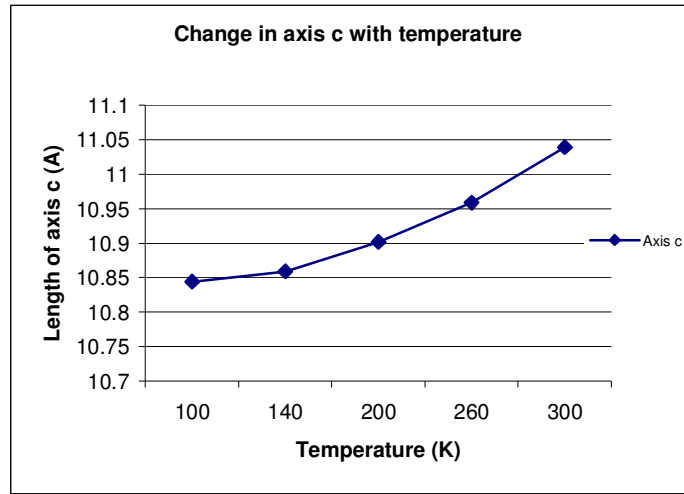


Figure 5.2.2: The trend in unit cell parameters and cell volume of pMHB with respect to temperature, from the single crystal experiments.

		τ_1°	Change $^\circ$	τ_2°	Change $^\circ$
Molecule 1	100K	-2.8(5)	2.6	0.9(5)	5.0
	LT	-4.3(2)	1.1	0.7(2)	4.8
	RT	-5.4		-4.1	
	300K	-3.0(4)	2.4	1.0(4)	5.1
Molecule 2	100K	2.9(6)	0.2	-0.2(6)	3.0
	LT	1.5(2)	1.6	1.4(2)	1.4
	RT	3.1		2.8	
	300K	3.0(5)	0.1	-0.6(4)	3.4
Molecule 3	100K	-1.6(6)	3.9	-0.2(5)	6.8
	LT	3.0(2)	0.7	-1.1(2)	5.9
	RT	2.3		-7.0	
	300K	-2.0(4)	4.3	-1.2(4)	5.8

Table 5.1: Torsion angle data from low temperature form (LT), room temperature form (RT), our 100K data and our 300K data. (See figure 5.1 for a definition of the torsion angles.)

Having produced single crystal structures, the torsion angles were investigated to assess the likelihood of conformational polymorphism being present. Comparing the torsion angles in the 100K and 300K structures (Table 5.1) showed no significant differences, and allied with the continuous nature of the development of the XRPD patterns as a function of temperature, argue against this.

5.3 Conclusions

These single crystal studies, backed up with XRPD data, enable us to give the opinion that there is not a low temperature phase transition as postulated in the literature²². This is merely a contraction of the unit cell occurring as temperature is decreased. The results verify that there is an expansion of the *b* axis as temperature is decreased and a contraction of the *a* and *c* axis resulting in an overall unit cell contraction.

Through these studies, the changes in torsion angles between 100K and 300K are not as severe as stated in the literature²². We have found no overall changes in torsion angles of greater than 7° for torsion two and only one over 4° for torsion one (Figure 5.1), which was calculated to be 4.3°. This is therefore not believed to be a significant change in the crystal structure to allow it to be deemed a conformational polymorph and a simpler explanation of a unit cell contraction and minor changes in the molecular geometry as the temperature is lowered is justified.

Chapter 6. Scattering studies of bromo-substituted compounds: towards signal enhancement and halogen interactions

6.1: Dissolution and MZW studies of Methyl 2,5-dibromobenzoate

Following on from the initial liquid studies carried out on methyl 4-hydroxybenzoate (pMHB), it was decided to also study a second molecule containing heavier atoms, which may scatter X-rays better and potentially lead to distinctive signatures that can be identified in liquid scattering studies. For this part of the work, a related molecule containing two bromine atoms was selected, methyl 2,5-dibromobenzoate (MDBB; Figure 6.1.1).

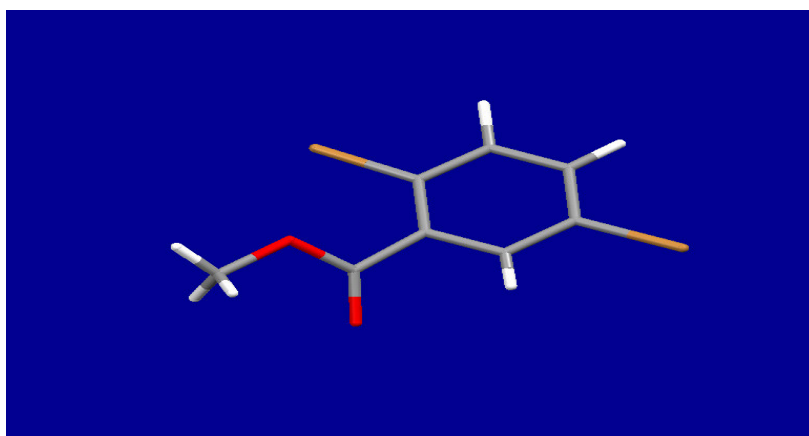


Figure 6.1.1: Methyl 2,5-dibromobenzoate

An added benefit of selecting this molecule was that its crystal structure was previously unknown, so all studies on this molecule including its initial crystallisation, while linking in with previous work would give a new understanding of the solution behaviour as well as revealing its solid-state structure and packing. All molecules behave differently in solution so all solution studies on this new system had to be carried out as for the first case study presented in Chapter 4, using the same techniques and instrumentation, to see any changes in behaviour that may occur. Due to the low melting point value of 48-51°C for MDBB, dissolution and metastable zone width studies were carried out from 20 to 35°C, at 5°C intervals as before. This resulted in a narrower range of study than before but was carried out to the same

accuracy. It was also decided to study a mixed solvent system, in this case ethanol and water, to decrease the concentrations of the solutions used. MDBB is soluble in ethanol but not in water and it was hoped that the presence of this antisolvent would help produce good quality crystals for analysis.

The wavelength range used in the ATR-UV studies was 200 – 270nm as the maximum UV absorbance occurs at ~ 237nm. This is smaller than that used for pMHB. For the calibration stage, five solutions were set up; 3%, 7%, 12%, 16% and 20% w/w MDBB/solvent (Figure 6.1.2). The temperature was ramped from 20°C at a rate of 1° every 6 mins up to 35°C. This enabled a suitable mixing time and accurate measurements using the ATR-UV could be taken. As before, this was crucial as unknown concentrations were assessed against these calibration results at each temperature during the dissolution and metastable zone width experiments.

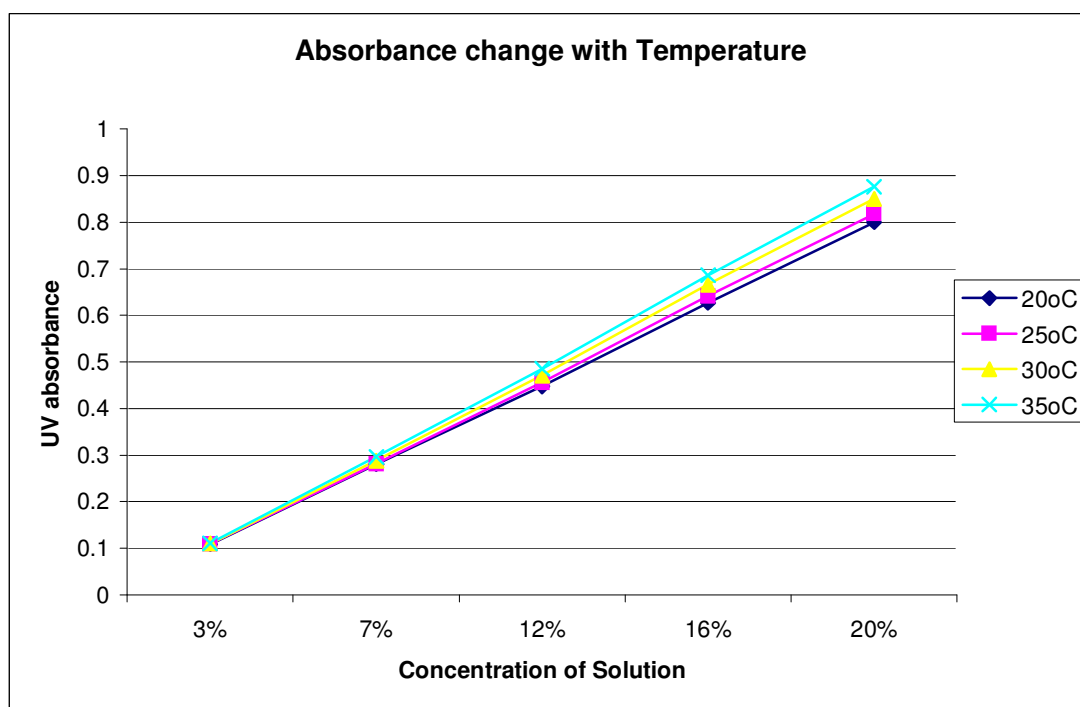


Figure 6.1.2: The absorbance changes for each calibration solution as a function of temperature.

The dissolution experiments were carried out in 150ml of solvent (1:1 v/v, ethanol : water), generating solubility curves using both out of the bottle and recrystallised MDBB. The process was changed from that of pMHB due to the lower solubility and lower temperature range that could be studied. In this instance, the MDBB was still added before the experiment commenced, however due to the mixed solvent system being studied, the solutions were left at the four temperatures for longer to ensure complete dissolution. Figure 6.1.3 shows the two dissolution curves that were produced, where the blue curve is for straight from the bottle MDBB and the pink curve is using recrystallised MDBB. It is noted that as previously, there is no big difference between these results and therefore either can be used for the MZW determination.

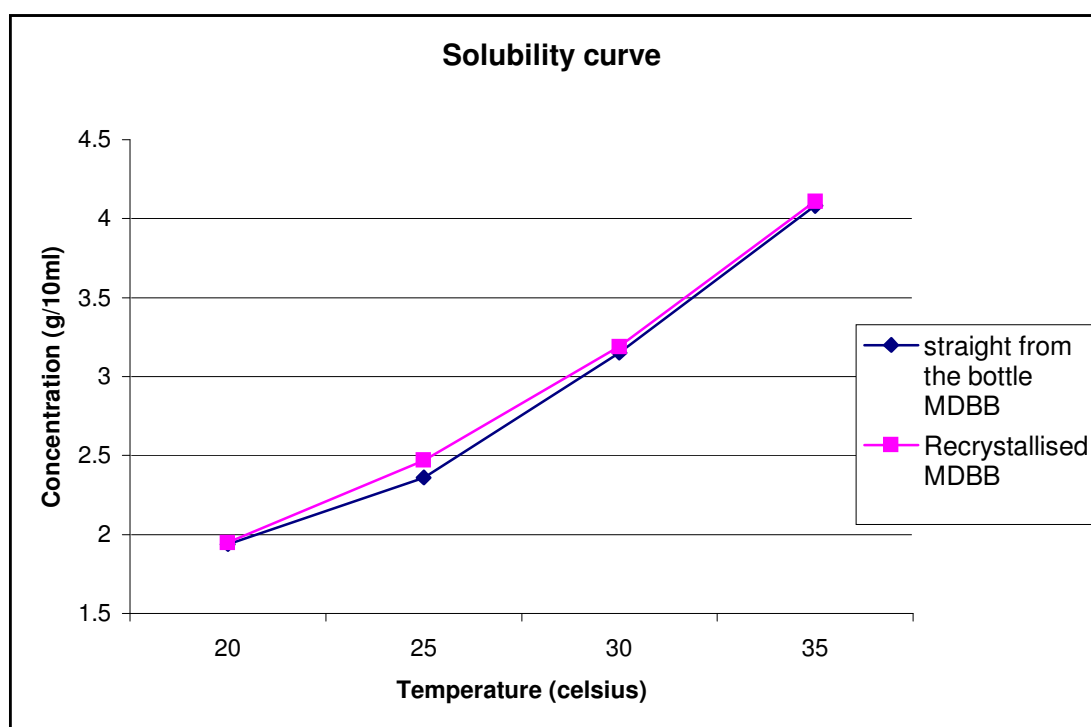


Figure 6.1.3: Solubility curves of MDBB from dissolution experiments.

The concentrations generated from the mixed solvent system were also decreased from the pMHB case and this is highly beneficial for crystallisation purposes considering the large scale of the reactor vessel.

Metastable zone width experiments were carried out based upon these results. Solutions were prepared at each of the temperatures and left to sit in the sealed vessel for two hours to ensure that crystallisation was not going to be spontaneous. The solutions were then cooled at $0.1^{\circ}\text{C min}^{-1}$ until the FBRM detected that particles were emerging from solution. This was noted as the crystallisation point for the experiment, and the MZW was then defined as the area between the solubility curve and the point where crystallisation occurred (Figure 6.1.4).

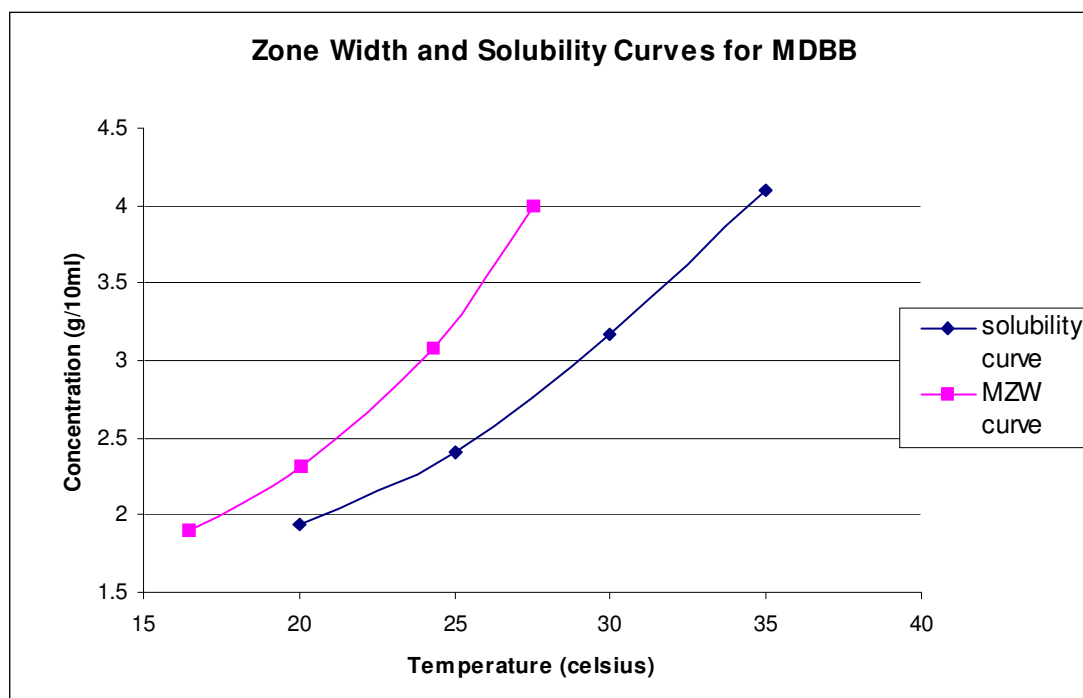


Figure 6.1.4: Solubility and supersolubility curves for MDBB indicating the metastable zone.

It should be noted that the crystallisation profiles for the two test compounds are completely unrelated. The MZW for MDBB is narrower than for that of pMHB, which would indicate that the solution is not as stable *i.e.* that over a shorter time period, crystallisation would be more likely to occur within the metastable zone. This can be explained by the simple notion that for any point within the metastable zone, the distance to the supersolubility curve is less for MDBB than for pMHB and thus any loss of solvent would result in the solution becoming more concentrated and spontaneous crystallisation would be more likely to occur. This, of course, could be anticipated as no two molecules are likely to have similar solution behaviour especially when the crystal structures show them to be completely unrelated.

Crystallisation is a complex process governed by both thermodynamics and kinetics, so therefore it is impossible to predict exactly how these molecules will react in solution and is impossible to have a feel for crystallisation profiles before carrying out the experiments.

6.1.1: Conclusions on MZW Experiments

Throughout the metastable zone width (MZW) experiments, it has been possible to monitor crystallisation *in-situ*; however it should be remembered that this pre-crystallisation work is on the micron scale and crystallisation, and its onset, occurs at much shorter length scales than this. The work carried out during these experiments has generated a new method for monitoring solubility and concentrations in solution. This is a highly advantageous technique that has been developed, as it is now possible to calculate concentration changes as experiments are being carried out without the need for sampling and trying to maintain the sample at the desired temperature. This is of huge benefit in the pharmaceutical industry especially, where solubility studies are of vital importance during the drug development stage. The complimentary techniques of using FBRM and ATR-UV, *in-situ*, provide the further benefit of being able to detect the sizes of particles present in solution, and arguably their shape. This is due to the scanning of the laser over the particles in solution, which detects particle sizes of distinct lengths and separates these in a chord length distribution (CLD) plot. The theory behind being able to analyse shape relies on the assumption that each shape will have varying lengths that will be scanned and identifies the proportionality of each length being scanned by the laser.

This theory has been studied in smaller scale crystallisations⁵¹ and is of importance when monitoring the possible changes in polymorphs (and the associated particle morphology) that can occur. These changes in polymorph that do not affect the solubility in solution would go unnoticed using the technique which has been adopted in this work, however using purely FBRM and detailed analysis it should be possible to determine when relevant shape changes have occurred.

6.2 Structural Studies of Methyl 2,5 dibromobenzoate

One of the reasons that MDBB was chosen was that it had an unknown crystal structure and no studies had been carried out to investigate polymorphism *via* crystallisation with other solvents. A quick solubility study showed that MDBB was soluble in only polar solvents and these results were analysed by X-ray powder diffraction to see if there was any change caused by recrystallisation from different solvents.

Single crystal studies have shown that even though a literature value of the melting point is given as 48-51°C for this compound, it sublimes at room temperature when given enough time. This was observed when carrying out single crystal studies when the diffraction from the crystal seemed to ‘disappear’. When the run was repeated with the crystal attached to the pip with superglue, the same thing occurred, indicating that the disappearance of the diffraction was not due simply to the crystal merely falling off. To prove what was happening some single crystals of MDBB were left on a slide at room temperature and over time these crystals also ‘disappeared’ to indicate that sublimation was occurring.

The diffraction data for MDBB were collected on the Bruker AXS Apex-II diffractometer at 100K and solved and refined using SHELXS⁸⁴ in the WinGX⁸⁵ program. Although it was only possible to collect data on a twinned crystal, from this it was still possible to deduce the crystal structure. The molecule was found to crystallise in the triclinic space group $P\bar{1}$, and cell parameters $a=4(2)\text{\AA}$, $b=7.1682(9)\text{\AA}$, $c=16.0658(16)\text{\AA}$, $\alpha=76.995(3)$, $\beta=89.205(15)$ and $\gamma=84.943(15)$, cell volume = 433.545\AA^3 , with $Z = 2$.

Figure 6.2.1 shows the crystal structure viewed along the a axis and from this it is interesting to notice the halogen contacts involved in the crystal packing. Halogen bonding ($X\cdots O$, $X\cdots N$) has been known to exist for many years and is commonly understood to have the strength of a moderate hydrogen bond (i.e. 4-15 kJ mol^{-1})⁶¹. In this molecule, however, as well as the presence of a $\text{Br}\cdots\text{O}$ halogen bond, there is

also the weaker halogen – halogen ($\text{Br}\cdots\text{Br}$) interaction present. Although this type of interaction is weaker, with no hydrogen bonding possible in this particular case, it is an interesting observation that may indicate this interaction may contribute to the packing in the crystal structure. This could be studied further in the presence of hydrogen bonds to assess whether this is a significant contribution to the structure of the molecule or definitely a secondary interaction.

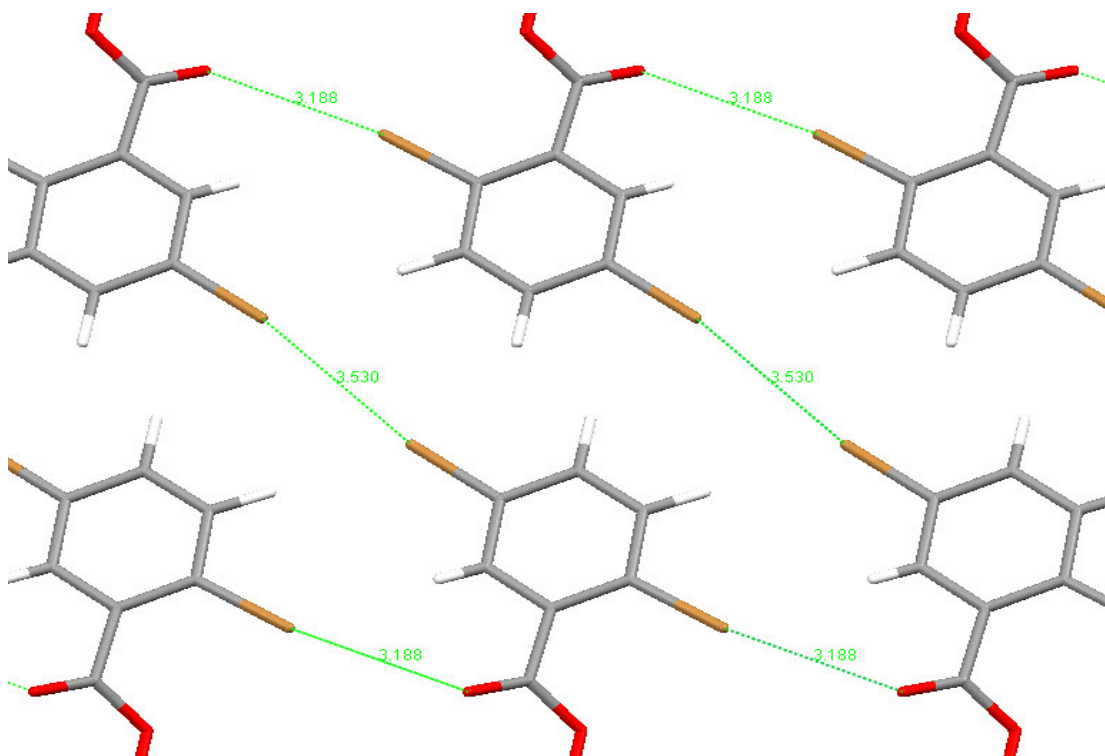


Figure 6.2.1: Crystal structure of MDBB viewed along the a axis, with halogen - oxygen bonds and halogen – halogen interactions highlighted and the distances shown in Å.

While the strength of the interactions were not calculated, by looking at the sum of the van der Waals radii these can be determined to be a close contact and likely to be significant in the absence of any other stabilising interactions. The contact distance of the halogen bond, $\text{Br}\cdots\text{O}$, was measured to be $3.188(2)\text{Å}$, which corresponds to 94.8% of the sum of the van der Waals radii, while the halogen interaction, $\text{Br}\cdots\text{Br}$, is found to be $3.5(1)\text{Å}$, corresponding to 95.4% of the sum of the van der Waals radii. Whilst it is recognised that these contacts are not significantly less than the sum of their

respective van der Waals radii, they are likely to be important and can be further investigated in other studies.

Due to the difficulties in being able to solve the crystal structure from single crystal analysis, XRPD was also carried out for a direct comparison against the powder pattern calculated from the solved single crystal structure. This confirms that the correct structure had been produced – the calculated powder pattern from the structure solved and refined from the twinned crystal at 100K is shown in Figure 6.2.2. When compared with the pattern collected from the powder sample on the Bruker AXS D8 diffractometer at room temperature, it can be seen that the two patterns generally match well. There is some indication of splitting of peaks from the predicted pattern, but this is known to occur for some peaks during the temperature range of 100 – 300K due to lattice expansion and is not a significant effect in this case. The first five peaks from the predicted pattern correspond almost perfectly with the first five peaks from the pattern collected experimentally and thus a close correspondence is observed. This supports the conclusion that the correct crystal structure has been solved even though it was from a twinned crystal.

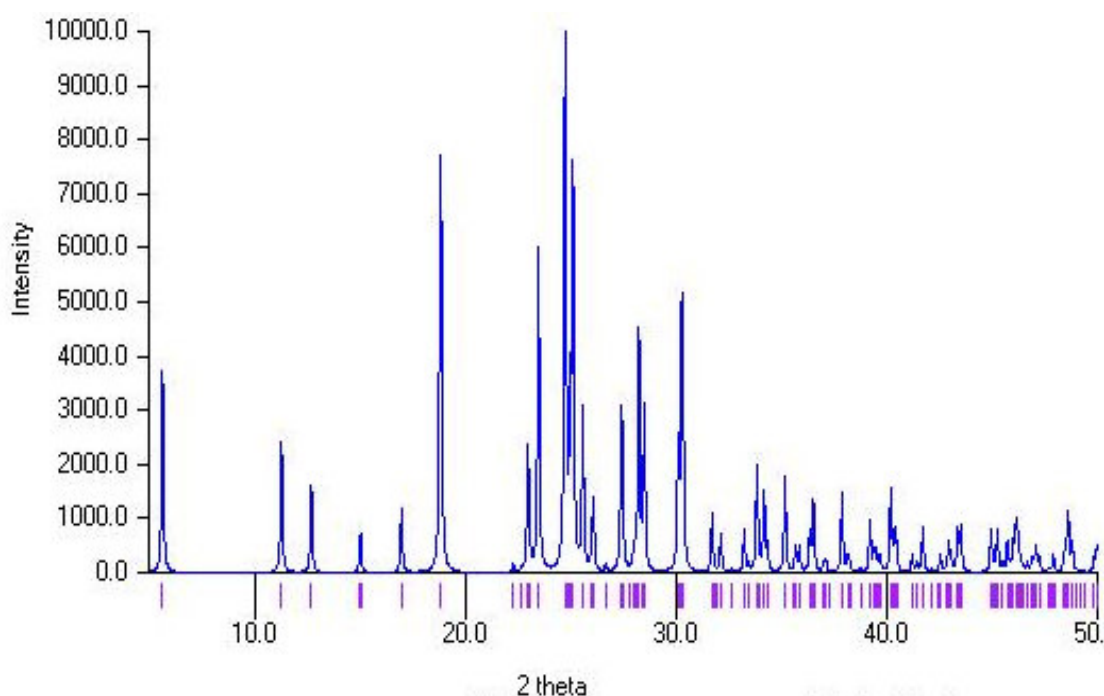


Figure 6.2.2: Predicted powder pattern of MDBB calculated from the crystal structure solved from the twinned crystal at 100K.

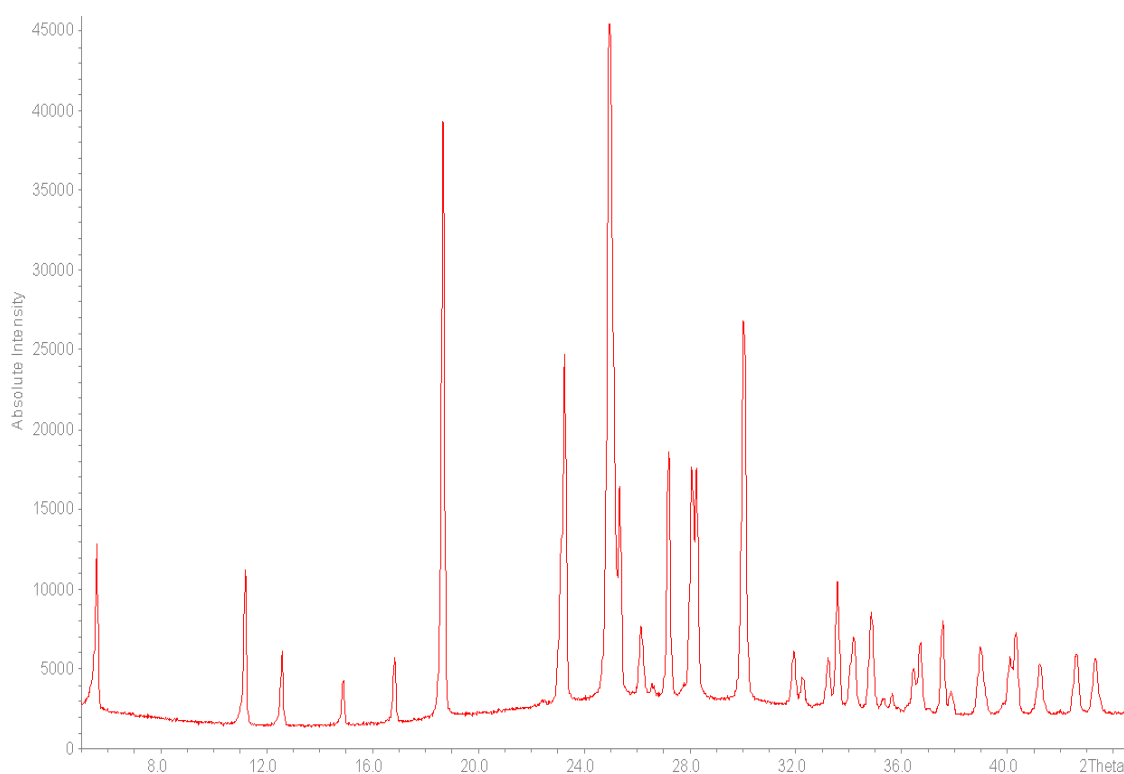


Figure 6.2.3: Powder pattern of MDBB collected at 300K.

6.3 Preliminary SAXS studies of 2-bromobenzoic acid

During the beam time that was granted at Daresbury on Station 2.1, SAXS studies of 2-bromobenzoic acid were carried out. This sample was chosen as a substitute to the planned system, due to the fact that the concentrated solutions of methyl 2,5-dibromobenzoate that were prepared tended to crystallise whenever a sample was taken from the stock solution and prior to SAXS studies commencing on the beamline. Concentrated solutions of 2-bromobenzoic acid were thus used as an alternative sample. The choice of 2-bromobenzoic as an alternative to MDBB revolves around the fact that the compound is known to crystallise in the carboxylic acid dimer motif (Figure 6.3.1) and also contains a heavy (Br) atom, which was the prerequisite following on from the initial studies carried out on methyl 4-hydroxybenzoate, with the aim of enhancing the X-ray scattering in the system due to the presence of the heavier Br atom.

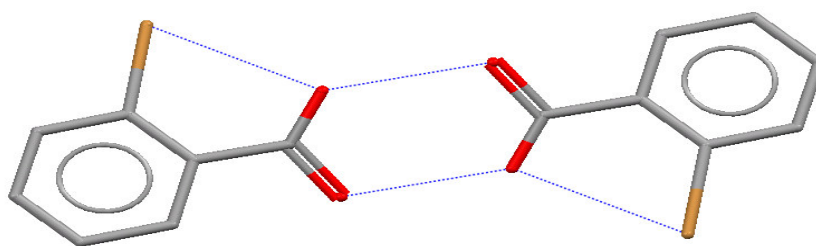


Figure 6.3.1: Typical dimer of 2-bromobenzoic acid, with hydrogen bonds and halogen bonds labelled in blue⁸⁸.

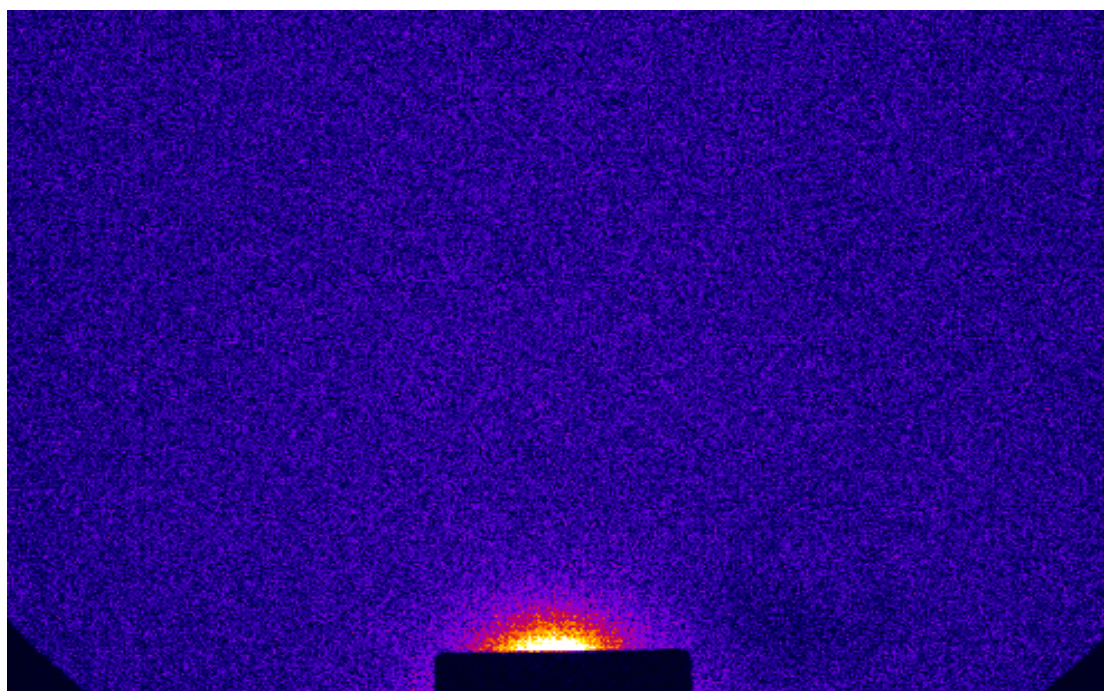


Figure 6.3.2: Scattering profile of MDBB.

SAXS studies were carried out using the identical method as for pMHB described in section 4.3. Figure 6.3.2 shows the scattering profile from the 2-bromobenzoic acid solution. From this it is easily noticeable that, as before, the scattering produced from the solution is focussed at very small angles around the beam stop and for this reason

analysis is not easy to carry out. The programs that are routinely used for the analysis of protein solutions were again used, including Fibrefix, GNOM and Primus, which are all available on line through the web-site of their author, Dmitri Svergun⁴³. Unfortunately due to the weak scattering that was produced from the solutions studied, in depth analysis was not possible using these programs, especially considering that such a small molecule system was being investigated.

It was however, possible to notice the overall changes in the scattering being observed from the pure methanol solution compared with that from the pMHB (Chapter 4) and 2-bromobenzoic acid solutions. Our hypothesis was indeed correct in suggesting that increased scattering would be observed from the 2-bromobenzoic acid solution due to the heavy atom present. This is shown in Figure 6.3.3 where the scattering profiles are overlaid, with obvious increases in scattering evident for the systems with solute present.

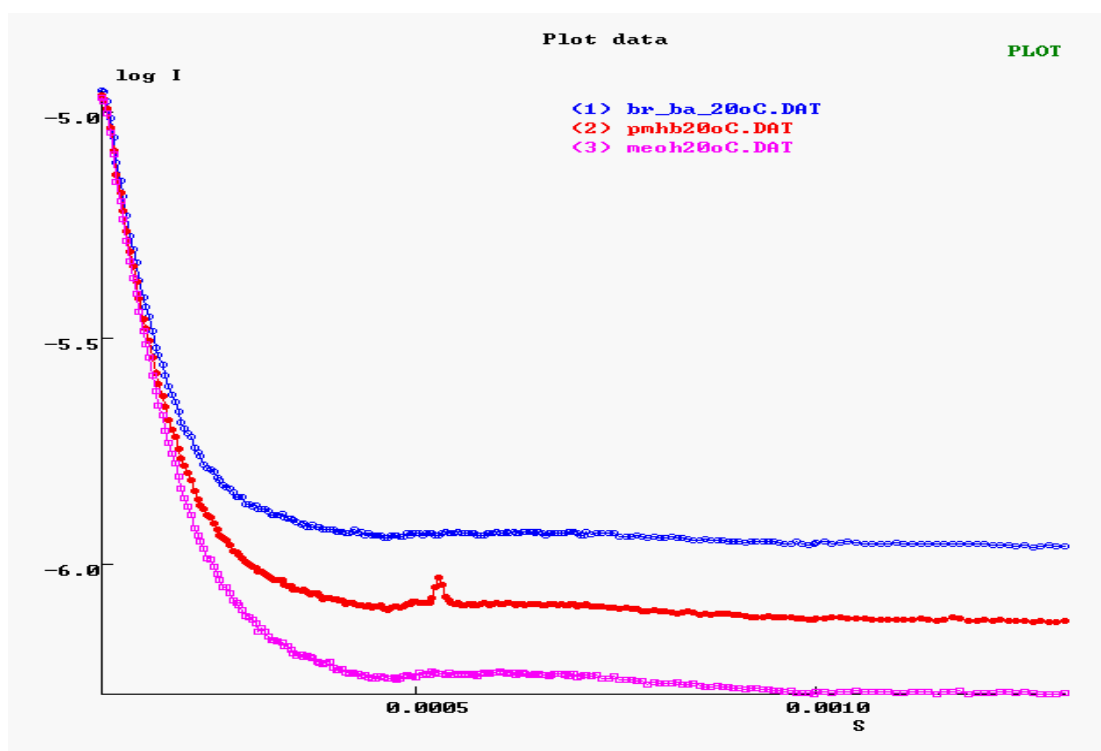


Figure 6.3.3: Scattering profile measured on Station 2.1 showing variations between the scattering from solutions of the two molecules investigated (2-bromobenzoic acid

in blue, pMHB in red, both in methanol solvent) and the control (methanol solvent-only) experiment (in pink).

It can be easily observed from this graph that the scattering patterns cannot overlay perfectly. This is due to the increased scatter observed for the solutions with solute present. The profile for the 2-bromobenzoic acid shows differences even at lower angle. The slope of the peak is seen to vary more significantly than for pMHB. This is as expected due to the presence of the bromine atom in the molecule being studied, however, even with this increased observed scattering, attempting to deduce any structural information from this was not possible with the analysis tools available.

One observation from the 2-bromobenzoic acid study that was not present in the pMHB study, was that of a slight temperature effect; it is not clear how important this may be. One of the initial hypotheses underlying this work was that prior to crystallisation, the particles in solution would become more ordered and increase the scattering from solution – this may be expected to lead to an increase in scattering as the temperature is lowered, potentially inducing more crystallisation. This turned out not to be the case in our experiments, during which crystallisation did not occur. However there is a small change observed in the scattering profiles of the 2-bromobenzoic acid solution between 10 and 20°C. This is shown in Figure 6.3.4 and can perhaps be attributed to changes in kinetics and thermal motion. It is to be expected that at higher temperatures particles move about a lot more than at lower temperatures and although the temperature change in this case is just 10°C this may explain the differences in scattering.

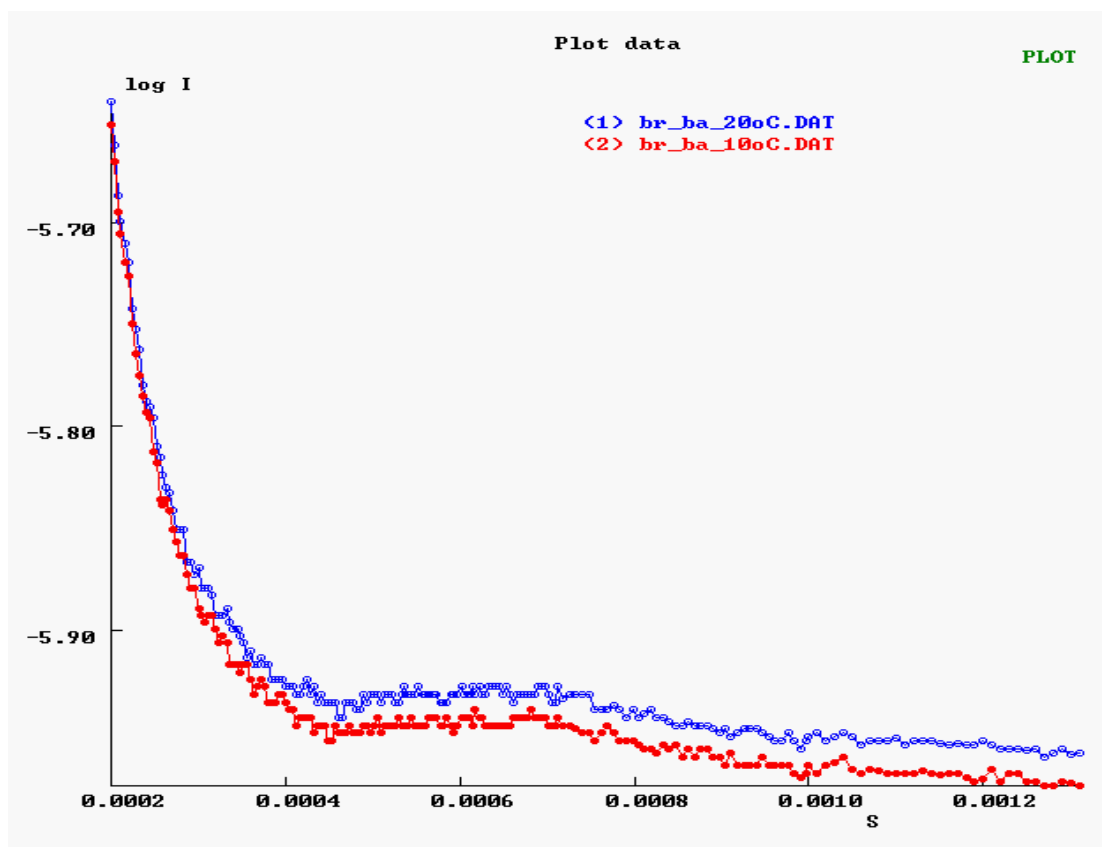


Figure 6.3.4: Scattering profile showing the variations in scattering of 2-bromobenzoic acid with temperature, with the increase between 10°C (red) and 20°C (blue) evident.

6.3.1: Conclusions

Through the SAXS studies that have been carried out it has been possible to observe scattering from the solutions containing our test molecules. This is a significant achievement considering the size of the molecules involved in the study and the shortage of studies carried out in this field to date. It is of course, a disappointment that there has not been an opportunity to get any structural information from the observed scattering, however this would require extra specialist analysis programs that are not currently available. Differences in the small angle liquid scattering for 2-bromobenzoic acid have however been observed as a function of temperature and this requires further investigation.

Chapter 7: Co-crystals of Brominated Compounds.

I. Bromanilic acid with picolines

7.1: Methyl 4-bromobenzoate

The structural studies of methyl 2,5-dibromobenzoate (Section 6.2), showed that halogen – halogen interactions and the stronger Br \cdots O halogen bond were present in the crystal structure. The related methyl-4-bromobenzoate was studied to examine whether these interactions were more significant in the absence of other ‘stronger’ interactions.

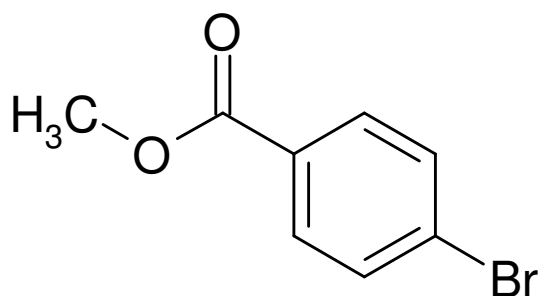


Fig 7.1.1: Methyl-4-bromobenzoate

The structures of the iodo- and chloro- analogues of methyl-4-bromobenzoate have previously been studied, although there are no three dimensional coordinates available for the chloro analogue⁸⁹, the iodo- has been solved by means of single crystal diffraction⁹⁰. The iodo- substituted derivative was found to crystallise in the Pbc_a space group and was found to contain I \cdots O halogen bonds, but no halogen – halogen interactions. The halogen bonds formed have a length of 3.203(4)Å and a C-I \cdots O angle of 172.5(2)°. This is equivalent to 91.5% of the sum of the van der Waals radii.

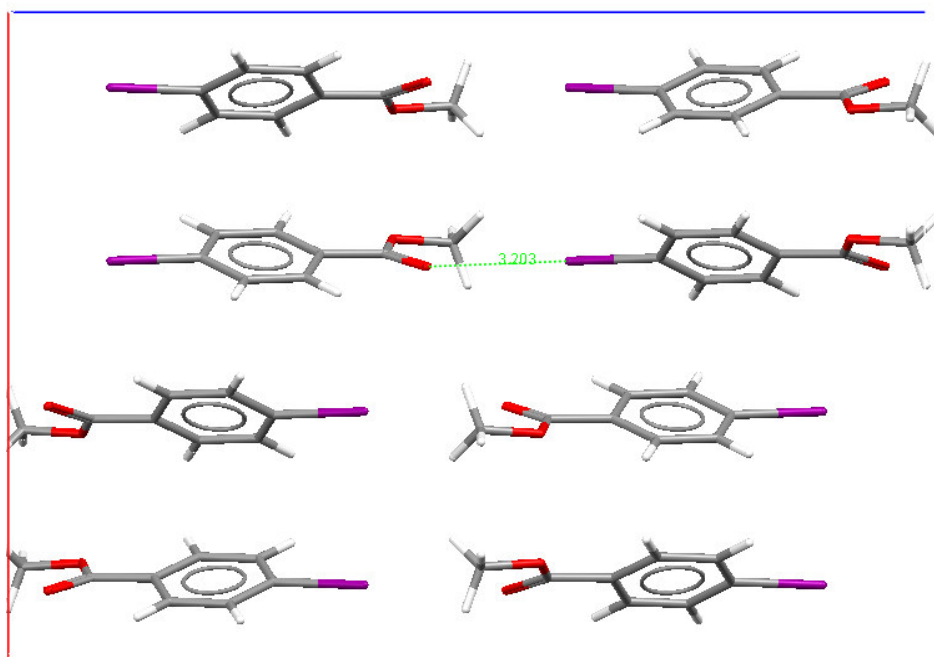


Fig 7.1.2: Crystal structure of methyl-4-iodobenzoate viewed along the *b* axis, with an O...I halogen bond highlighted.

A systematic recrystallisation study was carried out on methyl-4-bromobenzoate using a variety of solvents and conditions and analysed using XRPD to assess the possibilities for polymorphism.

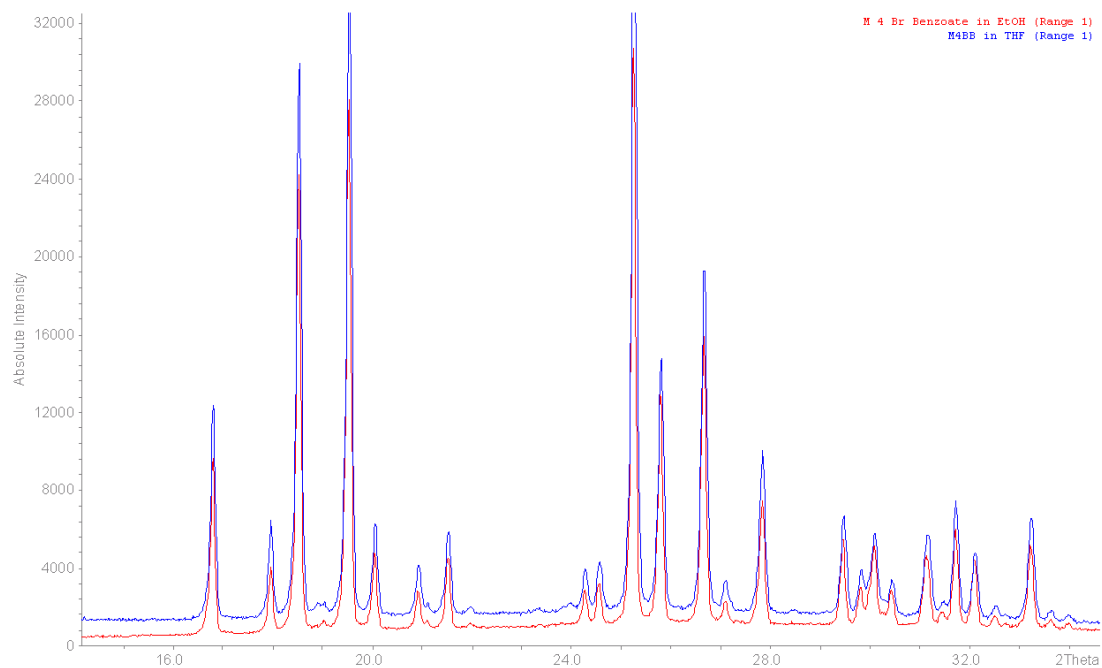


Fig 7.1.3: Overlay of representative XRPD patterns of methyl-4-bromobenzoate collected from samples recrystallised from different solvents.

Figure 7.1.3 shows an overlay of two data sets collected on a Bruker AXS D8 powder diffractometer. This clearly shows that although intensities may vary, that each peak is accounted for in both patterns. Only two patterns have been overlaid here to make it simple to notice the similarities between the patterns, however many more patterns were collected and all contain the same peaks, which would indicate that there is only one form present.

Following on from this initial analysis, a variable temperature single crystal X-ray diffraction analysis was carried out. The crystals were grown at room temperature using the slow evaporation technique from methanol solvent. Data were collected on a Bruker AXS Apex II diffractometer. The structure was solved using SIR⁸² within CRYSTALS⁸³ and refined using SHELXL⁸⁴. It was found to crystallise in the orthorhombic *Pbca* space group, with $Z = 8$, at all the temperatures that were investigated. Structures were solved every 50K between 100 and 300K so that analysis over a wide temperature range could be carried out.

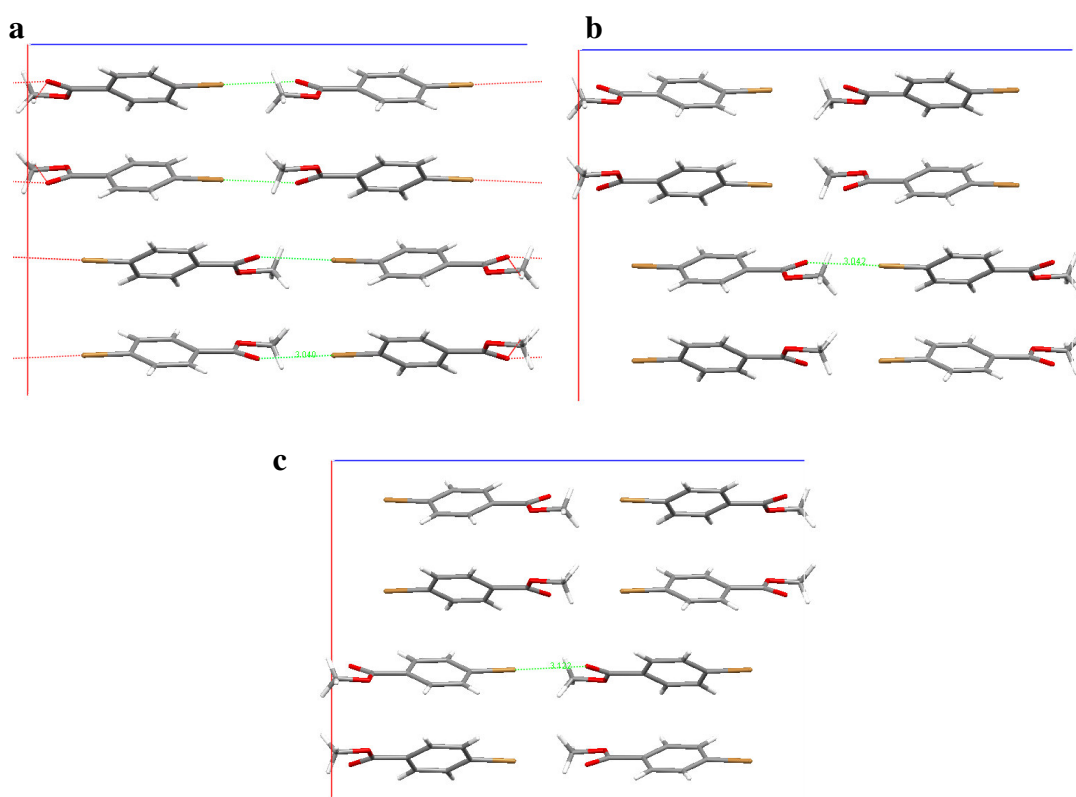


Fig 7.1.4 a-c: Crystal structures of methyl 4-bromobenzoate viewed along the *b* axis produced at 100, 200 and 300K respectively, with the halogen bond highlighted.

Figure 7.1.4a shows the crystal structure and packing of methyl-4-bromobenzoate along the b axis at 100K. This packing motif is the same across the temperature range studied and no phase transition was observed. The only variation is in the length of the bromine – oxygen contact. In the absence of hydrogen bonding in this system, halogen bonding is the strongest interaction present. At 100K, the Br \cdots O halogen bond measures 3.040(2)Å and represents 90% of the sum of the van der Waals radii, and the C-Br \cdots O angle was found to be 172.1(1)°. The length of this interaction varies as a function of temperature and is elongated to 3.122(3)Å at 300K, this however still represents 92.6% of the sum of the van der Waals radii with the C-Br \cdots O angle found to be 173.1(1)°.

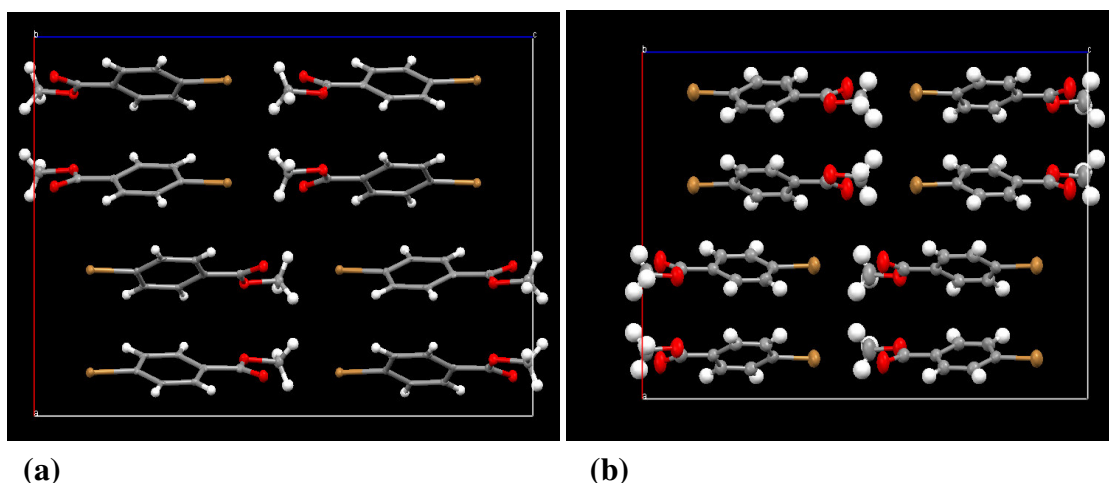


Figure 7.1.5: The variation of the thermal ellipsoids at 100K(a) and 300K(b) for methyl-4-bromobenzoate indicating that although the precision of the structure remains similar, the thermal motion, specifically around the methyl hydrogens increases considerably as would be expected for a librating methyl group.

The crystal structure is isostructural with that of the iodo derivative and shows no signs of polymorphism. During this study the crystal structure was published from a determination at 173K⁹¹ and is found to be in close agreement with the data we collected at 200K. The published halogen bond distance measures 3.047(3)Å and the C-Br \cdots O angle is 172.3(1)°. This study indicates that in the absence of hydrogen bonding, halogen bonding interactions are important intermolecular interactions in the stabilising of the crystal structure. The crystallographic data from the variable temperature study is available in Appendix 2.

7.2: Co- crystallisations of Bromanilic Acid – potential intermolecular halogen interactions

7.2.1: Introduction to bromanilic acid

Bromanilic acid belongs to a family of widely used and studied anilic acids with importance in organic synthesis⁹² and also widely studied in for its ferroelectric properties⁹³. It is the aim of this part of the project to examine the possibilities for potential uses in crystal engineering, due to the ability of bromanilic acid to hydrogen and halogen bond readily.

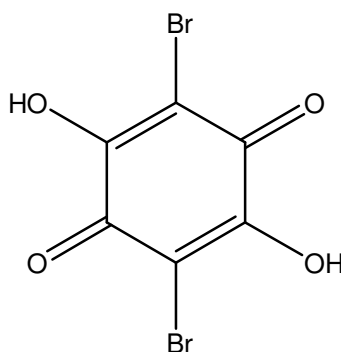


Fig 7.2.1: A schematic diagram of bromanilic acid, systematic name: 2,5-dibromo-3,6-dihydroxyl-1,4-benzoquinone.

Bromanilic acid, unlike other members of its family, is soluble in many solvents and crystallises mainly in deep purple cuboidal shapes. It is possible for bromanilic acid to co-crystallise with target molecules and lose either one or two protons to an acceptor on another molecule in a similar way to that seen for the related chloranilic acid^{92,94}. In studies carried out to date, there is only two examples of complete hydrogen atom transfer from both hydroxyl groups of the bromanilic acid molecule^{92,95}.

Robl solved the crystal structure of bromanilic acid from X-ray diffraction data in 1987⁹⁶ and it was found to crystallise in the space group $P2_1/n$. The most interesting characteristic of the crystal structure is that each bromanilic acid molecule has four hydrogen bonds to four separate bromanilic acid molecules. This without doubt is the

most stabilising interaction in the crystal structure with other weaker interactions such as Br \cdots Br being formed a result of the former interactions. The hydrogen bond formed is a moderate strength O-H \cdots O interaction and these are formed from each oxygen atom in the crystal structure (O \cdots O distance 2.781Å, O-H \cdots O angle 147.55°). The Br \cdots Br close contact of 3.434Å is measured as being 92.8% of the sum of the van der Waals radii.

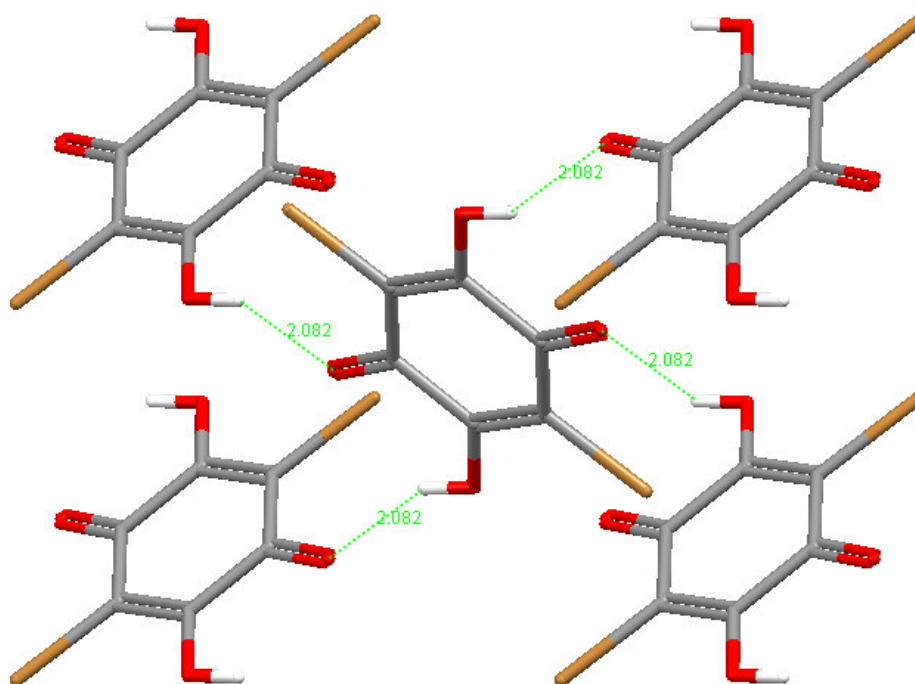


Figure 7.2.2: Crystal structure of bromanilic acid viewed along the *c* axis showing the four hydrogen bonds that are present from each bromanilic acid molecule⁹⁶.

Bromanilic acid has high potential for co-crystallisation due to the many routes by which it could potentially form intermolecular interactions to strengthen a crystal lattice. The obvious main routes would be through hydrogen bonding, with the ketone and hydroxyl groups present and there is a strong possibility of forming bifurcated hydrogen bonds as seen for the related chloranilic acid⁹⁷. The larger halogen atoms Br and I are known to form close contacts with themselves or with atoms such as oxygen, whereas F and Cl are more likely to interact with hydrogen atoms. Studies have shown that Cl \cdots Cl interactions are longer than Br \cdots Br interactions⁶⁰ thus backing this theory. For this reason it would be suggested that there should be a greater deal of halogen bonding, Br \cdots O, and halogen – halogen interactions, Br \cdots Br,

than in the associated chloranilic acid co-crystal compounds. There is also the possibility of halogen bonds and many other weaker interactions including $\pi - \pi$ stacking interactions. Hydrogen bonds are directional interactions and can be distinguished in their strength in the range of angles ($\angle D-H \cdots A$) between strong ($\sim 180^\circ$) and weak cases ($>90^\circ$). Due to the significant hydrogen bonding capability there is also the likelihood of solvates, most significantly hydrates, forming during co-crystallisation studies⁹⁸.

There are two instances of bifurcated hydrogen bonding involving bromanilic acid. Both of these instances are found in the same study carried out by Zaman *et al.*⁹². The first of these, a co-crystal complex of bromanilic acid with bis(4-(2-pyridyl)pyridinium) forms a three molecule interaction in a two to one ratio of the pyridinium to bromanilic acid. This results in deprotonation on both sides of the bromanilic acid and bifurcated hydrogen bonds forming. The second of these involves a co-crystal of bromanilic acid with ethyne-1-(4-pyridyl)-2-(4'-pyridinium) also in a two to one ratio as previously. This time however deprotonation only occurs on one side of the bromanilic acid.

Interestingly, on further examination of the CSD there are also two instances of $Br \cdots O$ halogen bond interactions^{92,99} with interactions of 3.190 and 3.251 Å, which are both shorter than the sum of the van der Waals radii of 3.37 Å. Zaman *et al.*⁹² show the complex interactions surrounding the anilic acids. Their study focuses on the co-crystallisation of 2,2'-bipyrimidine with cyanilic acid, chloranilic acid and bromanilic acid. The chloranilic acid and bromanilic acid co-crystal structures are both stabilised by hydrogen bonding from water molecules and interestingly both generate halogen – halogen interactions. These studies do not emphasise the significance of halogen bonding which has been found to be significant in previous crystal structures.

Bromanilic acid is soluble in a wide variety of solvents, which enables a variety of conditions to be used throughout the studies. Many of these trials were set up using the Microvate ReactarayTM, which allows 12 different temperature conditions to be used in parallel. This enables products to be collected in a much shorter time and screened by XRPD before altering conditions to promote the growth of single crystals.

Co-crystals incorporating bromanilic acid can exist in both 1:1 and 2:1 ratios depending on the experimental set up in terms of the ratio of starting materials, and other factors.

7.2.2: Initial studies of Bromanilic acid

A crystal structure is a compromise between interactions of varying strengths, directionalities and distance-dependence properties. Interactions in an organic crystal are numerous and of a range of strengths, therefore can the effect of hydrogen bonds and halogen bonds be studied in co-crystals with the possibility to contain both? For many years it has been known that there exists three separate types of hydrogen bonding for small molecules. The strengths of these interactions are upwards of 15 kJ mol⁻¹ for the very strong hydrogen bond and 4-15 kJ mol⁻¹ for the moderate hydrogen bonds and <4 kJ mol⁻¹ for weak hydrogen bonds⁶¹. In terms of small molecule crystallography, studies invariably centre around moderate strength hydrogen bonding. The hydrogen bonding in these small molecule systems has been studied for many years and now has an element of predictability associated with it. For this reason, it is the purpose of this work to examine the effect of additional halogen atom interaction capabilities in the construction of the co-crystals studied. This is a topic of great interest in terms of crystal engineering as halogen bonding is known to be a significant non-covalent interaction.

The crystallographic studies reported in Chapter 5 on methyl-2,5-dibromobenzoate, a material which was used in the metastable zone width studies, showed that there were two distinct interactions occurring in the absence of any hydrogen bonding. These were halogen – halogen interactions e.g. Br...Br and halogen bonding interactions e.g. O...Br; the latter of these is predominant and known to be comparable in strength to that of weak hydrogen bonds⁶⁰.

Co-crystallisation of bromanilic acid with a series of co-molecules has been used to try and monitor and possibly engineer these close halogen bonding interactions even in the presence of hydrogen bonding. These close halogen contacts have the potential to play a significant role in the crystal structure especially where only weak hydrogen

bonding is found to occur. Hydrogen bonding and possible halogen bonding patterns were evaluated with the aim of prediction of certain patterns that are likely to occur in related crystal structures.

Previous studies involving the related chloranilic acid show a significant number of Cl...Cl interactions and also the presence of halogen bonding interactions with both nitrogen atoms and oxygen atoms indeed both are found in the co-crystal structure of chloranilic acid and piperazine-2,5-dione¹⁰⁰. Indeed the crystal structures of pure chloranilic acid, and indeed the hydrated form, are found to contain Cl...Cl interactions^{101,102}. In related studies involving the co-crystallisation of chloranilic acid with the family of picolines there appears to exist a relationship between the ratio and the packing sequence. It has been found that the 1:1 chloranilic acid (C) : picoline (P) structures tend to form a P:C:C:P type structure, whereas the 1:2 structures tend towards P:C:P due to the hydrogen atoms being transferred from both hydroxyl groups of the bromanilic acid^{94,103}.

A systematic co-crystal study of bromanilic acid and a family of compounds, picolines and lutidines was thus completed in this work, to see if any halogen interactions were present and determine whether there were any cases in which it could be a short enough contact to compete with any hydrogen bonding involved.

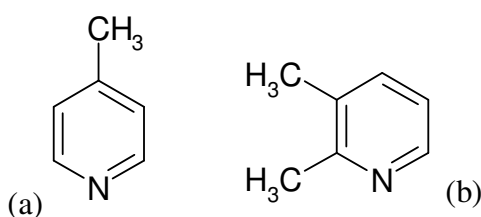


Fig 7.2.3: An example of a picoline and a lutidine molecule, in this example (a) 4-picoline and (b) 2,3-lutidine.

The molecules studied are all related and it is merely the positions of the methyl groups in the isomeric picolines and lutidines that vary. The main interactions expected in these co-crystal compounds would be hydrogen bonding between the nitrogen of the ring and the hydroxyl hydrogens on the bromanilic acid with only weak halogen interactions present if any at all. This could be altered by the presence of a halogen on the secondary molecule to compete for the interaction around the

hydroxyl group of the bromanilic acid molecule. Following on from this study it was decided to investigate whether the presence of a bromine atom on the 2nd molecule involved in the co-crystal would have any effect on the likelihood of halogen bonding or halogen – halogen interactions occurring. The hypothesis behind this is that by involving a halogen atom in the 2nd molecule this will enable competition between hydrogen bonding and halogen bonding, with the added possibility of halogen – halogen interactions between the bromine atoms.

Picolines, (chemical formula C₆H₇N) come in three isomeric forms, 2-, 3- and 4-picoline. They are all colourless liquids with a strong smell and have a high affinity for protons. For this reason it was hypothesised that hydrogen bonding would occur with the hydroxyl group after extracting a H atom and/or possibly forming a bifurcated hydrogen bond with a second interaction to the ketone group as well. This was anticipated to be the major stabilising interaction in the 2:1 co-crystal compounds studied, however in the 1:1 co-crystal studies it was suspected to be more likely that competing interactions from halogen bonding would occur.

Before commencing the co-crystal study, single crystals of bromanilic acid were grown from methanol by the slow evaporation method. Data were collected on a Bruker AXS Apex II diffractometer at 100 K and solved using SHELXS⁸⁴ using direct methods. The structure was refined using CRYSTALS⁸³ and found to crystallise in the monoclinic P2₁/c space group, with cell parameters of $a=5.4365(5)$ Å, $b=7.3128(6)$ Å, $c=9.5880(8)$ Å and $\beta=99.435(6)^\circ$, and a cell volume of $376.02(6)$ Å³. This was found to be in agreement with previously published data⁹⁶.

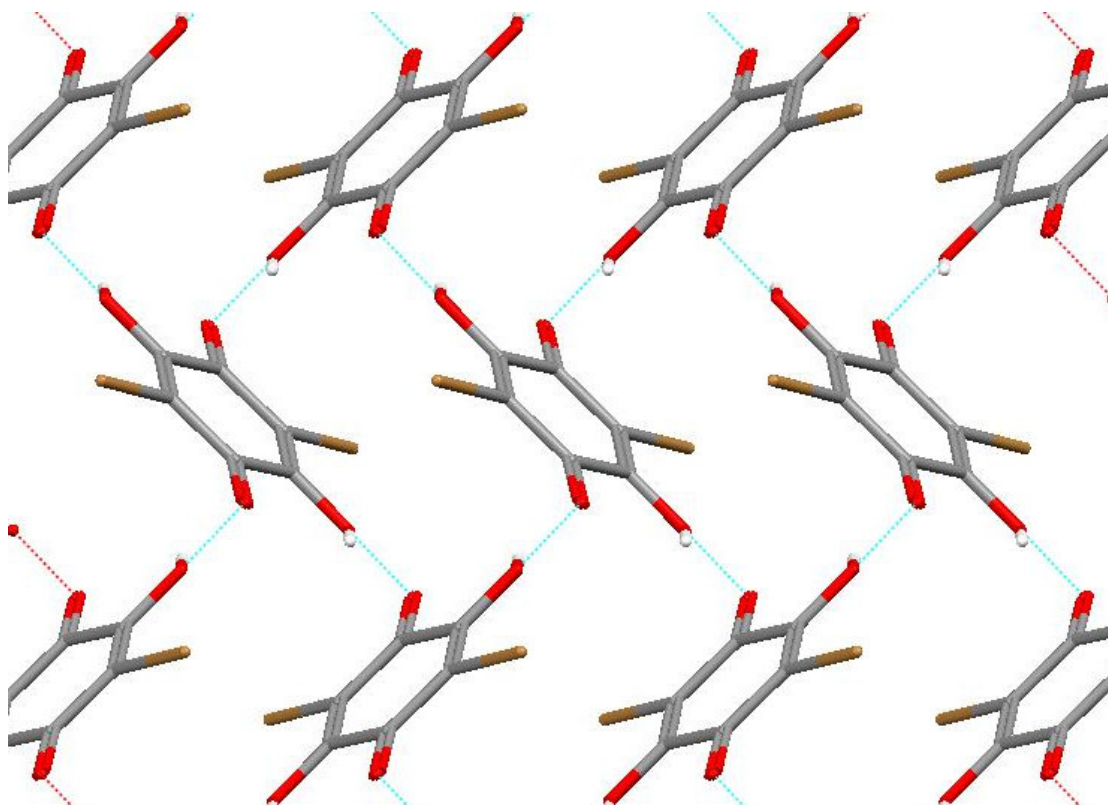


Fig 7.2.4: Crystal structure of bromanilic acid collected at 100K. Close contacts are shown with dashed lines.

Figure 7.2.4 shows the crystal structure of bromanilic acid with the hydrogen bonding extended. The hydrogen bonding is of the moderate variety forming zigzag chains of bromanilic acid molecules, which are highly symmetrical. For this reason, the full three-dimensional structure is held together by hydrogen bonding and any other close contacts are constrained to be present by these interactions. This initial survey of solvent and temperature crystallisation conditions yielded only one product and this indicated that no hydrates should be expected.

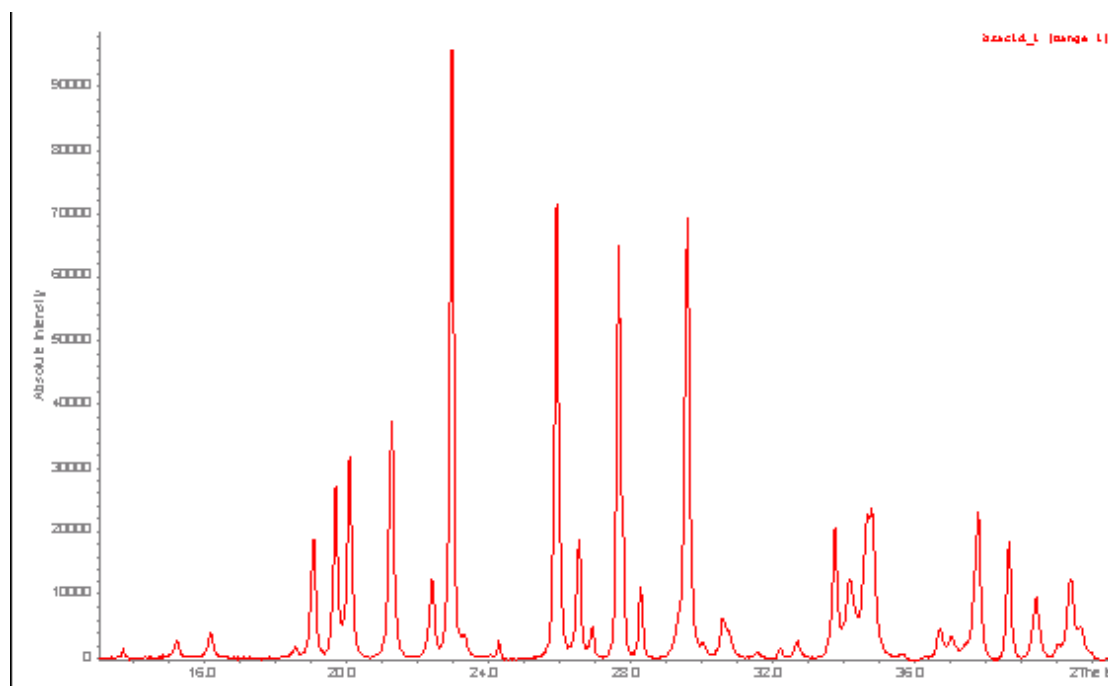


Figure 7.2.5: XRPD data from recrystallised sample of bromanilic acid

7.3: Co-crystallisation Studies of Bromanilic acid and Picolines

Co-crystallisation experiments were carried out using 2-, 3- and 4-picoline using a series of solvents and temperature regimes. Co-crystallisations were carried out attempting to crystallise in both 1:1 and 2:1, picoline : bromanilic acid ratios. All solid materials were initially characterised by XRPD. The co-crystallisations in this case used a liquid material as a second component. In spite of this, the XRPD patterns of the initially solid materials are crucial in such studies as this is always the first check when assessing whether a new co-crystal has been produced. The bromanilic acid spectra collected allows initial comparison with powder data collected from the co-crystals and this can indicate if bromanilic acid was crystallising out as the product, a valid and useful conclusion even in the absence of powder data for the other co-crystal molecules. The screening showed that new molecular complexes had been formed and single crystals were selected from these solid products. Single crystal data were collected from all new complexes. Higher quality single crystal data were collected from the 2:1 co-crystals, however the data collected from the 1:1 co-crystals also gave rise to some interesting features.

All crystals unless stated were grown via the slow evaporation method from alcohol solvents at room temperature. These were generated using molar quantities of the two components.

For all the reported structures, data were collected on a Bruker AXS Apex II diffractometer with a CCD detector and graphite monochromated Mo K α radiation ($\lambda = 0.7103\text{\AA}$) at 100K. Structures were solved by direct methods (SHELXS-97⁸⁴) and refined (SHELXL-97⁸⁴) by full matrix least-squares methods, as implemented in the WinGX software package⁸⁵. Absorption corrections were applied. Hydrogen atoms were introduced at calculated positions and refined isotropically.

7.3.1. *Bromanilic acid 3-picoline co-crystal structures*

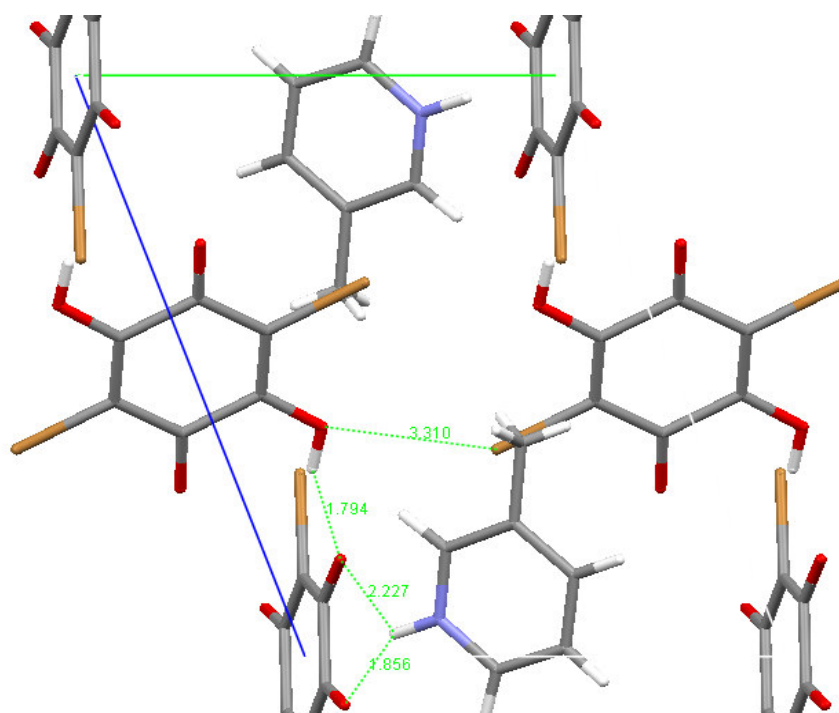


Figure 7.3.1: Crystal structure of bromanilic acid and 3-picoline in a 1:1 ratio viewed down the a axis collected at 100K.

Figure 7.3.1 shows the crystal structure of the 1:1 bromanilic acid and 3-picoline co-crystal collected at 100K. The crystal was grown from a methanol solution containing 10mg bromanilic acid and 31mg 3-picoline to account for the 1:1 ratio. This is a very intriguing co-crystal complex as it bears out the complexity of bromanilic acid due to the many states in which it can exist. It was found to crystallise in the $P\bar{1}$ space group, the complex has crystallised in a one picoline to 0.5 fully protonated bromanilic acid to 0.5 completely deprotonated bromanilic acid ratio. This is possible due to the symmetry of bromanilic acid, however this motif has never previously been generated. This also promotes the idea of salts or co-crystals. In this co-crystal complex one half has been deprotonated and the other remains fully protonated so by definition this could be determined to be a half salt, half co-crystal. To avoid confusion, all such structures will be described as co-crystals to avoid any terminology difficulties.

There is the presence of a bifurcated hydrogen bond between the 3-picoline and the fully deprotonated bromanilic acid molecule with N...O distances of 2.724(2)Å and 2.858(2)Å and angles equal to 148(2)° and 122(2)° respectively (Figure 7.3.2). There are also hydrogen bonds formed from the fully protonated bromanilic acid to the fully deprotonated measuring 2.587(2)Å with an angle of 152(2)° and further more the presence of two Br...O halogen bonds measuring 3.311(2)Å and 3.337(1), which due to the distances involved must be considered to be as a result of the stronger hydrogen bonding interactions rather than as a contributing interaction resulting in extra stabilisation of the crystal structure.

The three-dimensional structure is linked via these halogen bonding interactions, so they do play an important role in the crystal structure. The stabilisation of the deprotonated bromanilic acid molecule comes from the conjugation in the system. This is evident when compared with the C-O bond lengths from the protonated bromanilic acid. In the deprotonated form the C-O hydroxyl bond contracts (1.251(2)Å) and the carbonyl C=O elongates (1.246(2)Å) in comparison to the protonated form (1.316(2)Å and 1.220(2)Å).

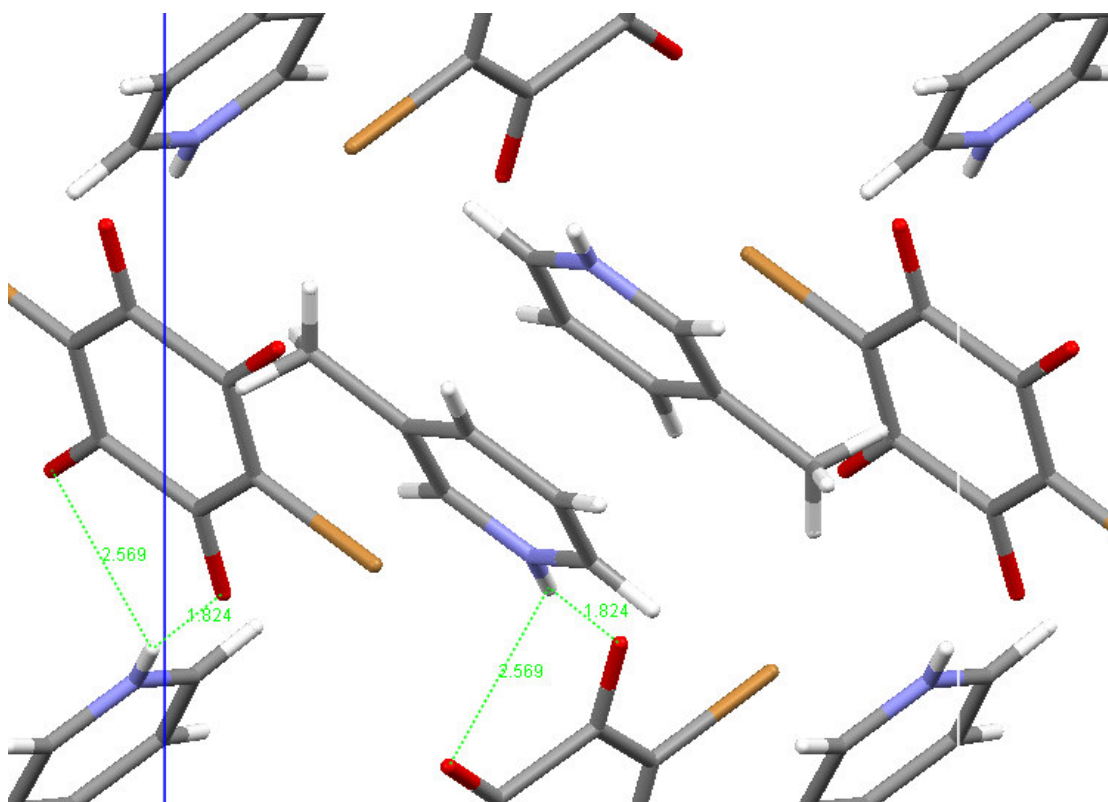


Figure 7.3.2: Crystal structure of bromanilic acid and 3-picoline in the ratio 1:2 viewed down the *a* axis, collected at 100K.

The crystal structure of bromanilic acid and 3-picoline in the 1:2 form was collected at 100K and found to crystallise in the monoclinic form with space group $P2_1/c$. The co-crystal was grown from a methanol solution containing 12mg bromanilic acid and 75mg 3-picoline left to slowly evaporate at room temperature. Due to the presence of two picoline molecules, this can fully deprotonate both sides of the bromanilic acid and it is found that the bromanilic acid exists in the fully deprotonated state and all picoline molecules have been protonated. In this instance only N-H \cdots O(O) bifurcated bonds were found to be present, once again in a major and minor variety. The major interaction, N \cdots O, measures 2.601(1) \AA , with the angle determined to be 168(2) $^\circ$. This follows the same hydrogen bonding motif as found for that of chloranilic acid⁹⁴ and again the bromanilic acid is found to be stabilised through conjugation with C-O bond lengths measuring 1.240(1) \AA and 1.265(1) \AA . In this 1:2 co-crystal compound, the weaker interactions that generate the 3-dimensional crystal structure again appear to involve the bromine with a close contact to the carbon atoms of the bromanilic acid molecule which lies perpendicular to the bromine atom (Figure 7.3.3).

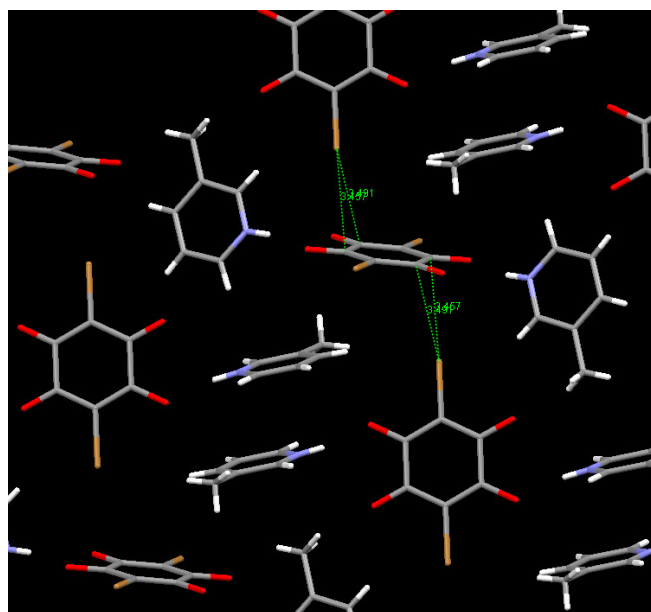


Figure 7.3.3: Close contacts involving bromine and the carbon atoms of the bromanilic acid molecule involved in the bifurcated hydrogen bonding with 3-picoline.

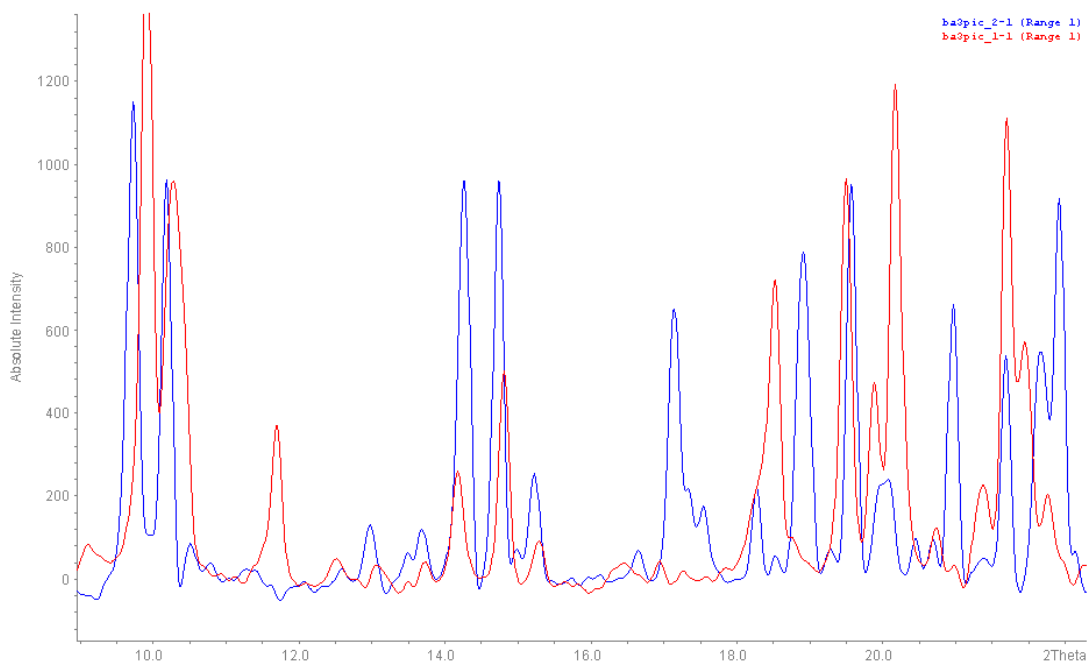


Figure 7.3.4: XRPD data showing the 1:1 and 1:2 co-crystal products of co-crystallisations of bromanilic acid and 3-picoline.

Figure 7.3.4 shows a cropped selection of the powder patterns collected for both the 1:1 and 1:2 bromanilic acid : 3 picoline complexes. These show very little similarity as would be expected considering there is no relationship between the two crystal structures and that the bulk products of both are different.

7.3.2 Bromanilic acid 2-picoline co-crystal structures

Bromanilic acid and 2-picoline only produced high enough quality single crystals in the 1:2 bromanilic acid : 2-picoline form for single crystal X-ray diffraction studies. The crystal used was grown from a methanol and water solution containing 8mg of bromanilic acid and 50mg 2-picoline. The solution was left to crystallise at 5°C and crystals were produced. The single crystal data collected for the 1:1 co-crystal was not of high enough quality to produce a reliable refined structure. As with the 2:1 3-picoline : bromanilic acid co-crystal, the bromanilic acid was found to be fully deprotonated and found to crystallise in the monoclinic $P2_1/c$ space group.

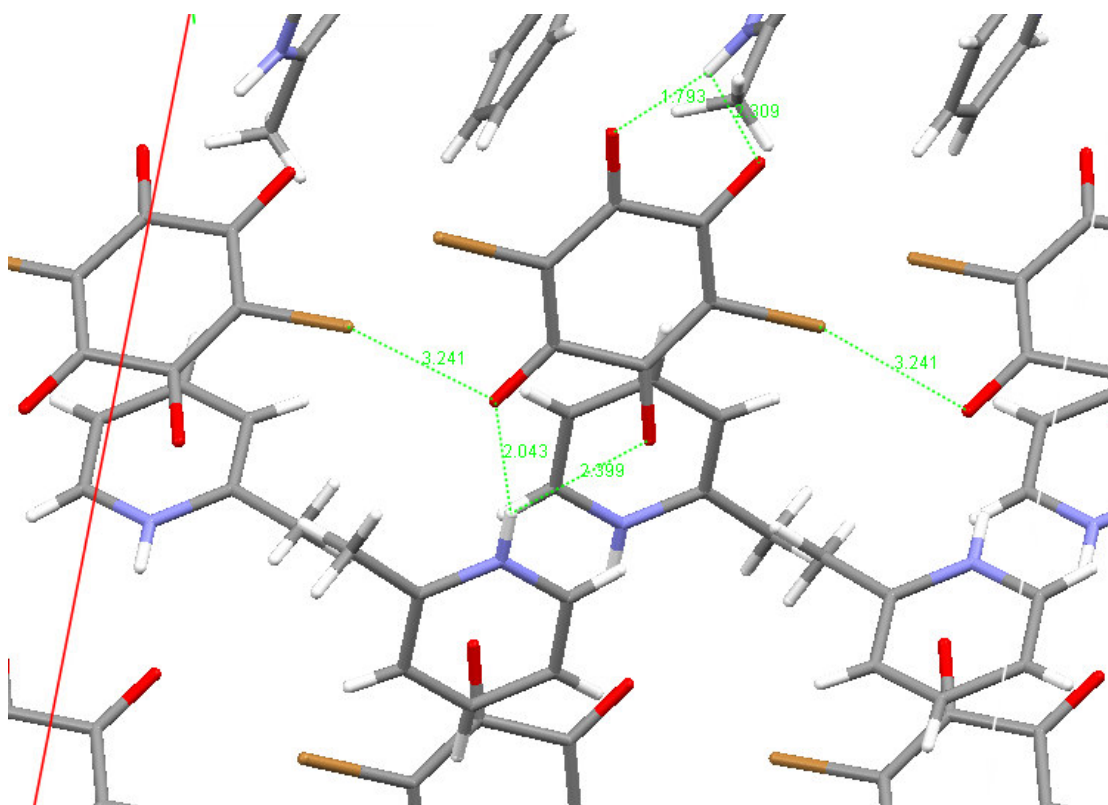


Figure 7.3.5: Crystal structure of Bromanilic acid and 2-picoline in the ratio 1:2 viewed along the b axis, collected at 100K

Once again the predominant interactions are bifurcated hydrogen bonds as a result of the hydrogen transferring over to the picoline molecule (Figure 7.3.5). However in this instance the dominant bifurcated hydrogen bond measures $2.841(4)\text{\AA}$, at an angle of $164(3)^\circ$. The hydrogen bonding incorporated in this crystal structure results in additional halogen bonding, $\text{Br}\cdots\text{O}$, being present in the 2-picoline co-crystal structure where none was visible in the 3-picoline structure. This $\text{Br}\cdots\text{O}$ interaction is of length $3.357(2)\text{\AA}$ and an angle of $162.5(1)^\circ$ and again these halogen bonds are found to be important in producing the three-dimensional crystal structure linking via halogen bonding to the carbonyl group. The conjugation present again helps to stabilise the deprotonated bromanilic acid molecule with C-O bond distances measuring $1.241(6)$ and $1.255(5)\text{\AA}$.

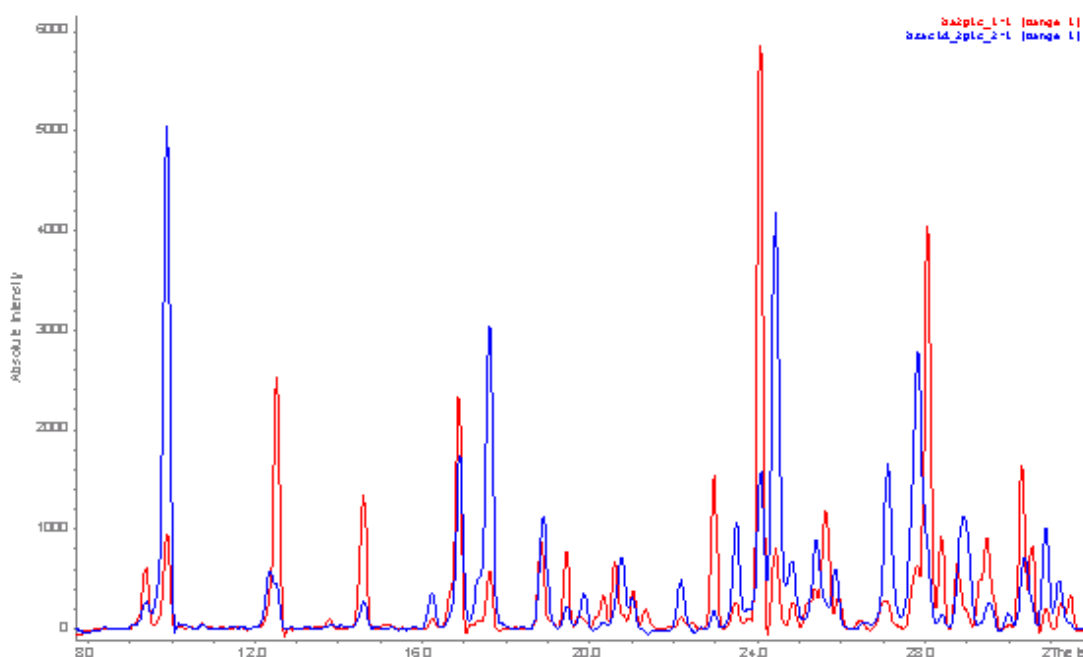


Figure 7.3.6: XRPD data showing the 1:1 and 1:2 bromanilic acid 2-picoline co-crystal products.

Figure 7.3.6 shows the XRPD data collected on result of the recrystallisation trials of both the 1:1 and 1:2 co-crystallisation attempts. From this it can be seen that both patterns show a great similarity to each other and from this it is understandable why only the 1:2 co-crystal structure could be obtained. Though showing marginal

changes, mainly in intensity, the peaks for both the 1:1 and 1:2 crystallisation products show enough to indicate that only the 1:2 product was successfully grown. This shows that even though crystallisations were prepared in a 1:1 ratio, only a 1:2 product was obtained. These trials were carried out in sample vials and further investigations using the Reactarray Microvate™ did not prove to be any more successful in producing the 1:1 complex.

7.3.3. Bromanilic acid 4-picoline co-crystal structures

The final picoline molecule in the sequence, 4-picoline, was successfully co-crystallised in both the 1:1 and 1:2 forms. Both 1:1 and 1:2 crystals were grown from acetone solution at 5°C using the Microvate™. The 1:1 co-crystal in this instance contains all the non-covalent interactions of interest in the study, possibly helped by the methyl group being as far away as possible from the nitrogen on the picoline molecule. In this instance, the bromanilic acid molecule remains fully protonated and unlike the 3-picoline co-crystal structure there is only one type of bromanilic acid present in the crystal structure. This results in essentially only a O-H...N hydrogen bond being present (Figure 7.3.7), however there is also a close contact between the nitrogen and the carbonyl oxygen of the bromanilic acid (3.021(9)Å). The hydrogen bond to the hydroxyl group has an N...O distance of 2.771(9)Å and a reduced angle of 138.1(5)°. There is also the presence of Br...O halogen bonding of 3.263(9)Å, angle 151.1(3)°, and also for the first time halogen – halogen interactions are also observed, Br...Br, of length 3.546(1)Å, representing 95.84% of the sum of the van der Waals radii.

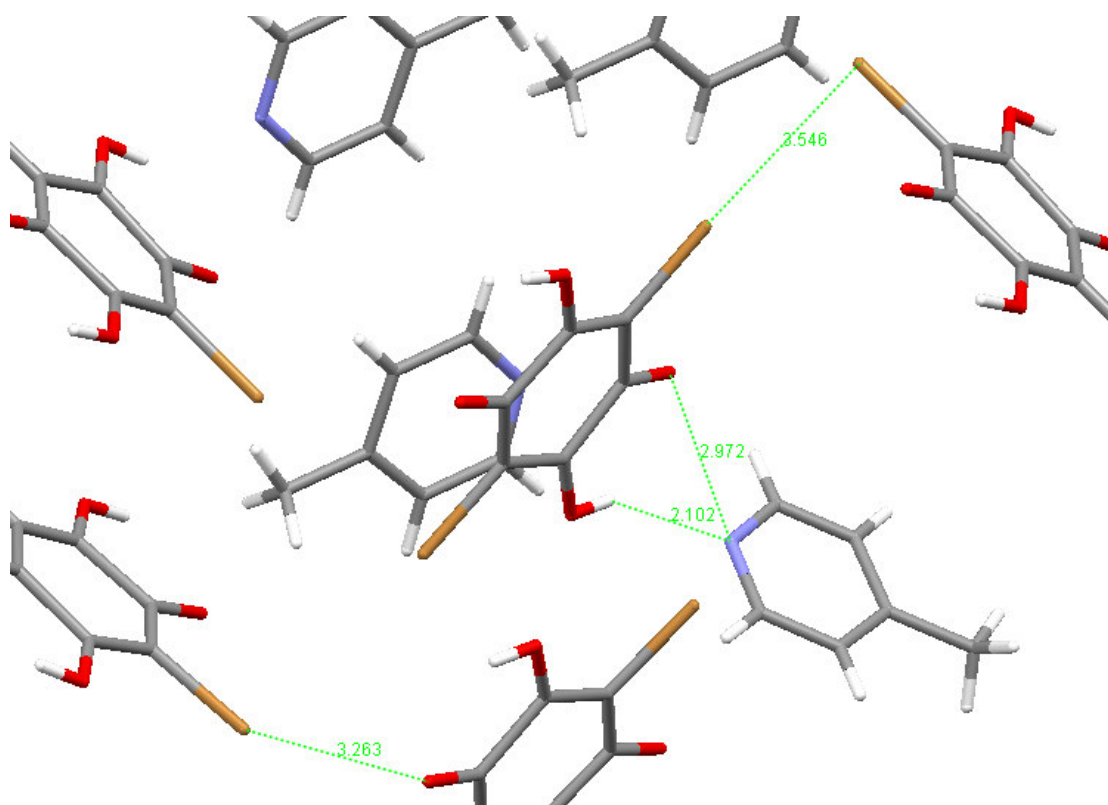


Figure 7.3.7: Crystal structure of bromanilic acid and 4-picoline in a 1:1 ratio determined at 100K

The 1:2 co-crystal complex of bromanilic acid with 4-picoline follows the same trend as the other 1:2 complexes studied whereby the bromanilic acid is fully deprotonated and hydrogen bonding occurs at both sides of the bromanilic acid molecule. This is the complex in which the nitrogen is nearest the centre of the two oxygen atoms of the bromanilic acid, however as can be seen there is still one dominant hydrogen bond in this case measuring $2.762(2)\text{\AA}$, with an angle measured to be $142(2)^\circ$ (Figure 7.3.8). This is in comparison to the longer $\text{N}\cdots\text{O}$ distance measuring $2.860(2)\text{\AA}$ with an angle of $137(2)^\circ$. In comparison to the other bifurcated hydrogen bonds, Table 7.1, this is much more of a central bifurcated bond. This co-crystal complex has no other non-covalent interactions present. In this co-crystal structure there are found to be many other weaker interactions involved to stabilise the structure in 3-dimensions involving the hydrogen in the 2 position of the picoline generating close contacts with the oxygen, from the shorter of the two C-O bonds, and the bromine atom of another bromanilic acid molecule. The bromanilic acid molecule in this instance has been stabilised significantly by the conjugation of the molecule with C-O distances of $1.242(2)\text{\AA}$ and $1.245(2)\text{\AA}$.

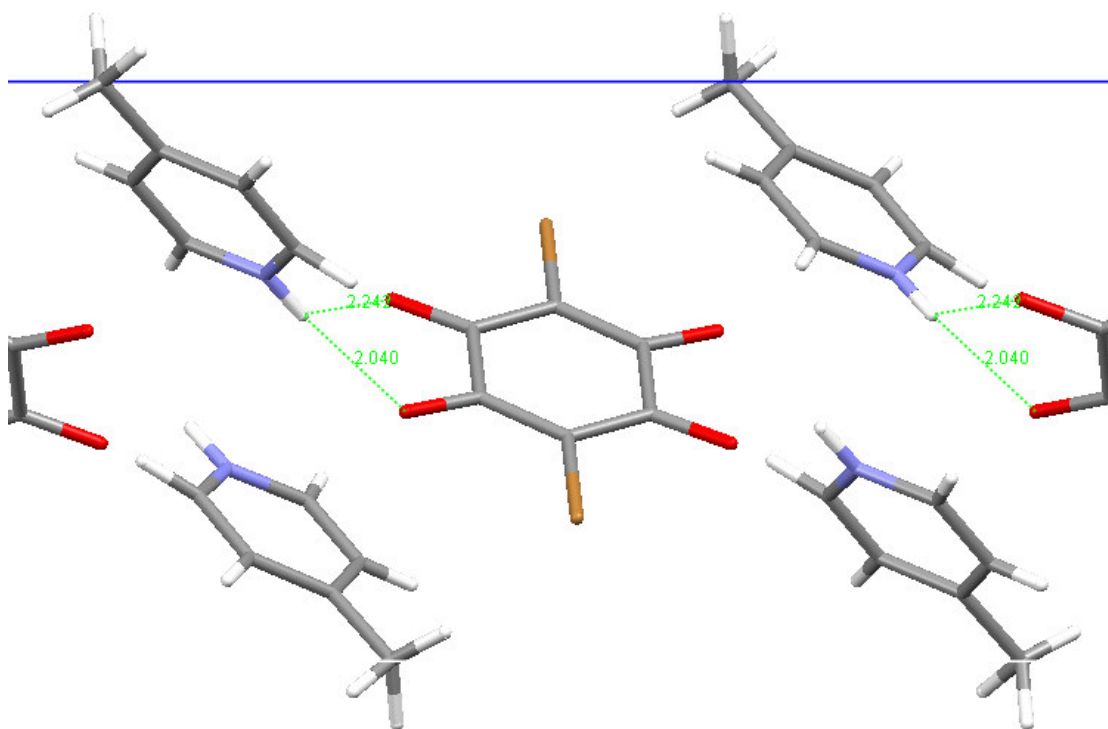


Figure 7.3.8: Crystal structure of bromanilic acid and 4-picoline in the ratio 1:2 viewed along the b axis, collected at 100K.

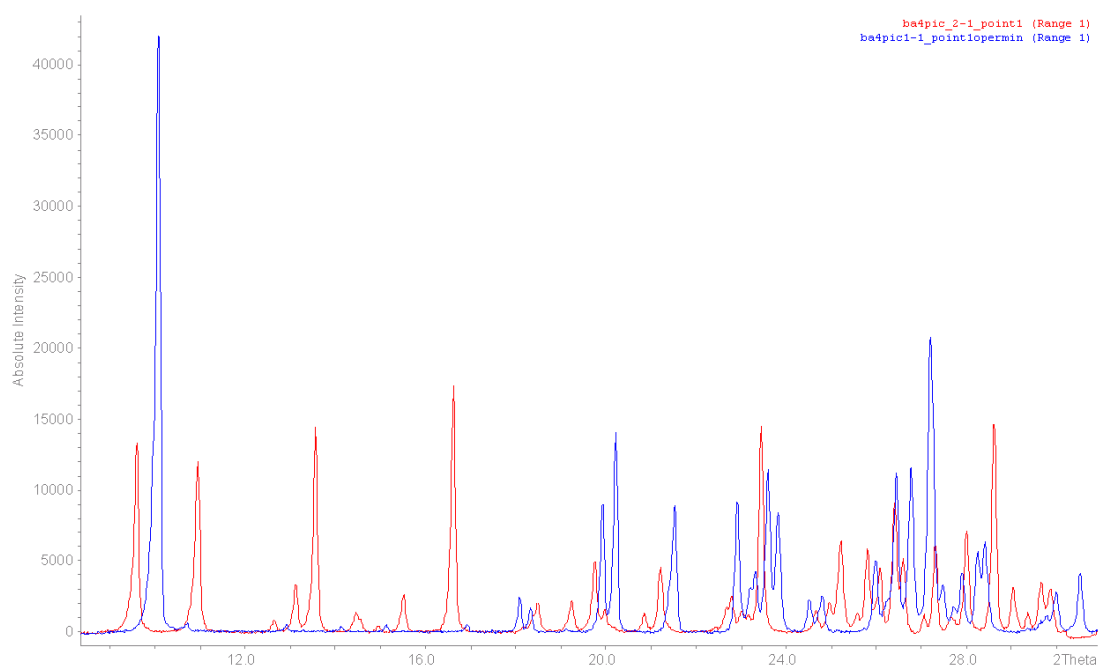


Figure 7.3.9: XRPD data showing the 1:1 and 1:2 co-crystal products of bromanilic acid with 4-picoline.

Figure 7.3.9 shows an overlay of the XRPD data for both the 1:1 and 1:2 co-crystal complexes of bromanilic acid and 4-picoline. This is a pure powder pattern where the 1:1 pattern (blue) and the 1:2 pattern (red) have completely unique peaks thus suggesting that there is only one product in each crystallisation and there are no mixtures.

Table 7.1: Distances and angles for the bifurcated hydrogen bond in the bromanilic acid (Ba) picoline (pic) complexes and other important close contacts. The angles shown represent the plane of the bifurcated hydrogen bond.

Co-crystal	N – O ₁ (Å)	N – O ₂ (Å)	N – H (Å)	H – – O ₁ (Å)	H – – O ₂ (Å)	Br – – O (Å)	Br – – Br (Å)	N-H- - O ₁ (°)	N-H - - O ₂ (°)	O- - H- - O (°)	Overall (°)
Ba : 2pic 1:2	2.841(4)	2.961(4)	0.89(3)	1.98(3)	2.40(3)	3.357(2)		164(3)	121(2)	74(1)	359(3)
Ba : 3pic 1:1	2.724 (2)	2.858(2)	1.07(2)	1.76(2)	2.15(3)	3.311(2) 3.337(1)		148(2)	122(2)	85(1)	355(2.5)
Ba : 3pic 1:2	2.601(1)	3.041(1)	0.83(1)	1.79(1)	2.59(1)			168(2)	116(1)	73.0(5)	357.0(1.8)
Ba : 4pic 1:1	2.771(9)	3.021(9)		0.820(5)*		3.263(9)	3.546(1)				
Ba : 4pic 1:2	2.762(2)	2.860(2)	0.76(2)	2.13(2)	2.25(3)			142(2)	137(2)	74.3(8)	353.3(2.4)

*It should also be noted from the table that there is no bifurcated hydrogen bond for the bromanilic acid : 4-picoline 1:1 cocystal as the hydrogen atom was located on the hydroxyl group.

Table 7.2: The crystallography data produced from single crystal diffraction.

Compound	Ba:2pic 1:2	Ba:3pic 1:1	Ba:3pic 1:2	Ba:4pic 1:1	Ba:4pic 1:2
Formula	C ₁₂ H ₉ Br ₂ N O ₄	C ₁₂ H ₉ Br ₂ N O ₄	C ₁₂ H ₉ Br ₂ N O ₄	C ₁₂ H ₉ Br ₂ N O ₄	C ₁₂ H ₉ Br ₂ N O ₄
Molecular weight (g mol ⁻¹)	390.51	390.51	390.51	390.51	390.51
Temperature (K)	100	100	100	100	100
Space Group	P 1 21 / c 1	P-1	P 1 21 / c 1	C c	P 1 21/c 1
<i>a</i> (Å)	16.4608(17)	7.6036(4)	8.9526(7)	18.4569(10)	8.1345(8)
<i>b</i> (Å)	7.8053(8)	8.4569(4)	9.6149(8)	11.1776(6)	6.1517(6)
<i>c</i> (Å)	14.5632(15)	11.1195(5)	10.4275(8)	14.0787(7)	17.7868(17)
α (°)		69.350(2)			
β (°)	99.593(5)	86.849(2)	103.935(4)	117.532(3)	96.177(7)
γ (°)		74.752(2)			
Volume (Å ³)	1844.9(3)	644.96(6)	871.17(12)	2575.6(2)	884.90(15)
Z	5	2	2	8	3
θ range (°)	1.255 – 21.035	1.959 – 34.393	2.344 – 28.870	2.21 – 36.21	2.303 – 32.816
Reflections Collected	11969	17647	10143	13032	14768
Independent	1970	4832	2280	3526	3237
Refln Observed I > 2 σ (I)	1610	4144	2050	3040	2516
R _{int}	0.0455	0.0393	0.0329	0.0485	0.0460
No. Parameters	283	199	142	353	142
GooF on F ²	0.9733	1.0373	1.3223	1.019	0.8521
R ₁ (Observed)	0.0393	0.0344	0.0289	0.0588	0.0403
R ₁ (all)	0.0746	0.0396	0.0337	0.0731	0.0579
wR ₂ (all)	0.0665	0.0750	0.0740	0.1472	0.1004

7.3.4. Summary

From this study it can be concluded that in terms of predictable stabilising interactions, the bromanilic acid and picolines in the 1:2 form will always result in full deprotonation with bifurcated hydrogen bonding occurring at both sides of the bromanilic acid molecule. This is entirely predictable given the knowledge of picolines to have a high affinity for protons. This is also in complete agreement with work carried out previously⁹⁴ where a P:C:P structure was generated with picolines and chloranilic acid. This motif stands up here as well with regards to a predictable P:B:P structure being produced.

From the crystal structures produced of the 1:1 co-crystals there does not appear to be a predictable motif present. With regards to the bromanilic acid : 3-picoline co-crystal there is a P:B:P, three molecule interaction present, however as the bromanilic acid crystallises in two different types (protonated and deprotonated), this is not present throughout. The protonated bromanilic acid produces a O-H...O hydrogen bond and a Br...O halogen bond is also found. The bromanilic acid : 4-picoline co-crystal crystallises in a completely different space group and the bromanilic acid is found to hydrogen bond only to one picoline molecule with other significant halogen bonding present. Hydrogen transfer to the picoline does not occur for this system. For this reason there is currently no specific motif present for the 1:1 structures, however these 1:1 structures are more likely to contain additional halogen bonding interactions and the only instance of halogen – halogen interactions was with that of the 4-picoline co-crystal.

Chapter 8: Co-crystals of Brominated Compounds. II.

Bromanilic acid with lutidines

8.1: Co-crystallisations of bromanilic acid and the family of lutidine molecules.

Lutidines or dimethylpyridines are commonly found in coal tar and bone oil and are strong smelling liquids. These compounds have been studied routinely in terms of organometallic compounds where the lone pair on the nitrogen is attracted to the metal centre. There have been significant studies using a range of lutidine compounds in co-crystal studies, including a study by Schmidtman and Wilson⁶⁴ in which a whole family of co-crystals with pentachlorophenol were produced. This was intended to study hydrogen transfer in the series, however attention should be given to 2,6-lutidine pentachlorophenol co-crystal where hydrogen transfer has occurred from one of the two pentachlorophenol molecules in the crystal lattice⁶⁴. Further research of structures available on the CSD only provides one further example of a significant co-crystallisation study using lutidines and fumaric acid by D.A. Haynes *et al*¹⁰⁴. During this work the full family of co-crystals was produced using lutidines with both fumaric and succinic acid, which resulted in salt formation.

Ishida *et al* have also used lutidines to produce co-crystals with chloranilic acid in the 1:1 ratio⁹⁷. These structures all formed a chloranilic acid dimer and the lutidine molecule interaction with the hydroxyl group of the other half of the bromanilic acid. In only the 2,5-lutidine – chloranilic acid structure can this be described as a bifurcated hydrogen bond as the other co-crystals appear to be hydrogen bonded from the nitrogen to the hydroxyl group. An interesting feature in this study is the importance of the hydrogens on the lutidine ring and also from the methyl group. For the 2,5-lutidine co-crystal the hydrogen on the 6 position of the lutidine develops an interaction with the carbonyl group, whereas in the 2,4- and 2,6-lutidine co-crystal compounds, it is a hydrogen on the methyl group that appears to form this close contact to stabilise the crystal structure.

The family of lutidine molecules studied involved 2,3-, 2,4-, 2,5- and 3,5-lutidine. These present a set of simple molecules to examine structural motifs that may be

present and in common between them. These are similar to the family of picolines though containing an extra methyl group on the aromatic ring. These co-crystals were studied in the 1:1 form with bromanilic acid. This was due to the 1:1 picolines showing an increased presence of non-covalent interactions in addition to hydrogen bonding.

8.1.1: Bromanilic acid 2,3-lutidine

Bromanilic acid and 2,3-lutidine were found to crystallise in the monoclinic $P2_1/n$ space group at 100K. Crystals were grown from a 2-propanol solution containing 6mg bromanilic acid and 16mg 2,3-lutidine, by slow evaporation at room temperature. Due to the 1:1 ratio it is unsurprising that deprotonation has only occurred on one of the hydroxyl groups of the bromanilic acid molecule and this will be the case in all the subsequent lutidine co-crystals, however it is the subsequent interactions that are of interest. Due to this deprotonation a bifurcated hydrogen bond is formed, with a dominant interaction being present (Figure 8.1.1). The conjugation of the bromanilic acid molecule changes with the carbonyl and hydroxyl groups shortening on the deprotonated side (1.218(3)Å, 1.258(3)Å) and them both elongating on the protonated side (1.240(3)Å, 1.335(3)Å).

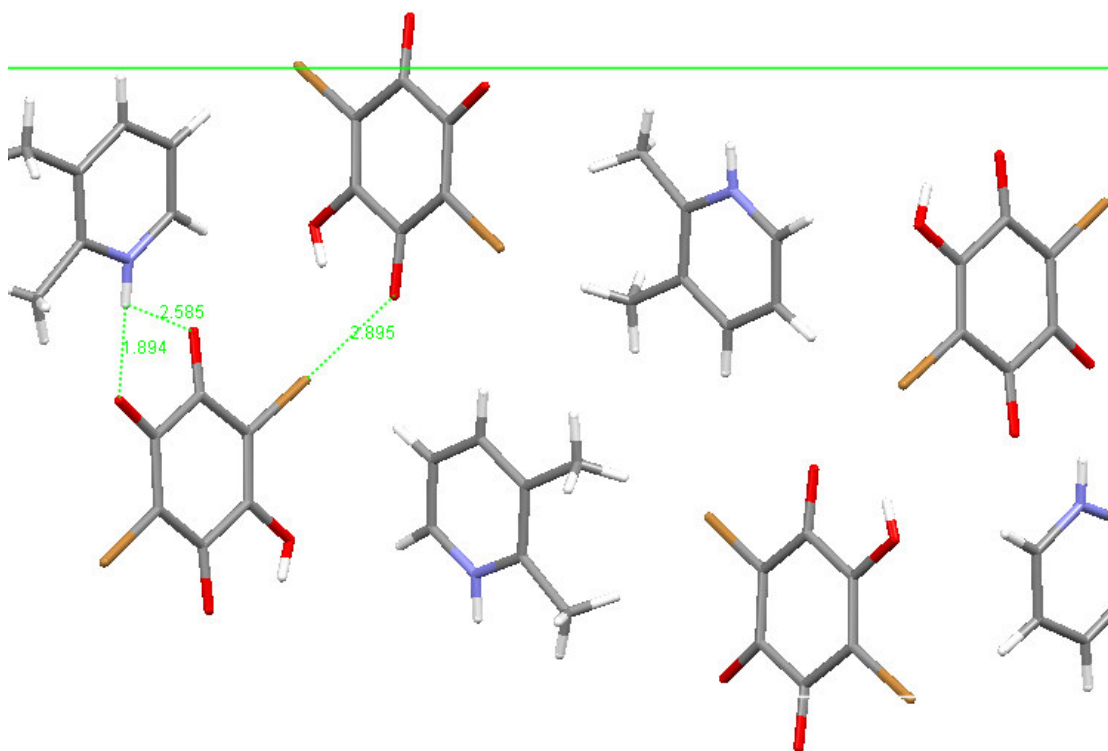


Figure 8.1.1: Crystal structure of bromanilic acid and 2,3-lutidine in a 1:1 ratio viewed down the a axis, collected at 100K.

All the data from the bifurcated hydrogen bonds and also the halogen bonds is presented in Table 8.1. However, the major N···O bifurcated bond interaction measures 2.772(3)Å and has an N-H- - O angle of 175(3)°. This is significant as this is similar to that of a strong hydrogen bond even though it is bifurcated and has a second significantly weaker interaction (3.039(3)Å, 113(3)°). The environment of the transferred hydrogen is also interesting as the sum of the three angles involved in the bifurcated hydrogen bond N-H···O, N-H···O and O···H···O is roughly equal to 360°. This shows that the bifurcated hydrogen bond is almost planar in this example.

As well as showing a clear distinction between the major and minor interactions for the bifurcated bonds, each bromanilic acid molecule has a Br···O halogen bond present (Figure 8.1.2) measuring 2.895(2)Å from the bromine of one bromanilic acid molecule to the carbonyl group adjacent to the protonated hydroxyl group. This is a significant discovery in the study as the aim was to investigate halogen bonding and this instance is the first that has been discovered where the interatomic distances have been sufficiently close to describe this as a major interaction in the crystal structure. This is also the main route by which the three-dimensional crystal structure is produced. Another feature of this crystal structure is the availability of a hydrogen on each bromanilic acid molecule that is not involved in any hydrogen bonding throughout the crystal structure and indeed the only close contacts involving the hydroxyl group are to a bromine atom as a result of the significant halogen bond it has already formed to the adjoining carbonyl group. As it is known that hydrogen bonding is the strongest non covalent interaction this would not be expected.

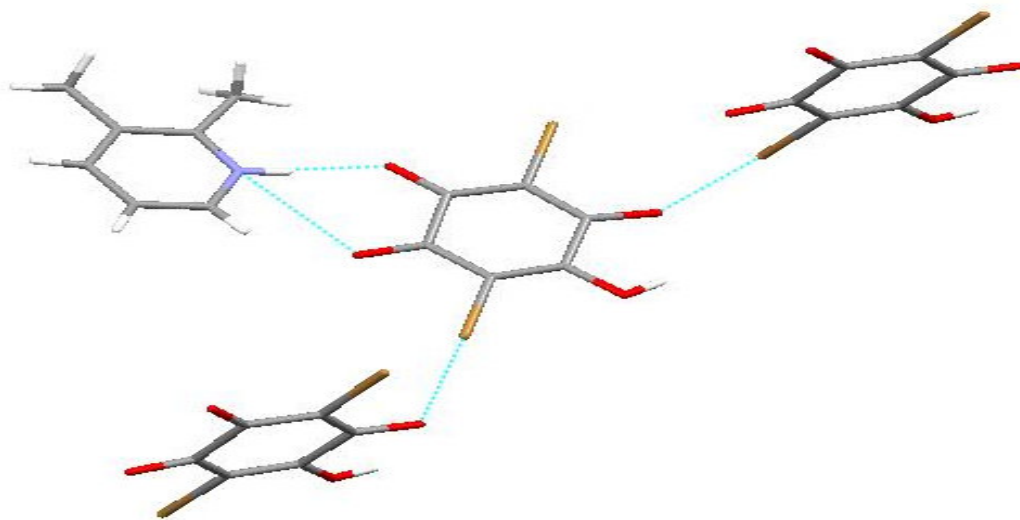


Figure 8.1.2: All the interactions from one molecule of bromanilic acid in the co-crystal structure with 2,3-lutidine.

Furthermore as was discovered by Ishida *et al*⁹⁷, the methyl group in the two position also forms a close contact with the deprotonated hydroxyl group of the bromanilic acid.

8.1.2: *Bromanilic acid 2,4-lutidine*

Bromanilic acid and 2,4-lutidine were found to crystallise in the monoclinic $P2_1/c$ space group and had very little resemblance to the crystal structure of bromanilic acid and 2,3-lutidine. The crystal was grown from a methanol and water solution containing 10mg bromanilic acid and 26mg 2,4-lutidine left to evaporate at room temperature. The crystal structure in this instance was found to have undergone hydrogen atom transfer to the lutidine molecule at each end to form a four molecule unit. The bromanilic acid forms centrosymmetric dimers joined by two O-H...O hydrogen bonds (Figure 8.1.3). The dimers are linked to the lutidine *via* bifurcated bonds on either side forming this four-molecule unit (Figure 8.1.4). In this example the bifurcated bonding is not as strong, as shown by the bond lengths and angles in Table 8.1, however the hydrogen atom is exactly planar between all atoms involved in the bifurcated bonding. This crystal structure is also layered and π - π stacking interactions are also significant in the crystal structure.

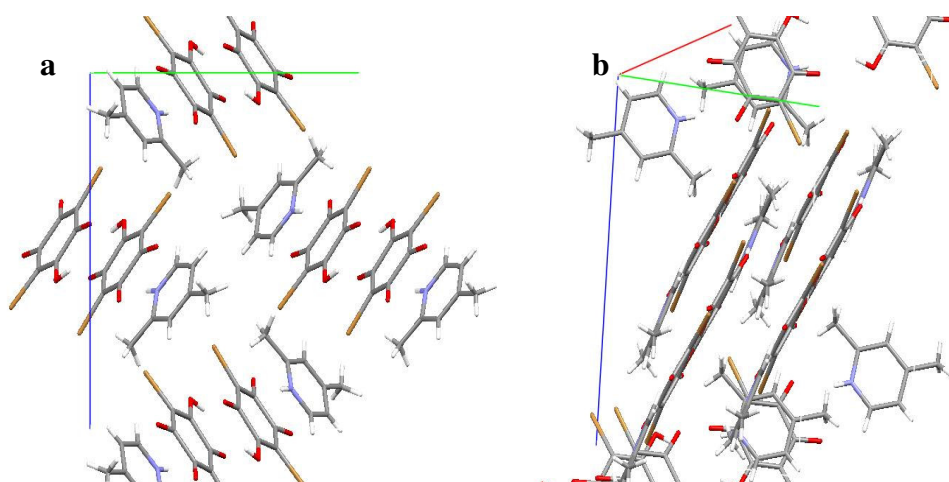


Figure 8.1.3: (a) shows the existence of the four molecule interaction in bromanilic acid 2,4-lutidine and (b) shows that each of these four molecule interactions has staggered four molecule interactions layered below it providing π - π stacking interactions.

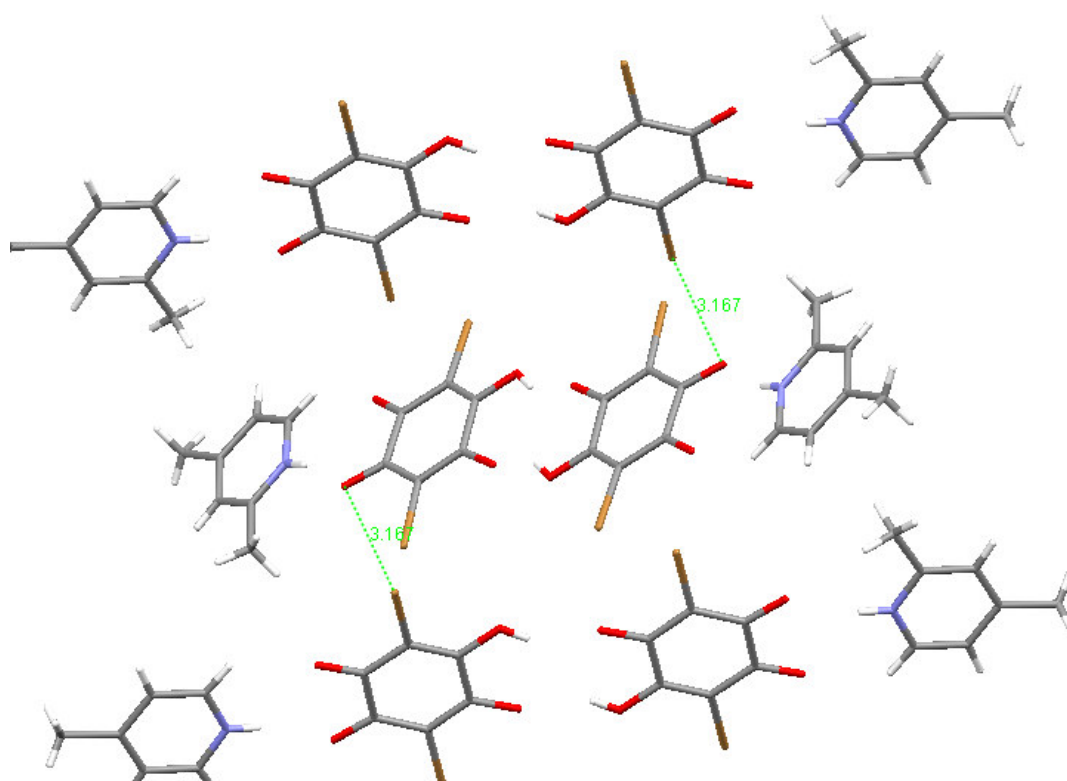


Figure 8.1.4: Crystal structure of bromanilic acid and 2,4-lutidine in a 1:1 ratio collected at 100K showing the halogen bonding and how it links the four-molecule units.

Each of these four-molecule units is linked to two other four molecule units *via* halogen bonding to the deprotonated hydroxyl group. Although this may not be as short a contact as that of the 2,3-lutidine co-crystal compound, measuring 3.152(2)Å, it is obviously a very important stabilising interaction as it is fundamental in producing the three-dimensional structure.

8.1.3: Bromanilic acid 2,5-lutidine

The co-crystal used was grown from a methanol and water solution left to evaporate slowly at room temperature containing 8mg bromanilic acid and 22mg 2,5-lutidine. The bromanilic acid and 2,5-lutidine co-crystal complex crystallised in a similar way to the 2,4-lutidine co-crystal in the $P2_1/c$ space group and forming the same four molecule unit, however the subsequent intermolecular interactions vary considerably. The bifurcated bonds in this co-crystal do not have as distinct major and minor interactions present as the nitrogen is much closer to the centre of the two oxygen atoms. The four molecule unit with the bifurcated N---O distances of 2.882(2)Å and 2.983(2)Å indicating that unlike previous examples, this co-crystal has a nearly symmetrical interaction with both hydrogens (Figure 8.1.5). A small twist of the lutidine molecule with respect to the plane of the bromanilic acid dimer can also be determined, with the torsion angle between the plane of the lutidine and the plane of the bromanilic acid measuring 6.6(1)°, and this slight distortion moves the hydrogen atom away from being in an exactly planar position.

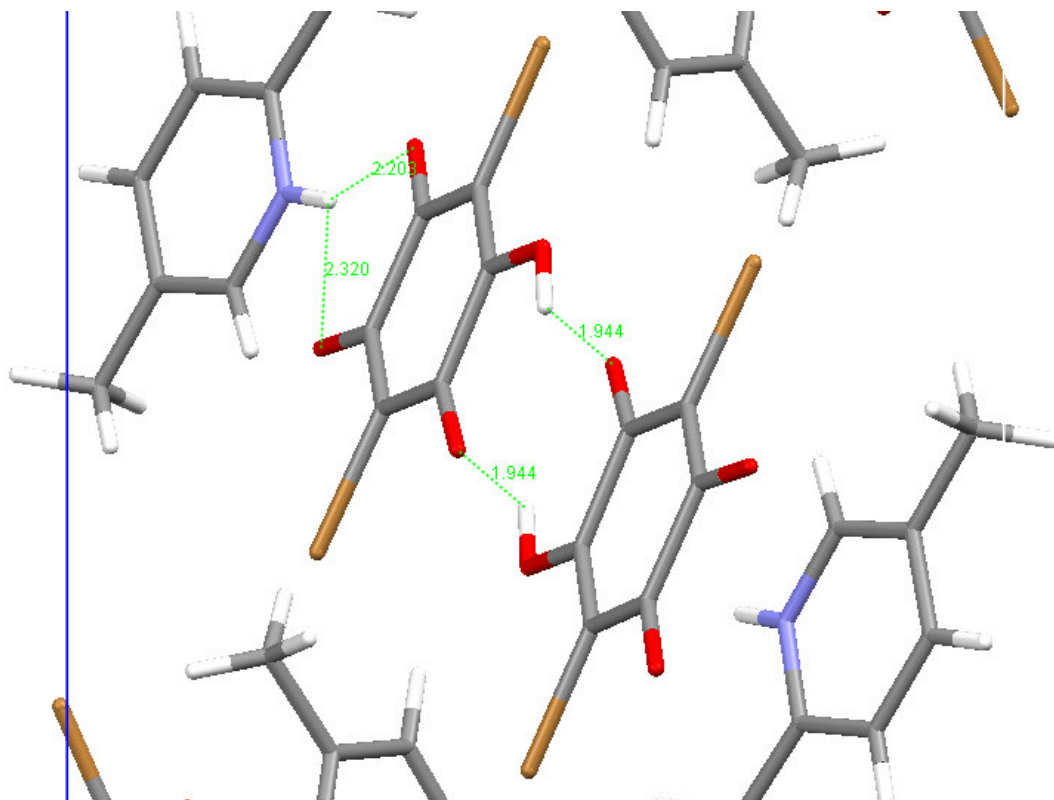


Figure 8.1.5: Crystal structure of bromanilic acid and 2,5-lutidine in a 1:1 ratio viewed along the a axis, collected at 100K.

The other main interaction present in the crystal structure is the presence of π - π stacking interactions from staggered layers of four molecule interactions (Figure 8.1.6), which encourages the theory that in the four molecule system present there is no requirement for further stabilisations via any other interactions. This is in contrast to the first system studied, which did not have the same four molecule motif and therefore the halogen bonding present was a significant interaction.

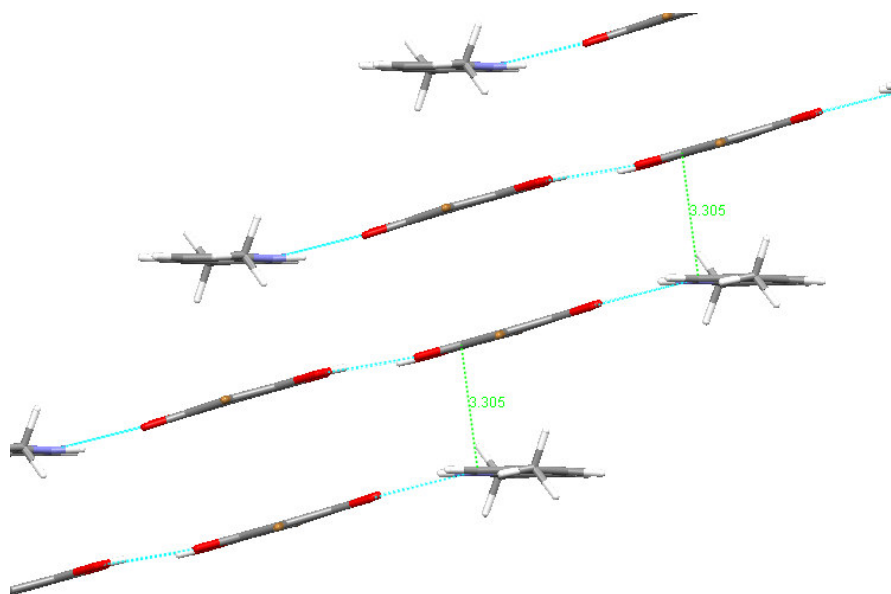


Figure 8.1.6: The layers in the bromanilic acid 2,5-lutidine co-crystal that are present as a result of π - π stacking interactions between the four molecule units.

The only other interactions that are present to help generate the three-dimensional crystal structure are weaker interactions involving bromine – hydrogen interactions, which lie between the layers and link between two lutidine molecules from separate layers via interactions with a methyl hydrogen from one lutidine ($C-H\cdots Br$) and a hydrogen on the ring of the other ($\pi-H\cdots Br$). Whilst these interactions are not thought to be overly significant in terms of strength, they do provide a role of generating the entire three-dimensional crystal structure.

8.1.4: Bromanilic acid 3,5-lutidine

The bromanilic acid and 3,5-lutidine co-crystal that was formed from a 2-propanol solution containing 10mg bromanilic acid and 26mg 3,5-lutidine, crystallised in the $P2_1/c$ space group and also follows the same four molecule motif described in the structures of 2,4- and 2,5-lutidine (Figure 8.1.7). In this crystal structure however, the O-H...O dimer interactions are longer at $2.757(2)\text{\AA}$, which is supplemented by the hydrogen bond angle measuring $133(2)^\circ$ indicating a weaker hydrogen bond interaction. The major component of the bifurcated bond however, is clearly present

and measures 2.671(2)Å. This is the shortest N...O interaction found in this co-crystal study (Table 8.1). Br- - - O halogen bonding is also found to be present in the crystal structure and plays a significant role in the generation of the three-dimensional crystal structure as in the 2,4-lutidine co-crystal complex. The halogen bonding is from the carbonyl group of the deprotonated side of the bromanilic acid molecule and is again used to link the central four molecule unit to two other four molecule units.

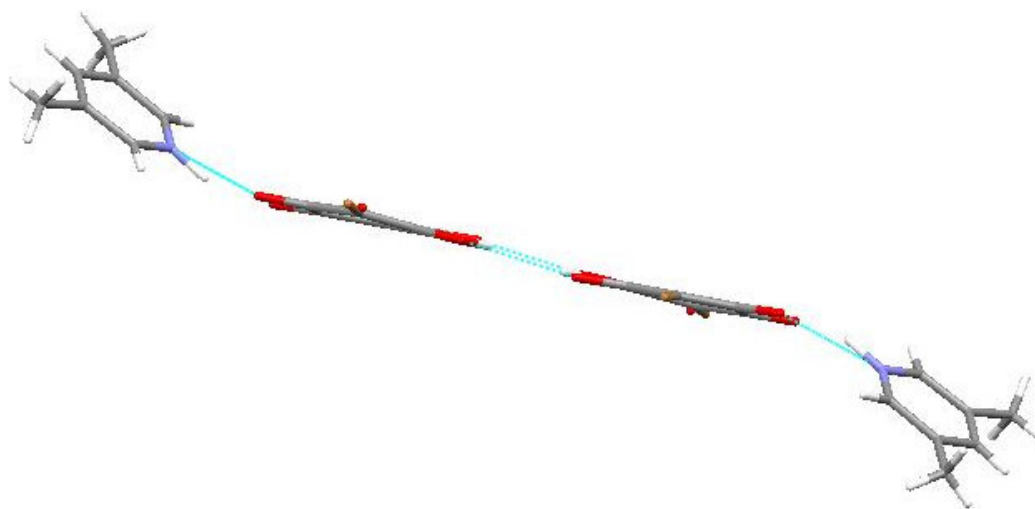


Figure 8.1.7: Four molecule interaction of bromanilic acid with 3,5-lutidine.

The four molecule interaction shown in Figure 8.1.7 shows a distinct change to the others that have been noted in the study. This is due to a relatively planar O-H - - - O interaction between the bromanilic acid molecules, however as can be seen the lutidine molecule in this instance is nowhere near co-planar with the bromanilic acid dimer. As a result of this there are no π - π stacking interactions present in the crystal structure. In this case the torsion angle between the plane of the lutidine molecule and that of the bromanilic acid is found to be 21.5(1)°, which is considerably higher than that of the 2,5-lutidine complex which was found to be 6.6(1)°. The conjugation of the bromanilic acid molecule is similar throughout with the C-O bond distances found to be 1.219(2)Å and 1.242(2)Å for the deprotonated side and 1.240(2)Å and 1.334(2)Å for the protonated side. This is found to be similar to that of the 2,3-lutidine co-crystal complex, thus the position of the methyl groups must play a key role. In this case the methyl groups are on symmetrical positions away from the bromanilic acid molecule and this extra bulk may play a key role in the significant change on torsion angle.

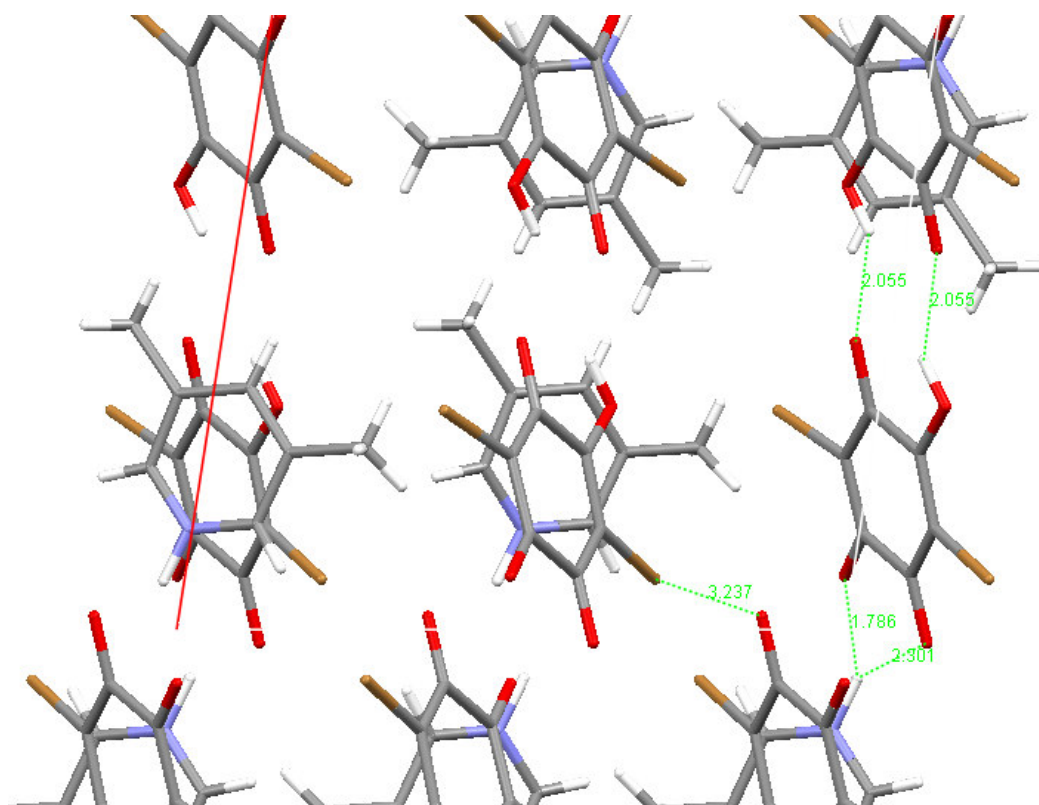


Figure 8.1.4.2: Crystal structure of bromanilic acid and 3,5-lutidine in a 1:1 ratio viewed along the b axis, collected at 100K.

In the 3,5-lutidine co-crystal complex there are also other weaker interactions that help generate the 3-dimensional structure (Figure 8.1.8), however the presence of the halogen bonding interactions is highly significant and was found to be so in both the 2,3- and 2,4-lutidine co-crystal complexes as well.

Table 8.1: Distances and angles for the bifurcated hydrogen bond in the bromanilic acid (ba) lutidine (lut) complexes and brominated methylpyridines (mepyr) complexes and other important close contacts. The angles shown represent the plane of the bifurcated hydrogen bond.

Co-crystal	N – O ₁ (Å)	N – O ₂ (Å)	N – H (Å)	H – – O ₁ (Å)	H – – O ₂ (Å)	Br – – O (Å)	Br – – Br (Å)	N-H – – O ₁ (°)	N-H – – O ₂ (°)	O – – H – – O (°)	Overall
Ba : 2,3lut	2.772(3)	3.039(3)	0.88(3)	1.89(3)	2.59(3)	2.895(2)		175(3)	113(3)	72(1)	360(3.5)
Ba : 2,4lut	2.839(2)	2.974(3)	0.78(4)	2.07(3)	2.48(4)	3.152(2)	3.6086(6)	167(4)	123(3)	71(1)	360(4)*
Ba : 2,5lut	2.882(2)	2.983(2)	0.84(2)	2.20(2)	2.32(3)			155(2)	125(2)	72.2(7)	352.2(2.4)
Ba : 3,5lut	2.671(2)	2.999(2)	1.00(2)	1.79(2)	2.30(2)	3.237(1)		145(2)	126(2)	80.5(8)	351.5(2.4)
*Ba : 2- br-3- mepyr	2.618(5)		1.75(5)	0.88(5)		2.850(3)					
Ba : 3-br- 4-mepyr	2.675(3)	2.915(3)	0.78(4)	1.92(4)	2.52(4)	3.114(2) 3.274(2)		164(4)	113(3)	73(1)	350(4)

*It should be noted that there is not bifurcated hydrogen bond in the crystal structure of bromanilic acid : 2-bromo-3-methylpyridine.

Table 8.2: The crystallography data produced from single crystal x-ray analysis.

Compound	Ba:2,3lut	Ba:2,4lut	Ba:2,5lut	Ba:3,5lut	Ba:2br3mepyr	Ba:3br4mepyr
Formula	C13 H11 Br2 N1 O4	C12 H8 Br3 N1 O4	C12 H8 Br3 N1 O4			
Molecular weight (g mol ⁻¹)	405.04	405.04	405.04	405.04	469.91	469.91
Temperature (K)	100	100	100	100	100	100
Space Group	P 1 21/n 1	P 1 21/c 1	P 1 21/c 1			
<i>a</i> (Å)	4.9786(4)	8.2948(2)	7.7357(4)	11.6766(5)	5.2866(3)	10.2229(4)
<i>b</i> (Å)	23.181(3)	12.1560(4)	11.1416(6)	10.4926(5)	13.3814(8)	5.5760(2)
<i>c</i> (Å)	12.2811(13)	13.9544(5)	15.8011(9)	11.5221(5)	20.3576(13)	24.5300(9)
α (°)	90	90	90	90	90	90
β (°)	100.794(3)	102.966(2)	94.269(3)	98.834(2)	91.556(4)	95.802(3)
γ (°)	90	90	90	90	90	90
Volume (Å ³)	1392.3(2)	1371.17(8)	1358.09(13)	1394.92(11)	1439.61(15)	1391.12(9)
Z	4	4	4	4	4	4
θ range (°)	1.757 – 23.601	2.247 – 35.962	2.239 – 42.111	1.765 – 31.543	1.821 – 27.237	1.669 – 32.153
Reflections Collected	9997	23034	39052	14464	14783	21156
Independent	2053	6064	9404	3817	3202	4796
Refln Observed <i>I</i> > 2 σ (<i>I</i>)	1680	4673	6404	3178	2394	3457
<i>R</i> _{int}	0.0442	0.0407	0.0557	0.0304	0.0680	0.0537
No. Of Parameters	214	214	214	225	205	205
Goof on F ²	0.9544	0.9449	1.0298	0.9901	0.9925	0.9179
<i>R</i> ₁ (Observed)	0.0382	0.0381	0.0468	0.0314	0.0513	0.0475
<i>R</i> ₁ (all)	0.0568	0.0575	0.0769	0.0423	0.0836	0.0835
<i>wR</i> ₂ (all)	0.0873	0.0944	0.0986	0.0588	0.1063	0.1114

8.2: Summary

As can be determined by this study, in the 1:1 crystal structures of bromanilic acid with lutidines, the main stabilising interaction that is present is the four molecule interaction involving centrosymmetric dimers joined by two O-H...O hydrogen bonds, with each bromanilic acid molecule involved in bifurcated hydrogen bonding to the lutidine molecule. Where this motif is present, these are the most significant non-covalent interactions, however as noted this motif is not present across the whole family of lutidines. In the case of 2,3-lutidine and bromanilic acid, there was only one type of hydrogen bonding interaction, a weakly bifurcated hydrogen bond showing a large degree of asymmetry and in this instance the presence of a halogen bond stabilised the crystal structure. This however has been the only instance in which halogen bonding has had a significant impact on the co-crystallisation behaviour of bromanilic acid.

Furthermore the presence of halogen bonding has been found to be significant in three of the co-crystal complexes that were produced. This enables the three-dimensional crystal structure to be generated and the absence of this in the 2,3-lutidine co-crystal complex was noted, however this complex was found to contain π - π stacking interactions from staggered layers of four molecule interactions. Once again however the presence of Br...Br interactions was only produced in the 2,4-lutidine co-crystal complex so it is difficult to put any emphasis on this at this stage.

8.3: Co-crystals of bromanilic acid and other bromo substituted compounds.

Further research was carried out involving co-crystallisations with related compounds incorporating extra bromine atoms, to examine the affect these extra bulky atoms have on the co-crystal structure involving bromanilic acid. The compounds selected were 2-bromo-3-methylpyridine and 3-bromo-4-methylpyridine; these are fundamentally similar to the picoline compounds used previously as they contain one methyl group on the aromatic ring but also contain a bromine atom to attempt to produce halogen bonding interactions with the bromanilic acid molecule.

These co-crystallisation studies were carried out in the same way as the other co-crystallisation trials, involving dissolving equimolar amounts of both compounds in a minimum amount of methanol and left to slowly evaporate. The co-crystals produced were then evaluated by single crystal X-ray diffraction. The aim was to see if crystallisation could be affected by the presence of these heavy atoms, which would also act as a possibility for stabilisation as in the case of bromanilic acid and 2,3-lutidine. The 1:1 co-crystal structures with picolines reported in Chapter 7 had no obvious motif, with the 3-picoline co-crystal showing hydrogen transfer onto the nitrogen atom, whereas the 4-picoline co-crystal does not show hydrogen transfer. In the case of the lutidine co-crystal complexes, the most notable motif involved the four molecule interaction (P:B:B:P). The aim of this study however was to try and encourage the bromine atoms to play a more significant role in the crystal structure.

8.3.1: 2-bromo-3-methylpyridine : bromanilic acid

The 1:1 2-bromo-3-methylpyridine:bromanilic acid co-crystal structure was found to crystallise in the monoclinic $P2_1/c$ space group when recrystallised from a methanol solution containing 10mg bromanilic acid and 14mg 2-bromo-3-methylpyridine left to crystallise at 5°C. In this crystal structure each bromanilic acid molecule is found to be fully protonated, each containing four hydrogen bonded interactions and two halogen bonding interactions meaning each atom capable of hydrogen or halogen bonding is involved. Due to the symmetrical nature of bromanilic acid these

interactions are the same on each side meaning there are three unique non covalent interactions (Figure 8.3.1).

Figure 8.3.1 shows the presence of the O-H...N and O-H...O hydrogen bonds and also the presence of a Br...O halogen bond, which was found to be crucial in the generation of the three-dimensional structure of the lutidine co-crystal complexes. The presence of the bromine atom in the 2 position of the methyl pyridine ring could also explain the absence of any hydrogen transfer due to the increased bulk around the nitrogen acceptor.

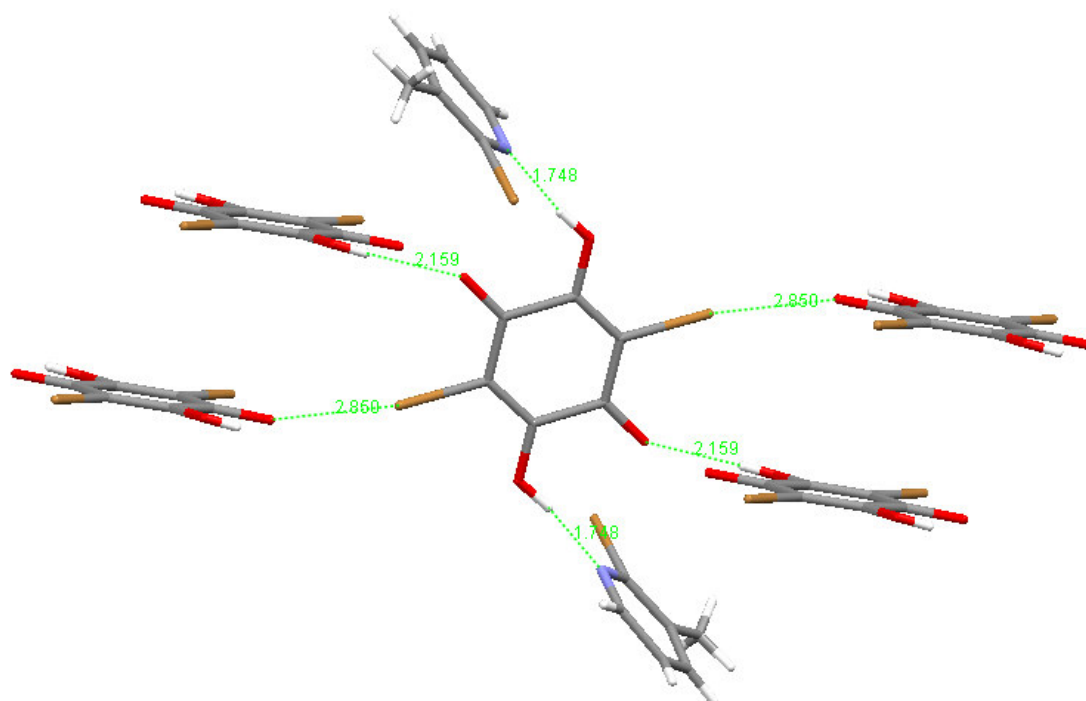


Figure 8.3.1: Crystal structure of bromanilic acid and 2-bromo-3-methylpyridine showing the interactions present around each bromanilic acid molecule collected at 100K.

The findings from this co-crystal complex are once again intriguing due to the relatively long and weaker O-H...O hydrogen bond, 2.793(4)Å, short and strong O-H...N hydrogen bond, 2.618(5)Å with an angle of 171(5)°, and the presence of a relatively strong halogen bond, 2.850(3)Å for only the second time (Table 8.1).

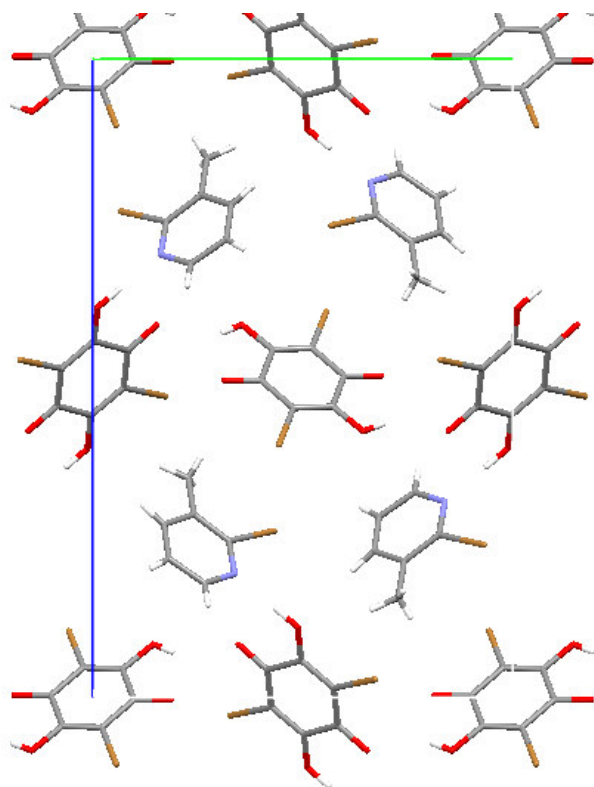


Figure 8.3.2: The crystal packing of bromanilic acid (ba) and 2-bromo-3-methylpyridine (mp) showing apparent a-b-a-b type layers, when viewed along the *a* axis.

Figure 8.3.2 shows the build up of the 3-dimensional crystal structure, which shows an apparent layered motif composed of ba:mp:ba:mp. The layers of mp form a hydrogen bond to a hydroxyl group from the layer below and then the next hydrogen bonds to the hydroxyl group from the layer above. This integrates each layer in the crystal structure.

8.3.2: 3-bromo-4-methylpyridine : bromanilic acid

The 3-bromo-4-methylpyridine – bromanilic acid 1:1 co-crystal was found to crystallise in the monoclinic $P2_1/c$ space group when recrystallised from a methanol and water solution containing 10mg bromanilic acid and 14mg 3-bromo-4-methylpyridine left to slowly evaporate at room temperature. In this structure however, the hydrogen atom has transferred onto the nitrogen atom from one half of the bromanilic acid molecule, whereas it remains on the oxygen on the other side of the molecule to form a similar dimer interaction to that present in the 1:1 bromanilic

acid : lutidines complexes (Figure 8.3.3). As was discussed previously, by moving the bulky bromine atom away from the nitrogen acceptor of the methylpyridine molecule, this frees up the nitrogen to act as an acceptor in the same way as it did previously in the case of the lutidines. This results in a four molecule interaction (Figure 8.3.4), which stabilises the compound and the presence of halogen bonding interactions, bromine to the carbonyl adjacent to the deprotonated hydroxyl group as seen previously, measuring $3.274(2)\text{\AA}$. There is also a halogen bond from the bromine of the methylpyridine to the hydroxyl oxygen on the bromanilic acid, measuring $3.114(2)\text{\AA}$, which is still protonated and generates the 3-dimensional structure. The halogen bonding is elongated in this cocrystal in comparison to that of the 2-bromo-3-methylpyridine structure (Table 8.1), however it has been possible to engineer a further halogen bonding interaction to generate the three-dimensional structure by including an extra bromine atom on the methylpyridine ring.

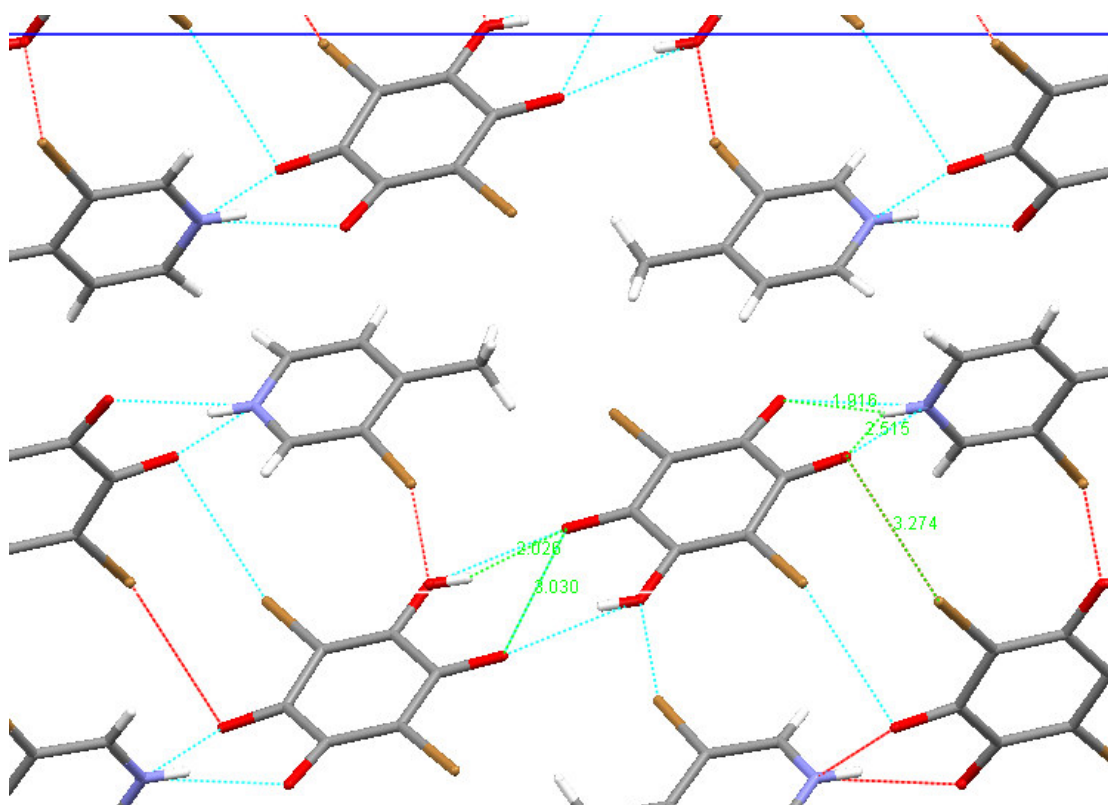


Figure 8.3.3: Crystal structure of bromanilic acid and 3-bromo-4-methylpyridine in a 1:1 ratio viewed along the b axis, collected at 100K.

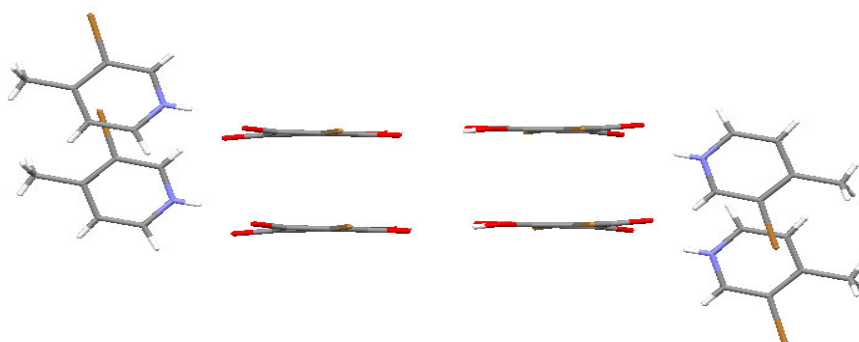


Figure 8.3.4: Four molecule unit in crystal structure of 3-bromo-4-methylpyridine and bromanilic acid

Figure 8.3.4 shows the four molecule unit is highly similar to that found in the bromanilic acid and 3,5-lutidine co-crystal structure. This relies on the bromanilic acid molecules being close to planar with the plane of the 3-bromo-4-methylpyridine in this case being close to perpendicular with the nitrogen and hydrogen donor between the two oxygen acceptors. This is in contrast to the 2-bromo-3-methylpyridine and bromanilic acid co-crystal, which does not possess the four molecule interaction and contains chains of bromanilic acid molecules interspaced by rows of the 2-bromo-3-methylpyridine constituent of the co-crystal.

8.4: Conclusions/Summary

During these studies it has been possible to engineer a further halogen bonding contact with bromanilic acid with the presence of a bromine atom on the methylpyridine ring of the 3-bromo-4-methylpyridine co-crystal structure. This resulted in the same four molecule interaction being observed as was in the case of the bromanilic acid : lutidine co-crystal complex. This was further stabilised and the three-dimensional crystal structure generated via these halogen bond interactions. The halogen bond interactions are found to be shorter in the case of the 2-bromo-3-methylpyridine cocrystal, however this does not generate the four molecule unit, possibly due to the presence of the bromine atom in the 2 position preventing hydrogen atom transfer from occurring.

Chapter 9: Conclusions and Forward Look

9.1 Liquid Scattering Studies

This aspect of the project was funded under an “adventurous chemistry” theme, due to its challenging nature from the outset - to try and monitor small molecule nucleation. Progress has been made with a significant increase in knowledge of the requirements and associated challenges, which can only be gained by experience. It has been a huge success to be able to monitor scattering from the small molecule solutions that were trialled. However to develop this work still further, it would be more beneficial to trial solutes with heavier atoms present than the ones studied in this work. Unfortunately future proposals for beam time were not successful to enhance this study.

The metastable zone width work carried out at Strathclyde Institute of Pharmacy and Biomedical Sciences (SIPBS) in developing new and more practicable routes to monitor crystallisation from solution and carry out solubility studies yielded very significant results. These have been generated without the need for sampling and concentration changes can be monitored on-line alongside particle size distribution plots, commonly referred to as chord length distribution (CLD) plots. We have successfully produced two robust metastable zone width diagrams by these methods with the solubilities of the pMHB from our method in close correspondence with the literature values⁸⁷.

Carrying out these experiments prior to SAXS studies enabled us to prepare suitably concentrated solutions that would encourage an increase in the scattering due to the likelihood of the presence of nucleating particles. This also enabled us to ascertain an idea of the behaviour of the solution as it was cooled, albeit on a much larger scale than that used for the SAXS studies. To continue these studies still further it would be a possibility to attempt these studies, possibly even in a co-crystallisation situation by selecting a complex with long range ordering such as halogen – halogen interactions and also short-range stronger interactions such as hydrogen bonding, however again it would be recommended to attempt these with molecules containing heavy atoms.

9.2 Structural studies of methylbenzoate derivatives and the assessment of conformational polymorphism

This aspect of the project focused on taking the original; target models for the dissolution/nucleation studies and carrying out crystallographic studies on their structures. These were successful and included the solution of the previously unknown structure of methyl 2,5-dibromobenzoate (MDBB), as presented in Chapter 6.

A wide range of variable temperature crystallographic studies were carried out on these systems, with a particular focus on the postulated conformational polymorphism in methyl 4-hydroxybenzoate (pMHB), as presented in Chapter 4. By carrying out detailed XRPD scans, backed up by accurate molecular geometry determinations by single crystal diffraction, it was shown that this was actually due to a gradual change in selected torsion angles and an expected unit cell expansion. The work thus did not support the existence of conformational polymorphism in this material.

9.3 Co-crystal Studies and the Attempts to Engineer Halogen Bonding Interactions

The co-crystal studies involving bromanilic acid and the picolines, lutidines and the bromo-substituted pyridines enabled a wide range of structures to be produced and their bonding motifs to be examined. The 1:1 co-crystals with the range of picolines did not, unfortunately, produce any reproducible, predictable motifs, but instead showed a wide range of possible configurations and a higher occurrence of halogen bonding than in the 2:1 complexes. The 4-picoline 1:1 complex was the most anomalous, with no proton transfer from the bromanilic acid to the picoline observed; instead, the bromanilic acid remains fully protonated and the only halogen-halogen interaction in these systems is induced. In the 1:2 ratio a P:B:P motif is generated. This results in complete deprotonation of the bromanilic acid molecule and both picolines are fully protonated in the bifurcated hydrogen bond interactions that are formed.

Following on from this a selection of 1:1 co-crystals were produced with bromanilic acid and a range of lutidine molecules. In all but one of these co-crystal complexes a L:B:B:L motif was observed with hydrogen atom transfer occurring on one hydroxyl group of the bromanilic acid, and the other being involved in a hydrogen bonded dimer with its mirror image on the other molecule. It should also be noted that in the absence of this four molecule interaction such as the case with 2,3-lutidine, the presence of a short halogen bonding interaction is present. Although there are other instances of halogen bond interactions in all of the lutidine complexes, it is in the absence of the four molecule unit that it becomes shortest and it would be expected that at this point it plays a key role in the stabilising of the packing of the molecules in the unit cell.

To try and produce further halogen bonding interactions, bromanilic acid was co-crystallised with bromo-substituted pyridines. In the case of the 2-bromo-3-methylpyridine co-crystal complex, there is no hydrogen transfer to the pyridine group, possibly due to steric hindrance by the presence of the bromine atom in the 2-position. This means that no bifurcated hydrogen bonding takes place and again the bromine plays a more prominent role in the crystal structure. In the second of these co-crystals, this time with 3-bromo-4-methylpyridine, hydrogen transfer does occur from the bromanilic acid onto the pyridine group. This enables the generation of the four molecule unit, which once again results in an elongated halogen bonding interaction. However, due to the presence of the bromine on the methylpyridine ring, a second halogen bonding interaction is produced, also to an oxygen of a bromanilic acid molecule. This signifies a success in generating extra stabilising interactions in these co-crystal systems.

To probe these interactions further co-crystallisations should be targeted where there is not the presence of a stabilising interaction such as that of a four molecule interaction. In this instance it could be possible to produce more than one strong halogen bonding interaction, even if possible weaker hydrogen bonding is present.

References:

1. B. Rodriguez-Spong, C.P. Price, A. Jayasankar, N. Rodriguez-Hornedo, *Advanced Drug Delivery Reviews*, **2004**, *56*, 241-274
2. Joop H ter Horst, P.W. Cains, *Crystal Growth and Design*, **2008**, *8*, 7, 2537-2542
3. J. Bernstein, *Polymorphism in Molecular Crystals*; Oxford University Press, Oxford, 2002
4. J.D. Dunitz and J. Bernstein, *Acc. Chem. Res.*, **1995**, *28*, 193-200
5. J.M. Rubin-Preminger, J. Bernstein, *Crystal Growth and Design*, **2005**, *5*, 4, 1343-1349
6. I. Barsky, J. Bernstein, P.W. Stephens, K.H. Stone, E. Cheung, M.B. Hickey, J.O. Henck, *Crystal Growth and Design*, **2008**, *8*, 1, 63-70
7. H. Haisa, S. Kashino, R. Kawai, H. Maeda, *Acta Cryst* **1976**, *B32*, 1283-1285
8. H. Haisa, S. Kashino, H. Maeda, *Acta Cryst.* **1974**, *B30*, 2510-2512
9. Tatyana N. Drebuschak, E.V. Boldyreva, *Z Kristallogr.* **2004**, *219*, 506-512
10. C.C. Wilson, *Z Kristallogr.* **2000**, *215*, 693-701
11. J.P. Reboul, B. Cristau, J.C. Soyfer, J.P. Astier, *Acta Cryst B*, **1981**, *37*, 10, 1844-1848
12. V.L. Himes, A.D. Mighell, W.H. de Camp, *Acta Cryst B*, **1981**, *37*, 12, 2242-2245
13. M.M.J. Lowes, M.R. Caira, A.P. Lotter, J.G. Van der Watt, *J. Pharm. Sci.* **1987**, *76*, 9, 744-752
14. A.L. Grzesiak, M.D. Lang, K. Kim, A.J. Matzer, *J. Pharm. Sci.* **2002**, *91*, 4, 1186-1190
15. A.J. Florence, A. Johnston, S.L. Price, H. Nowell, A.R. Kennedy, N. Shankland, *J. Pharm. Sci.* **2006**, *95*, 9, 1918-1930
16. Aurora J Cruz Cabeza, G.M. Day, W.D.S. Motherwell, W. Jones, *Crystal Growth and Design*, **2006**, *6*, 8, 1858-1866
17. Lian Yu, G.A. Stephenson, C.A. Mitchell, C.A. Bunnell, S.V. Snorek, J. Bowyer, T.B. Borchardt, J.G. Stowell, S.R. Byrn, *Journal of the American Chemical Society*, **2000**, *122*, 585-591
18. C. A. Mithell, L. Yu, M.D. Ward, *Journal of the American Chemical Society*, **2001**, *123*, 10830-10839
19. Shuang Chen, I.A. Guzei, L. Yu, *Journal of the American Chemical Society*, **2005**, *127*, 9881-9885
20. J. van de Streek, *Cryst Eng Comm*, **2007**, *9*, 350-352

21. Lin Xianti, *Chinese J. Struct. Chem.*, **1983**, 2,213
22. D.Vujovic, L.R. Nassimbeni, *Crystal Growth and Design*, **2006**, 6, 1595-1597
23. T.Threlfall, T. Gelbrich, *Crystal Growth and Design*, **2007**, 7, 11, 2297
24. J. Dunitz, *Acta Cryst B*, **1995**, 51, 619-631
25. G. Desiraju, *Organic Solid State Chemistry*. Amsterdam: Elsevier, 1987
26. M.S.Hoard, S.D. Elakovich, *Phytochemistry*, **1996**, 43, 5, 1129-1133
27. T. Friscic, W.Jones, *Faraday Discuss.* **2007**, 136, 167-179
28. I. Weissbuch, M. Lahav, L. Leiserowitz, *Crystal Growth and Design*, **2003**, 3, 125-150
29. L.J.Chyall, J.M. Tower, D.A. Coates, T.L. Houston, S.L. Childs, *Crystal Growth and Design*, **2002**, 2, 6, 505-510
30. R.J.Davey, J. Garside, A.M. Hilton, D. McEwan, J.W. Morrison, *Journal of Crystal Growth*, **1996**, 166, 971-975
31. R.J.Davey, A.M. Hilton, J. Garside, *Trans IchemE*, **1997**, 75A, 245-251
32. D.Erdemir, A.Y. Lee, A.S. Myerson, *Current Opinions in Drug Discovery and Development*, **2007**, 10, 746-755
33. T.Bergfors, *Journal of Structural Biology*, **2003**, 142, 66-76
34. M. Fujiwara, Z.K. Nagy, J.W. Chew, R.D. Braatz, *Crystal Growth and Design*, **2002**, 2, 363-370
35. B.M.Epelbaum, M. Bickermann, A. Winnacker, *Crystal Growth and Design*, **2005**, 275, 479-484
36. Z. Ji, J. Warzywoda, A. Sacco Jr, *Microporous and Mesoporous Materials*, **2005**, 81, 201-210
37. R.J.Davey, *Nature*, **2004**, 428, 374-375
38. F.F.da-Silva, P.J.B. Pereira, L. Gales, M. Roessle, D. Svergun, P. Moradas-Ferreira, A.M. Damas, *Journal of Biological Chemistry*, **2006**, 281, 44, 33433-33440
39. D Svergun, *J. Appl. Cryst.* **2007**, 40, 10-17
40. N.Dimasi, M. Roessle, O. Moran, G. Candiano, D.I. Svergun, R. Biassoni, *Int.Journal of Biological Macromolecules*, **2007**, 40, 193-200
41. J.L.Haston, S.B. Engelsen, M. Roessle, J. Clarkson, E.W. Blanch, C. Baldock, C.M. Kielty, T.J. Wess, *J.Bio.Chem.* **2003**, 278, 42, 41189-41197
42. L.G.Jacobsohn, G. Capote, M.E.H. Maia da Costa, D.F. Franceschini, F.L. Freire Jr, *Diamond and Related Materials*, **2002**, 11, 1946-1951

43. <http://www.embl-hamburg.de/ExternalInfo/Research/Sax/software.html>
44. A.T.Hulme, S.L. Price, *J.Chem.Theory Comput*, **2007**, 3, 1597-1608
45. S.A.Barnett, A.T. Hulme, N. Issa, T.C. Lewis, L.S. Price, D.A. Tocher, S.L. Price, *New Journal of Chemistry*, **2008**, 32, 1761-1775
46. J.P.M.Lommerse, W.D.S. Motherwell, H.L. Ammon, J.D. Dunitz, A. Gavezzotti, D.W.M. Hoffman, F.J.J. Leusen, W.T.M. Mooij, S.L. Price, B. Schweizer, M.U. Schmidt, B.P. Van Eijck, P. Verwer, D.E. Williams, *Acta Cryst*, **2000**, B56, 697-714
47. W.D.S.Motherwell, H.L. Ammon, J.D. Dunitz, A. Dzyabchenko, P. Erk, A. Gavezzotti, D.W.M. Hoffman, F.J.J. Leusen, J.P.M.Lommerse, W.T.M. Mooij, S.L. Price, H. Scheraga, B. Schweizer, M.U. Schmidt, B.P. Van Eijck, P. Verwer, D.E. Williams, *Acta Cryst*, **2002**, B58, 647-661
48. G.M.Day, W.D.S.Motherwell, H.L. Ammon, S.X.M. Boerrigter, R.G. Della Valle, E. Venuti, A. Dzyabchenko, J.D. Dunitz, B. Schweizer, B.P. Van Eijck, P. Erk, J. C. Facelli, V. E. Bazterra, M. B. Ferraro, D.W.M. Hoffman, F.J.J. Leusen, C. Liang, C. C. Pantelides, P.G. Karamertzanis, S.L. Price, T.C. Lewis, H. Nowell, A. Torrisi, H. A. Scheraga, Y.A. Arnautova, M.U. Schmidt, P. Verwer, *Acta Cryst*, **2005**, B61, 511-527
49. G.M.Day, T.G. Cooper, A.J. Cruz-Cabeza, K.E. Hejczyk, H.L. Ammon, S.X.M. Boerrigter, J.S. Tan, R.G. Della Valle, E. Venutti, J. Jose, S.R. Gadre, G.R. Desiraju, T.S. Thakur, B.P. Van Eijck, J.C. Facelli, V.E. Bazterra, M.B. Ferraro, D.W.M. Hoffman, M.A. Neumann, F.J.J. Leusen, J. Kendrick, S.L. Price, A.J. Misquitta, P.G. Karamertzanis, G.W.A. Welch, H.A. Scheraga, Y.A. Arnautova, M.U. Schmidt, J.van de Streek, A.K. Wolf, B. Schweizer, *Acta Cryst*, **2009**, B65, 107-125
50. B.O'Sullivan, P. Barrett, G. Hsiao, A. Carr, B. Glennon, *Organic Process Research and Development*, **2003**, 7, 977-982
51. B.O'Sullivan, B. Glennon, *Organic Process Research and Development*, **2005**, 9, 884-889
52. E.Kougoulos, A.G. Jones, M.W. Wood-Kaczmar, *Journal of Crystal Growth*, **2005**, 273, 529-534
53. P.Barrett, B. Glennon, *Part. Part. Syst. Charact.* **1999**, 16, 207-211
54. D.R.Thompson, E. Kougoulos, A.G. Jones, M.W. Wood-Kaczmar, *Journal of Crystal Growth*, **2005**, 276, 230-236

55. P.Barrett, B. Glennon, B. O'Sullivan, *TransIChemE*, **2002**, 80, part A, 799-805
56. A.Abbas, D. Nobbs, J.A. Romagnoli, *Meas. Sci. Technol.* **2002**, 13, 349-356
57. L.Pauling, *J. Am. Chem. Soc.* **1931**, 53,137-140
58. W.M. Latimer, W.H.Rodebush, *J. Am. Chem. Soc.* **1920**, 42, 1419-1423
59. M.L.Huggins, *J. Phys. Chem.* **1922**, 26, 601-625
60. G.R.Desiraju, T.Steiner, *The Weak Hydrogen Bond: in Structural Chemistry and Biology*, Oxford University Press, Oxford, 1999
61. G.A.Jeffrey, *An Introduction to Hydrogen Bonding*, Oxford University Press, Oxford, 1997
62. C.C.Wilson, *Acta Cryst*, **2001**, B57, 435-439
63. A.Parkin, C.C Seaton, N. Blagden, C.C. Wilson, *Cryst. Growth and Design*, **2007**, 7, 3, 531-534
64. M.Schmidtman, C.C. Wilson, *Cryst Eng Comm*, **2008**, 10, 177-183
65. R.E.Marsh, *Acta Cryst*, **1958**, 11, 651-663
66. S.K.Sikka, R. Chidambaram, *Acta Cryst*, **1967**, 23, 107-111
67. G.M.J.Schmidt, *Pure. Appl. Chem.* **1971**, 27, 4, 647
68. S.L.Price, A.J. Stone, J. Lucas, R.S. Rowland, A.E. Thornley, *J. Am. Chem. Soc.* **1994**, 116, 11, 4910-4918
69. G.R.Desiraju, R. Parthasarathy, *J. Am. Chem. Soc.* **1989**, 111, 23, 8725-8726
70. G.R.Desiraju, *Angew. Chem. Int. Ed. Engl.* **1995**, 34, 2311-2327
71. S.C.Nyburg, C.H. Faerman, *Acta. Cryst.* **1985**, B41, 274-279
72. I.Csoregh, T. Brehmer, P. Bombicz, E. Weber, *Crystal Engineering*, **2001**, 4, 343-357
73. C.B.Aakeroy, M. Fasulo, N. Schultheiss, J. Desper, C. Moore, *J. Am. Chem. Soc.* **2007**, 129, 13772-13773
74. C.B.Aakeroy, N.C. Schultheiss, A. Rajbanshi, J. Desper, C. Moore, *Cryst. Growth and Design*, **2009**, 9, 1, 432-441
75. C.B.Aakeroy, M.E. Fasulo, J. Desper, *Molecular Pharmaceutics*, **2007**, 4, 3, 317-322
76. A.V.Trask, W.D.S. Motherwell, W. Jones, *Cryst. Growth and Design*, **2005**, 5, 3, 1013-1021
77. P.Fernandes, K. Shankland, W.I.F. David, A.J. Markvardsen, A.J. Florence, N. Shankland, C.K. Leech, *J.Appl.Cryst.* **2008**, 41, 1089-1094
78. W.C.Rontgen, *Nature*, **1896**, 53, 274-276

79. D.Sherwood, Crystals X-rays and Proteins; Longman Group Limited, 1976
80. W.H.Bragg, W.L. Bragg, *Proc. Royal Soc. Lon. A* **1913**, 88, 428
81. 11th BCA/CCG X-ray structure analysis school
82. A.Altomare, M. Camalli, G. Cascarano, C. Giacovazzo, A. Guagliardi, A.G.G. Moliterni, G. Polidori, R. Spagna, SIR 97: A new program for solving and refining crystal structures.
83. P.W.Betteridge, J.R. Carruthers, R.I. Cooper, K. Prout, D.J. Watkin, *J. Appl. Cryst.* **2003**, 36, 1487
84. SHELXL/SHELXS: G.M.Sheldrick, *Acta Cryst*, **2008**, A64, 112-122
85. WINGX/MAPVIEW: L.J.Farrugia *J.Appl.Cryst.* **1999**, 32, 837-838
86. ApexII: Bruker AXS, 2007
87. C.K.L. Perumal, A. Arulchakkaravarthi, P. Santhanaraghavan, *J.Crystal Growth*, **2002**, 241, 200-205
88. G.Ferguson, G.A. Sim, *Acta Cryst*, **1962**, 15, 346
89. S.K.Roy, B. Amitha, M. Sridhar, J. Uchil, *J. Mater, Sci. Lett.* **1993**, 12, 570-571
90. C.P.Brock, *Acta Cryst*, **1987**, C43, 1748
91. M.Bolte, J. Wissler, *Acta Cryst*, **2006**, E62, o1192-o1193
92. Zaman.Md.B, *J. Org. Chem.* **2001**, 66, 5987-5995
93. S.Horiuchi, R. Kumai, Y. Tokura, *J. Am. Chem. Soc.* **2005**, 127, 5010-5011
94. M.Adam, A. Parkin, L.H. Thomas, C.C. Wilson, *Cryst Eng Comm*, **2009**, in press
95. L.H.Thomas, B. Boyle, L.A. Clive, A. Collins, L.D. Currie, M. Gogol, C. Hastings, A.O.F. Jones, J.L.Kennedy, G.B. Kerr, A. Kidd, L.M. Lawton, S.J. Macintyre, N.M. MacLean, A.R.G. Martin, K. McGonagle, S. Melrose, G.A. Rew, C.W. Robinson, M. Schmidtman, F.B. Turnbull, L.G. Williams, A.Y. Wiseman, M.H. Wocial, C.C. Wilson, *Acta Cryst.* **2009**, E65, o1218
96. C.Robl, A. Weiss, *Mat.Res.Bull.* **1987**, 22, 497-504
97. H.Ishida, S. Kashino, *Acta Cryst.* **2004**, E60, o974
98. Md.B.Zaman, M. Tomura, *Cryst. Growth and Design*, **2004**, 4, 585
99. M. Tomura, Y. Yamashita, *Cryst Eng Comm*, **2000**, 2, 92
100. Tzy-Jiun.M.Luo, G.T.R. Palmore, *Cryst Growth and Design*, **2002**, 2, 337
101. E.K.Andersen, *Acta Cryst.* **1967**, 22, 188
102. E.K.Andersen, *Acta Cryst.* **1967**, 22, 191
103. M.Adam, 2008, An Investigation of Hydrogen Bonded Molecular Systems Using X-ray and Neutron Diffraction

104. D.Haynes, W. Jones, W.D.S. Motherwell, *Crystl Eng Comm*, **2006**, 8, 830-840

Appendix 1: Crystallography data generated from the single crystal studies of pMHB in chapter 5.

Compound	pMHB	pMHB	pMHB	pMHB	PMHB
Formula	C ₈ H ₈ O ₃				
Molecular weight (gmol ⁻¹)	152.15	152.15	152.15	152.15	152.15
Temperature (K)	100	150	200	250	300
Space Group	Cc	Cc	Cc	Cc	Cc
<i>a</i> (Å)	12.9679(8)	13.0278(9)	13.1838(7)	13.4110(11)	13.548(3)
<i>b</i> (Å)	17.2935(8)	17.2195(11)	17.1399(9)	17.0261(14)	16.963(4)
<i>c</i> (Å)	10.8438(10)	10.8588(7)	10.9015(6)	10.9589(9)	11.039(3)
α (°)	90	90	90	90	90
β (°)	119.139(4)	119.288(3)	119.478(2)	119.745(2)	119.857(9)
γ (°)	90	90	90	90	90
Volume (Å ³)	2124.1(3)	2124.6(3)	2144.5(2)	2172.6(3)	2200.1(9)
Z	12	12	10	12	12
θ range (°)	2.149 – 27.476	2.147 - 34.819	2.136 - 28.431	2.119 - 39.502	2.108 - 32.067
Reflections Collected	21970	35402	1715	22962	44548
Independent	2428	4588	1664	6385	3792
Refln observed I > 2 σ (I)	1649	3327	1463	3514	2216
No. Of Parameters	370	370	298	370	370
Goof on F ²	0.9828	1.2988	1.0405	0.8176	1.0420
<i>R</i> ₁ (Observed)	0.0317	0.0336	0.0326	0.0508	0.0374
<i>R</i> ₁ (all)	0.0452	0.0431	0.0371	0.0904	0.0592
<i>wR</i> ₂ (all)	0.0702	0.0444	0.0639	0.1467	0.1039

Appendix 2: Crystallography data generated from the single crystal studies of methyl-4-bromobenzoate in Chapter 7.

Compound	M4BB	M4BB	M4BB	M4BB	M4BB
Formula	C8 H7 Br1 O2				
Molecular weight / gmol ⁻¹	215.05	215.05	215.05	215.05	215.05
Temperature (K)	100	150	200	250	300
Space Group	P b c a	P b c a	P b c a	P b c a	P b c a
<i>a</i> (Å)	13.801(2)	13.8553(19)	13.968(2)	14.0262(11)	14.1505(11)
<i>b</i> (Å)	5.8977(9)	5.8950(8)	5.9306(7)	5.9211(4)	5.9558(4)
<i>c</i> (Å)	19.673(3)	19.652(3)	19.683(2)	19.7175(12)	19.7875(15)
α (°)	90	90	90	90	90
β (°)	90	90	90	90	90
γ (°)	90	90	90	90	90
Volume (Å ³)	1601.3(5)	1605.1(4)	1630.5(4)	1637.5(2)	1667.6(2)
Z	8	8	8	8	8
θ range/°	2.070 - 27.048	2.073 - 29.022	2.069 - 26.950	2.066 - 28.107	2.058 - 31.410
Reflections Collected	9044	10136	9044	11646	20724
Independent	1752	2024	1752	1972	2718
Refln (obs.I>2theta(I))	1200	1512	1200	1147	1354
R _{int}	0.0433	0.0392	0.0433	0.0535	0.0449
Parameters	121	121	121	121	121
Goof on F ²	1.0973	1.0632	1.0977	0.9638	1.0660
R ₁ (Observed)	0.0268	0.0305	0.0266	0.0332	0.0353
R ₁ (all)	0.0454	0.0415	0.0451	0.0615	0.0766
wR ₂ (all)	0.0538	0.0844	0.0548	0.0983	0.1116

Appendix 3:

_atom_site_label
_atom_site_fract_x
_atom_site_fract_y
_atom_site_fract_z
_atom_site_U_iso_or_equiv
_atom_site_occupancy
_atom_site_adp_type

Bromanilic Acid : 3 Picoline, 1 : 1

C1. 0.4625(2) 0.8771(2) 0.45069(15) 0.0094 1.0000 Uani
C2. 0.3846(2) 1.0717(2) 0.38450(15) 0.0093 1.0000 Uani
C3. 0.4335(2) 1.1871(2) 0.43963(15) 0.0095 1.0000 Uani
Br4. 0.34134(3) 1.43029(2) 0.356445(16) 0.0132 1.0000 Uani
O5. 0.28228(17) 1.12111(15) 0.28996(11) 0.0141 1.0000 Uani
O6. 0.42281(18) 0.77526(16) 0.39557(12) 0.0137 1.0000 Uani
C7. 0.1818(2) -0.0184(2) 0.94923(16) 0.0104 1.0000 Uani
C8. 0.1504(2) -0.0841(2) 1.09632(15) 0.0100 1.0000 Uani
C9. -0.0284(2) -0.0617(2) 1.13586(15) 0.0121 1.0000 Uani
Br10. -0.06715(3) -0.13980(2) 1.315021(16) 0.0163 1.0000 Uani
O11. 0.29247(17) -0.15350(16) 1.16703(11) 0.0142 1.0000 Uani
O12. 0.34376(17) -0.04253(16) 0.91671(12) 0.0149 1.0000 Uani
C13. 0.1960(2) 0.5441(2) 0.77057(16) 0.0140 1.0000 Uani
C14. 0.3195(3) 0.3824(2) 0.81357(17) 0.0146 1.0000 Uani
N15. 0.3831(2) 0.3102(2) 0.93524(14) 0.0149 1.0000 Uani
C16. 0.3323(3) 0.3881(2) 1.02311(17) 0.0156 1.0000 Uani
C17. 0.2067(3) 0.5494(2) 0.98529(18) 0.0176 1.0000 Uani
C18. 0.1402(3) 0.6278(2) 0.85967(18) 0.0163 1.0000 Uani
C19. 0.1315(3) 0.6248(3) 0.63220(19) 0.0233 1.0000 Uani
H161. 0.389(3) 0.318(2) 1.111(2) 0.0206 1.0000 Uiso
H171. 0.167(3) 0.607(3) 1.040(2) 0.0219 1.0000 Uiso
H181. 0.048(3) 0.749(3) 0.8266(19) 0.0203 1.0000 Uiso
H191. 0.129(3) 0.718(3) 0.606(2) 0.0257 1.0000 Uiso
H192. 0.257(3) 0.587(3) 0.587(2) 0.0257 1.0000 Uiso
H193. 0.023(3) 0.573(3) 0.609(2) 0.0257 1.0000 Uiso
H1. 0.366(4) 0.327(3) 0.757(2) 0.0500 1.0000 Uiso
H5. 0.496(4) 0.197(3) 0.963(2) 0.0500 1.0000 Uiso
H8. 0.351(4) 0.840(3) 0.314(3) 0.0500 1.0000 Uiso

Bromanilic Acid : 3 Picoline, 1 : 2

C1. 0.47315(12) 0.11327(11) 0.57957(11) 0.0135 1.0000 Uani
C2. 0.35756(13) 0.08050(11) 0.46586(12) 0.0134 1.0000 Uani
C3. 0.38778(13) -0.04363(11) 0.38114(12) 0.0133 1.0000 Uani
O4. 0.28233(9) -0.07389(8) 0.28055(8) 0.0181 1.0000 Uani
O5. 0.23310(9) 0.14209(8) 0.42753(8) 0.0181 1.0000 Uani
Br6. 0.434429(13) 0.263929(11) 0.686095(12) 0.0171 1.0000 Uani
C7. 1.00763(14) 0.35162(12) 0.59764(12) 0.0160 1.0000 Uani
N8. 1.01585(12) 0.46308(10) 0.67562(10) 0.0178 1.0000 Uani
C9. 0.89114(15) 0.53639(13) 0.68119(12) 0.0190 1.0000 Uani
C10. 0.86846(13) 0.30601(11) 0.52009(12) 0.0135 1.0000 Uani
C11. 0.73842(13) 0.38217(12) 0.52713(12) 0.0158 1.0000 Uani
C4. 0.74976(14) 0.49704(12) 0.60731(13) 0.0178 1.0000 Uani
C5. 0.86173(16) 0.18305(14) 0.43151(15) 0.0212 1.0000 Uani
H71. 1.0932(15) 0.3027(14) 0.5950(12) 0.0194 1.0000 Uiso
H91. 0.9073(14) 0.6167(13) 0.7376(13) 0.0238 1.0000 Uiso
H111. 0.6494(15) 0.3573(12) 0.4777(13) 0.0194 1.0000 Uiso

H41. 0.6703(15) 0.5470(13) 0.6152(13) 0.0219 1.0000 Uiso
H51. 0.7811(16) 0.1769(14) 0.3714(14) 0.0259 1.0000 Uiso
H52. 0.8585(15) 0.1002(13) 0.4767(13) 0.0259 1.0000 Uiso
H53. 0.9522(16) 0.1666(14) 0.4108(13) 0.0259 1.0000 Uiso
H6. 1.1053(18) 0.4864(16) 0.7110(15) 0.0500 1.0000 Uiso

Bromanilic Acid : 2 Picoline, 1 : 2

C1. 0.7783(3) 0.0885(4) 0.1096(2) 0.0344 1.0000 Uani
C2. 0.7063(3) -0.0042(5) 0.0865(3) 0.0385 1.0000 Uani
C3. 0.6910(3) -0.0973(5) -0.0098(3) 0.0393 1.0000 Uani
C4. 0.7484(3) -0.0768(4) -0.0681(2) 0.0374 1.0000 Uani
C5. 0.8212(3) 0.0193(4) -0.0456(3) 0.0370 1.0000 Uani
C6. 0.8391(3) 0.1041(4) 0.0533(3) 0.0364 1.0000 Uani
O7. 0.90612(19) 0.1785(3) 0.07350(16) 0.0513 1.0000 Uani
O8. 0.87468(18) 0.0408(3) -0.09503(17) 0.0504 1.0000 Uani
Br9. 0.72794(3) -0.18929(6) -0.18549(2) 0.0556 1.0000 Uani
O10. 0.62649(19) -0.1856(4) -0.02641(16) 0.0600 1.0000 Uani
O11. 0.6513(2) -0.0248(3) 0.13430(18) 0.0624 1.0000 Uani
Br12. 0.79779(3) 0.19975(5) 0.22786(2) 0.0491 1.0000 Uani
C13. 0.9458(3) -0.2408(5) 0.1371(3) 0.0438 1.0000 Uani
N14. 0.9780(2) -0.2366(4) 0.0586(2) 0.0407 1.0000 Uani
C15. 0.9453(3) -0.3239(6) -0.0183(3) 0.0476 1.0000 Uani
C16. 0.8794(3) -0.4243(5) -0.0176(3) 0.0570 1.0000 Uani
C17. 0.8447(3) -0.4370(6) 0.0618(4) 0.0624 1.0000 Uani
C18. 0.8786(3) -0.3472(7) 0.1384(4) 0.0625 1.0000 Uani
C19. 0.9857(4) -0.1396(6) 0.2167(3) 0.0681 1.0000 Uani
C20. 0.4680(3) 0.4474(6) -0.1197(2) 0.0472 1.0000 Uani
N21. 0.4694(2) 0.2795(5) -0.1037(2) 0.0541 1.0000 Uani
C22. 0.5311(4) 0.1769(7) -0.1188(3) 0.0598 1.0000 Uani
C23. 0.5959(3) 0.2413(6) -0.1541(3) 0.0574 1.0000 Uani
C24. 0.5968(4) 0.4119(7) -0.1725(3) 0.0587 1.0000 Uani
C25. 0.5346(4) 0.5139(6) -0.1549(3) 0.0551 1.0000 Uani
C26. 0.3963(4) 0.5472(7) -0.1001(3) 0.0746 1.0000 Uani
H151. 0.978(2) -0.307(4) -0.071(2) 0.0618 1.0000 Uiso
H161. 0.860(3) -0.482(5) -0.063(3) 0.0730 1.0000 Uiso
H171. 0.804(3) -0.512(5) 0.066(3) 0.0778 1.0000 Uiso
H181. 0.861(3) -0.347(5) 0.195(2) 0.0744 1.0000 Uiso
H221. 0.529(3) 0.063(5) -0.103(2) 0.0729 1.0000 Uiso
H231. 0.640(3) 0.162(5) -0.171(2) 0.0759 1.0000 Uiso
H241. 0.644(3) 0.458(5) -0.191(3) 0.0735 1.0000 Uiso
H251. 0.534(3) 0.619(4) -0.161(2) 0.0678 1.0000 Uiso
H261. 0.408(3) 0.665(5) -0.120(3) 0.0938 1.0000 Uiso
H262. 0.384(3) 0.485(5) -0.045(3) 0.0938 1.0000 Uiso
H263. 0.355(3) 0.515(6) -0.145(3) 0.0938 1.0000 Uiso
H2. 0.949(2) -0.099(5) 0.245(2) 0.0500 1.0000 Uiso
H6. 0.423(2) 0.251(4) -0.079(2) 0.0500 1.0000 Uiso
H8. 1.023(2) -0.174(4) 0.058(2) 0.0500 1.0000 Uiso
H9. 0.996(3) -0.048(4) 0.206(3) 0.0500 1.0000 Uiso
H25. 0.998(2) -0.224(4) 0.272(2) 0.0500 1.0000 Uiso

Bromanilic Acid : 4 Picoline, 1 : 1

H1. 0.513(6) 0.525(7) 0.325(8) 0.00(2) 1.0000 Uiso
H3. 0.208(6) -0.251(8) 0.077(7) 0.00(2) 1.0000 Uiso
Br1. 0.33421(5) 0.16939(7) 0.33141(6) 0.01589(19) 1.0000 Uani
Br2. 0.35842(5) 0.60836(7) 0.02358(6) 0.0164(2) 1.0000 Uani
O4. 0.4682(4) 0.3621(6) 0.3727(5) 0.0195(13) 1.0000 Uani
C18. 0.3373(5) 0.2915(7) 0.2413(7) 0.0141(17) 1.0000 Uani
O1. 0.4773(4) 0.5330(5) 0.2589(5) 0.0171(13) 1.0000 Uani
O2. 0.2214(4) 0.4238(6) -0.0212(5) 0.0165(13) 1.0000 Uani

O3. 0.2171(4) 0.2307(6) 0.0901(5) 0.0176(13) 1.0000 Uani
 H3A. 0.1879 0.2524 0.0283 0.026 1.0000 Uiso
 C15. 0.3514(5) 0.4841(6) 0.1110(6) 0.0104(15) 1.0000 Uani
 C16. 0.2787(6) 0.4066(7) 0.0672(7) 0.0155(18) 1.0000 Uani
 C13. 0.4077(5) 0.3674(7) 0.2844(6) 0.0131(16) 1.0000 Uani
 C17. 0.2749(5) 0.3020(7) 0.1344(6) 0.0121(16) 1.0000 Uani
 C14. 0.4088(6) 0.4663(7) 0.2094(7) 0.0153(18) 1.0000 Uani
 Br3. 0.41071(5) 0.07548(7) 0.08688(6) 0.0179(2) 1.0000 Uani
 Br4. 0.35206(6) -0.34572(8) 0.38002(7) 0.0238(2) 1.0000 Uani
 O8. 0.2687(4) -0.1044(5) 0.0353(5) 0.0184(13) 1.0000 Uani
 C21. 0.3140(6) -0.2059(8) 0.1991(8) 0.0193(19) 1.0000 Uani
 O7. 0.2442(4) -0.2643(6) 0.1434(6) 0.0226(14) 1.0000 Uani
 O6. 0.4952(4) -0.1669(6) 0.4411(5) 0.0201(13) 1.0000 Uani
 C22. 0.3668(5) -0.2233(7) 0.2992(7) 0.0138(17) 1.0000 Uani
 O5. 0.5154(4) 0.0147(5) 0.3313(4) 0.0151(12) 1.0000 Uani
 H5. 0.5405 -0.0076 0.3937 0.023 1.0000 Uiso calc R . .
 C19. 0.3972(6) -0.0411(7) 0.1763(7) 0.0148(18) 1.0000 Uani
 C23. 0.4433(6) -0.1523(7) 0.3512(7) 0.0130(17) 1.0000 Uani
 C24. 0.4544(6) -0.0496(7) 0.2826(8) 0.019(2) 1.0000 Uani
 C20. 0.3265(6) -0.1107(7) 0.1282(7) 0.0163(17) 1.0000 Uani
 N1. 0.1484(5) 0.8057(6) 0.3700(6) 0.0168(15) 1.0000 Uani
 C3. 0.1084(5) 0.9045(7) 0.1736(7) 0.0128(16) 1.0000 Uani
 C2. 0.0716(6) 0.7973(8) 0.1827(7) 0.0178(18) 1.0000 Uani
 H2. 0.0327 0.7592 0.1216 0.021 1.0000 Uiso calc R . .
 C4. 0.1641(6) 0.9589(8) 0.2650(8) 0.023(2) 1.0000 Uani
 H4. 0.1891 1.0295 0.2608 0.028 1.0000 Uiso calc R . .
 C6. 0.0843(6) 0.9571(9) 0.0637(8) 0.024(2) 1.0000 Uani
 H6A. 0.0444 0.9065 0.0098 0.036 1.0000 Uiso calc R . .
 H6B. 0.1317 0.9628 0.0525 0.036 1.0000 Uiso calc R . .
 H6C. 0.0615 1.0354 0.0592 0.036 1.0000 Uiso calc R . .
 C1. 0.0934(6) 0.7496(8) 0.2819(7) 0.0180(18) 1.0000 Uani
 H1A. 0.0701 0.6782 0.2881 0.022 1.0000 Uiso calc R . .
 C5. 0.1834(7) 0.9092(9) 0.3637(8) 0.025(2) 1.0000 Uani
 H5. 0.2206 0.9473 0.4260 0.031 1.0000 Uiso calc R . .
 C8. 0.1506(5) 0.4464(7) 0.2346(6) 0.0132(16) 1.0000 Uani
 H8. 0.1872 0.4865 0.2961 0.016 1.0000 Uiso calc R . .
 C7. 0.1319(6) 0.4945(8) 0.1365(7) 0.0182(18) 1.0000 Uani
 H7. 0.1556 0.5659 0.1312 0.022 1.0000 Uiso calc R . .
 C11. 0.0456(5) 0.3320(7) 0.0518(6) 0.0155(17) 1.0000 Uani
 H11. 0.0111 0.2922 -0.0110 0.019 1.0000 Uiso calc R . .
 C9. 0.1163(6) 0.3387(8) 0.2448(8) 0.0192(19) 1.0000 Uani
 N2. 0.0784(5) 0.4364(6) 0.0480(6) 0.0145(14) 1.0000 Uani
 C12. 0.1386(6) 0.2869(8) 0.3525(6) 0.0190(19) 1.0000 Uani
 H12A. 0.1760 0.3396 0.4070 0.029 1.0000 Uiso calc R . .
 H12B. 0.1640 0.2104 0.3587 0.029 1.0000 Uiso calc R . .
 H12C. 0.0903 0.2776 0.3610 0.029 1.0000 Uiso calc R . .
 C10. 0.0634(5) 0.2826(7) 0.1513(7) 0.0165(17) 1.0000 Uani
 H10. 0.0392 0.2107 0.1544 0.020 1.0000 Uiso calc R . .

Bromanilic Acid : 4 Picoline, 1 : 2

C1. 0.4281(2) 0.5693(3) 0.42464(10) 0.0160 1.0000 Uani
 C2. 0.5455(2) 0.3690(3) 0.43700(10) 0.0150 1.0000 Uani
 C3. 0.6118(2) 0.3196(3) 0.51063(10) 0.0165 1.0000 Uani
 Br4. 0.75109(2) 0.07117(3) 0.524928(11) 0.0189 1.0000 Uani
 O5. 0.57051(16) 0.26725(19) 0.37879(7) 0.0193 1.0000 Uani
 O6. 0.37844(16) 0.61446(19) 0.35800(7) 0.0198 1.0000 Uani
 C7. 0.1119(2) 0.4826(3) 0.66164(10) 0.0179 1.0000 Uani
 C8. 0.1774(2) 0.5631(3) 0.73151(11) 0.0204 1.0000 Uani
 C9. 0.2878(2) 0.4434(3) 0.77733(11) 0.0220 1.0000 Uani

N10. 0.3321(2) 0.2450(3) 0.75598(9) 0.0227 1.0000 Uani
C11. 0.2733(2) 0.1598(3) 0.68921(11) 0.0219 1.0000 Uani
C12. 0.1630(2) 0.2765(3) 0.64148(11) 0.0205 1.0000 Uani
C13. -0.0045(3) 0.6143(4) 0.60942(14) 0.0287 1.0000 Uani
H81. 0.153(3) 0.702(3) 0.7470(12) 0.0241 1.0000 Uiso
H91. 0.335(3) 0.494(3) 0.8230(12) 0.0239 1.0000 Uiso
H111. 0.307(3) 0.019(3) 0.6774(12) 0.0239 1.0000 Uiso
H121. 0.126(3) 0.220(3) 0.5978(12) 0.0240 1.0000 Uiso
H131. -0.082(3) 0.544(3) 0.5879(13) 0.0281 1.0000 Uiso
H132. -0.050(3) 0.734(3) 0.6351(12) 0.0281 1.0000 Uiso
H133. 0.052(3) 0.687(3) 0.5721(13) 0.0281 1.0000 Uiso
H3. 0.390(3) 0.183(4) 0.7847(15) 0.0500 1.0000 Uiso

Bromanilic Acid : 2,3 lutidine

C1. 0.6262(6) 0.29482(13) 0.0802(2) 0.0149 1.0000 Uani
C2. 0.6782(6) 0.29436(13) 0.1907(2) 0.0158 1.0000 Uani
C3. 0.5236(6) 0.33208(13) 0.2596(2) 0.0178 1.0000 Uani
C4. 0.3186(6) 0.36856(13) 0.2014(2) 0.0171 1.0000 Uani
C5. 0.2519(6) 0.37124(13) 0.0860(2) 0.0169 1.0000 Uani
C6. 0.4243(6) 0.33413(13) 0.0197(2) 0.0169 1.0000 Uani
O7. 0.3839(4) 0.33938(9) -0.08076(16) 0.0226 1.0000 Uani
O8. 0.0653(4) 0.40101(9) 0.02924(16) 0.0235 1.0000 Uani
Br9. 0.11293(6) 0.413336(14) 0.28552(2) 0.0238 1.0000 Uani
O10. 0.5921(4) 0.32669(9) 0.36148(16) 0.0228 1.0000 Uani
O11. 0.8656(4) 0.25999(10) 0.25003(16) 0.0228 1.0000 Uani
Br12. 0.81829(6) 0.247085(14) -0.00351(2) 0.0201 1.0000 Uani
C13. 0.6458(6) 0.43201(13) -0.2236(2) 0.0191 1.0000 Uani
C14. 0.5128(6) 0.43488(13) -0.3346(2) 0.0170 1.0000 Uani
C15. 0.5925(7) 0.39735(14) -0.4106(3) 0.0220 1.0000 Uani
C16. 0.8044(7) 0.35829(15) -0.3772(3) 0.0250 1.0000 Uani
C17. 0.9300(7) 0.35722(14) -0.2690(3) 0.0218 1.0000 Uani
N18. 0.8492(5) 0.39346(12) -0.1953(2) 0.0211 1.0000 Uani
C19. 0.2870(7) 0.47803(16) -0.3709(3) 0.0274 1.0000 Uani
C20. 0.5753(7) 0.46964(16) -0.1336(3) 0.0253 1.0000 Uani
H151. 0.492(6) 0.3999(13) -0.484(2) 0.0286 1.0000 Uiso
H161. 0.861(6) 0.3292(13) -0.427(2) 0.0315 1.0000 Uiso
H171. 1.068(6) 0.3315(13) -0.241(2) 0.0290 1.0000 Uiso
H191. 0.200(6) 0.4747(13) -0.447(3) 0.0349 1.0000 Uiso
H192. 0.353(6) 0.5159(14) -0.349(2) 0.0349 1.0000 Uiso
H193. 0.134(6) 0.4701(13) -0.330(2) 0.0349 1.0000 Uiso
H201. 0.679(6) 0.4631(14) -0.068(3) 0.0349 1.0000 Uiso
H202. 0.564(6) 0.5089(14) -0.159(2) 0.0349 1.0000 Uiso
H203. 0.393(6) 0.4619(13) -0.119(2) 0.0349 1.0000 Uiso
H7. 0.928(6) 0.3956(15) -0.125(3) 0.0500 1.0000 Uiso
H10. 0.862(7) 0.2665(16) 0.309(3) 0.0500 1.0000 Uiso

Bromanilic Acid : 2,4 lutidine

C1. 0.90439(16) 0.19216(11) 0.55354(10) 0.0140 1.0000 Uani
C2. 1.02992(15) 0.18826(12) 0.49595(10) 0.0144 1.0000 Uani
C3. 1.00553(15) 0.10940(11) 0.40708(9) 0.0130 1.0000 Uani
C4. 0.85658(15) 0.05016(11) 0.38354(9) 0.0130 1.0000 Uani
C5. 0.73824(15) 0.05279(11) 0.44134(9) 0.0125 1.0000 Uani
C6. 0.77043(15) 0.12613(11) 0.53096(9) 0.0127 1.0000 Uani
O7. 0.65620(12) 0.12713(9) 0.58358(8) 0.0175 1.0000 Uani
O8. 0.60470(11) 0.00120(9) 0.42414(7) 0.0182 1.0000 Uani
Br9. 0.811745(16) -0.039128(12) 0.269616(9) 0.0164 1.0000 Uani
O10. 1.12007(11) 0.10674(8) 0.36237(7) 0.0161 1.0000 Uani
O11. 1.15306(12) 0.24636(9) 0.51295(8) 0.0217 1.0000 Uani
Br12. 0.933870(16) 0.293269(12) 0.657859(10) 0.0193 1.0000 Uani

C13. 0.47281(16) 0.23292(13) 0.31099(10) 0.0190 1.0000 Uani
C14. 0.61209(17) 0.29593(14) 0.30823(12) 0.0231 1.0000 Uani
C15. 0.67700(17) 0.37022(14) 0.38130(13) 0.0245 1.0000 Uani
C16. 0.59599(17) 0.38271(13) 0.45804(13) 0.0235 1.0000 Uani
C17. 0.45777(17) 0.32123(13) 0.45950(11) 0.0197 1.0000 Uani
N18. 0.39968(14) 0.24881(11) 0.38723(9) 0.0158 1.0000 Uani
C19. 0.8323(2) 0.43393(18) 0.38094(19) 0.0377 1.0000 Uani
C20. 0.4001(2) 0.15064(17) 0.23506(12) 0.0277 1.0000 Uani
H141. 0.655(2) 0.2852(15) 0.2586(13) 0.0298 1.0000 Uiso
H161. 0.630(2) 0.4290(16) 0.5087(14) 0.0303 1.0000 Uiso
H171. 0.399(2) 0.3235(14) 0.5103(13) 0.0251 1.0000 Uiso
H191. 0.823(3) 0.5062(19) 0.4090(16) 0.0492 1.0000 Uiso
H192. 0.915(3) 0.3983(17) 0.4275(16) 0.0492 1.0000 Uiso
H193. 0.843(3) 0.4419(19) 0.3260(18) 0.0492 1.0000 Uiso
H201. 0.476(2) 0.1158(16) 0.2106(14) 0.0354 1.0000 Uiso
H202. 0.356(2) 0.0848(17) 0.2615(14) 0.0354 1.0000 Uiso
H5. 0.321(3) 0.2108(18) 0.3893(16) 0.0500 1.0000 Uiso
H7. 0.313(3) 0.1788(17) 0.1870(16) 0.0500 1.0000 Uiso
H11. 0.585(3) 0.0879(18) 0.5645(16) 0.0500 1.0000 Uiso

Bromanilic Acid : 2,5 lutidine

C1. 0.4371(2) 0.16236(14) 0.00087(11) 0.0126 1.0000 Uani
C2. 0.2819(2) 0.10049(14) -0.01685(10) 0.0123 1.0000 Uani
C3. 0.2489(2) 0.04872(14) -0.10566(10) 0.0118 1.0000 Uani
C4. 0.3629(2) 0.06041(14) -0.16561(10) 0.0119 1.0000 Uani
C5. 0.5272(2) 0.11945(14) -0.14685(11) 0.0126 1.0000 Uani
C6. 0.5642(2) 0.17565(15) -0.05707(11) 0.0144 1.0000 Uani
O7. 0.70451(16) 0.22867(14) -0.04458(9) 0.0262 1.0000 Uani
O8. 0.63916(15) 0.12864(12) -0.19702(8) 0.0192 1.0000 Uani
Br9. 0.31638(2) -0.007105(16) -0.274220(11) 0.0155 1.0000 Uani
O10. 0.09935(15) -0.00757(12) -0.12106(8) 0.0178 1.0000 Uani
O11. 0.16422(16) 0.08354(12) 0.03184(8) 0.0200 1.0000 Uani
Br12. 0.47839(2) 0.233092(15) 0.109386(11) 0.0153 1.0000 Uani
C13. 1.0291(2) 0.28269(15) -0.23866(11) 0.0153 1.0000 Uani
C14. 1.1652(2) 0.36306(16) -0.24366(12) 0.0178 1.0000 Uani
C15. 1.2332(2) 0.42206(16) -0.17219(12) 0.0182 1.0000 Uani
C16. 1.1677(2) 0.40251(16) -0.09346(12) 0.0168 1.0000 Uani
C17. 1.0319(2) 0.32299(16) -0.09112(12) 0.0165 1.0000 Uani
N18. 0.96688(18) 0.26690(14) -0.16205(9) 0.0154 1.0000 Uani
C19. 1.2398(3) 0.4662(2) -0.01527(14) 0.0240 1.0000 Uani
C20. 0.9481(3) 0.21598(19) -0.31251(13) 0.0220 1.0000 Uani
H141. 1.207(3) 0.3746(19) -0.2973(14) 0.0233 1.0000 Uiso
H151. 1.320(3) 0.4795(19) -0.1776(13) 0.0231 1.0000 Uiso
H171. 0.978(3) 0.3044(18) -0.0431(13) 0.0211 1.0000 Uiso
H191. 1.163(3) 0.454(2) 0.0293(14) 0.0300 1.0000 Uiso
H192. 1.355(3) 0.424(2) -0.0013(14) 0.0300 1.0000 Uiso
H193. 1.237(3) 0.553(2) -0.0248(15) 0.0300 1.0000 Uiso
H201. 1.005(3) 0.232(2) -0.3572(14) 0.0272 1.0000 Uiso
H4. 0.883(3) 0.221(2) -0.1561(16) 0.0500 1.0000 Uiso
H13. 0.038(3) -0.010(2) -0.0764(17) 0.0500 1.0000 Uiso
H17. 0.956(3) 0.135(3) -0.3007(17) 0.0500 1.0000 Uiso
H19. 0.827(3) 0.258(2) -0.3251(16) 0.0500 1.0000 Uiso

Bromanilic Acid : 3,5 lutidine

C1. 0.15121(18) 0.03215(17) 0.38885(15) 0.0128 1.0000 Uani
C2. 0.08214(17) 0.14144(17) 0.41329(14) 0.0123 1.0000 Uani
C3. 0.14290(18) 0.24873(17) 0.49386(15) 0.0131 1.0000 Uani
C4. 0.25927(17) 0.23342(17) 0.53944(15) 0.0117 1.0000 Uani
C5. 0.32706(17) 0.12879(17) 0.51171(14) 0.0125 1.0000 Uani

C6. 0.26537(18) 0.02854(16) 0.42882(15) 0.0130 1.0000 Uani
 O7. 0.33428(13) -0.06403(12) 0.40040(12) 0.0168 1.0000 Uani
 O8. 0.43042(12) 0.10762(13) 0.55013(11) 0.0166 1.0000 Uani
 Br9. 0.328043(18) 0.354531(17) 0.649864(16) 0.0148 1.0000 Uani
 O10. 0.08038(12) 0.33994(12) 0.51248(11) 0.0176 1.0000 Uani
 O11. -0.01997(12) 0.15509(13) 0.37328(11) 0.0184 1.0000 Uani
 Br12. 0.075664(18) -0.098738(17) 0.295329(16) 0.0167 1.0000 Uani
 C13. 0.35380(18) 0.67357(17) 0.55162(16) 0.0149 1.0000 Uani
 C14. 0.36248(19) 0.61039(19) 0.44674(16) 0.0159 1.0000 Uani
 C15. 0.26556(18) 0.56721(17) 0.37197(15) 0.0142 1.0000 Uani
 C16. 0.15909(19) 0.59052(18) 0.40496(16) 0.0152 1.0000 Uani
 N17. 0.15033(15) 0.65306(15) 0.50502(13) 0.0140 1.0000 Uani
 C18. 0.24403(19) 0.69348(17) 0.57821(16) 0.0146 1.0000 Uani
 C19. 0.2729(3) 0.4949(2) 0.26181(19) 0.0246 1.0000 Uani
 C20. 0.4571(2) 0.7156(2) 0.6361(2) 0.0233 1.0000 Uani
 H141. 0.4295(16) 0.5989(18) 0.4236(15) 0.005(5) 1.0000 Uiso
 H161. 0.0920(18) 0.5619(19) 0.3589(17) 0.017(6) 1.0000 Uiso
 H181. 0.2290(16) 0.7308(18) 0.6458(16) 0.008(5) 1.0000 Uiso
 H191. 0.215(2) 0.515(2) 0.197(2) 0.032(7) 1.0000 Uiso
 H192. 0.339(2) 0.511(2) 0.239(2) 0.032(8) 1.0000 Uiso
 H193. 0.2689(19) 0.414(2) 0.2700(19) 0.033(7) 1.0000 Uiso
 H201. 0.4561(18) 0.683(2) 0.708(2) 0.028(6) 1.0000 Uiso
 H202. 0.4617(16) 0.810(2) 0.6335(16) 0.014(5) 1.0000 Uiso
 H203. 0.519(2) 0.696(2) 0.615(2) 0.029(8) 1.0000 Uiso
 H7. 0.073(2) 0.667(2) 0.531(2) 0.051(8) 1.0000 Uiso
 H11. 0.403(2) -0.042(3) 0.444(2) 0.064(10) 1.0000 Uiso

Bromanilic Acid : 2bromo, 3methylpyridine

C1. 0.6948(8) 0.5219(3) 0.45322(19) 0.0138 1.0000 Uani
 C2. 0.6023(8) 0.5989(3) 0.4963(2) 0.0153 1.0000 Uani
 C3. 0.3986(8) 0.5712(3) 0.54446(19) 0.0143 1.0000 Uani
 O4. 0.3254(7) 0.6446(2) 0.58321(17) 0.0247 1.0000 Uani
 O5. 0.6710(6) 0.6861(2) 0.49645(15) 0.0245 1.0000 Uani
 Br6. 0.95526(9) 0.55600(4) 0.39595(2) 0.0184 1.0000 Uani
 C7. 0.3110(8) -0.0742(3) 0.4850(2) 0.0149 1.0000 Uani
 C8. 0.4677(9) -0.0838(3) 0.5434(2) 0.0159 1.0000 Uani
 C9. 0.6650(9) -0.0032(3) 0.5579(2) 0.0147 1.0000 Uani
 O10. 0.8075(6) -0.0120(2) 0.61070(16) 0.0204 1.0000 Uani
 O11. 0.4534(6) -0.1529(2) 0.58290(14) 0.0188 1.0000 Uani
 Br12. 0.06049(9) -0.17269(3) 0.47153(2) 0.0183 1.0000 Uani
 C13. 0.3389(8) 0.1754(4) 0.2549(2) 0.0181 1.0000 Uani
 C14. 0.3287(9) 0.2585(4) 0.2134(2) 0.0206 1.0000 Uani
 C15. 0.1497(10) 0.3298(4) 0.2290(2) 0.0246 1.0000 Uani
 C16. 0.0001(10) 0.3182(4) 0.2827(2) 0.0242 1.0000 Uani
 C17. 0.0311(10) 0.2337(4) 0.3211(2) 0.0234 1.0000 Uani
 N18. 0.1966(7) 0.1618(3) 0.30661(16) 0.0166 1.0000 Uani
 C19. 0.4981(12) 0.2722(5) 0.1567(3) 0.0309 1.0000 Uani
 Br20. 0.56859(10) 0.06826(4) 0.23907(2) 0.0284 1.0000 Uani
 H151. 0.139(9) 0.380(4) 0.200(2) 0.0331 1.0000 Uiso
 H161. -0.106(10) 0.358(4) 0.297(2) 0.0311 1.0000 Uiso
 H171. -0.069(9) 0.225(3) 0.355(2) 0.0292 1.0000 Uiso
 H191. 0.477(10) 0.335(4) 0.138(2) 0.0387 1.0000 Uiso
 H192. 0.652(10) 0.262(4) 0.166(3) 0.0387 1.0000 Uiso
 H193. 0.478(11) 0.244(4) 0.126(3) 0.0387 1.0000 Uiso
 H5. 0.382(11) 0.689(5) 0.572(3) 0.0500 1.0000 Uiso
 H15. 0.788(10) -0.062(4) 0.638(2) 0.0500 1.0000 Uiso

Bromanilic Acid : 3bromo, 4methylpyridine

C1. 0.2393(2) 0.2671(5) 0.91006(9) 0.0158 1.0000 Uani

C2. 0.1454(2) 0.1215(5) 0.93341(9) 0.0164 1.0000 Uani
C3. 0.0750(3) -0.0689(5) 0.89774(10) 0.0166 1.0000 Uani
C4. 0.1033(2) -0.1087(5) 0.84607(10) 0.0160 1.0000 Uani
C5. 0.2049(2) 0.0293(5) 0.82352(9) 0.0154 1.0000 Uani
C6. 0.2692(2) 0.2395(5) 0.85634(10) 0.0154 1.0000 Uani
O7. 0.34444(18) 0.3719(4) 0.83172(7) 0.0201 1.0000 Uani
O8. 0.24267(18) -0.0146(4) 0.77845(6) 0.0202 1.0000 Uani
Br9. 0.01729(3) -0.34999(5) 0.801722(10) 0.0188 1.0000 Uani
O10. -0.01434(19) -0.1956(4) 0.92112(7) 0.0219 1.0000 Uani
O11. 0.11429(17) 0.1393(4) 0.98104(6) 0.0204 1.0000 Uani
Br12. 0.31928(3) 0.51669(5) 0.954038(10) 0.0194 1.0000 Uani
C13. 0.7095(2) 0.1138(5) 0.86032(10) 0.0171 1.0000 Uani
C14. 0.6174(2) -0.0253(5) 0.88456(9) 0.0168 1.0000 Uani
C15. 0.5526(3) -0.2020(6) 0.85252(10) 0.0201 1.0000 Uani
C16. 0.5794(3) -0.2373(6) 0.79910(11) 0.0209 1.0000 Uani
N17. 0.6659(2) -0.0951(5) 0.77742(9) 0.0203 1.0000 Uani
C18. 0.7321(3) 0.0782(6) 0.80614(10) 0.0189 1.0000 Uani
C19. 0.5895(3) 0.0144(7) 0.94257(11) 0.0238 1.0000 Uani
Br20. 0.80540(3) 0.35720(6) 0.899664(11) 0.0233 1.0000 Uani
H151. 0.494(3) -0.310(5) 0.8652(11) 0.0243 1.0000 Uiso
H161. 0.538(3) -0.352(6) 0.7737(12) 0.0254 1.0000 Uiso
H181. 0.785(3) 0.177(6) 0.7910(12) 0.0257 1.0000 Uiso
H191. 0.530(3) -0.083(6) 0.9494(12) 0.0317 1.0000 Uiso
H192. 0.665(3) -0.012(6) 0.9677(12) 0.0317 1.0000 Uiso
H193. 0.558(3) 0.178(6) 0.9488(12) 0.0317 1.0000 Uiso
H9. 0.678(4) -0.106(7) 0.7466(15) 0.0500 1.0000 Uiso
H18. -0.025(4) -0.141(7) 0.9489(15) 0.0500 1.0000 Uiso